2018

Modeling and control of complex building energy systems

Venkatesh Chinde
Iowa State University

Modeling and control of complex building energy systems

by

Venkatesh Chinde

A dissertation submitted to the graduate faculty

in partial fulfillment of the requirements for the degree of

DOCTOR OF PHILOSOPHY

Major: Mechanical Engineering

Program of Study Committee:
Atul Kelkar, Major Professor
Soumik Sarkar
Shan Hu
Ananda Weerasinghe
Mehari Tekeste

The student author, whose presentation of the scholarship herein was approved by the program of study committee, is solely responsible for the content of this dissertation. The Graduate College will ensure this dissertation is globally accessible and will not permit alterations after a degree is conferred.

Iowa State University

Ames, Iowa

2018

DEDICATION

This dissertation is dedicated to the memory of my mother, Chinde Nagubai

TABLE OF CONTENTS

Page

LIST OF TABLES

Page

LIST OF FIGURES

Page

ACKNOWLEDGMENTS

There are many people I wish to thank for providing support throughout my Ph.D. journey. First and foremost, I would like to thank my advisor Dr. Atul Kelkar for finding me suitable for the project and accepting me as his student. Dr. Atul and I had a common interest in using passivity ideas for control in different engineering domains and also his immense experience in control theory helped me to pursue my goals. I feel grateful for the freedom he has given me not only in terms of research but also doing collaborative work for this dissertation. I also want to thank my program of study committee: Professors Soumik Sarkar, Shan Hu, Ananda Weerasinghe, and Mehari Tekeste for their valuable comments and suggestions that improved my work. I thank Iowa Energy Center for supporting my research.

I would like to thank Dr. Soumik Sarkar and Dr. Ramakrishna Pasumarthy for providing guidance throughout my Ph.D. The discussions we had were very helpful which shaped my dissertation very well. I also wish to thank Zhanhong Jiang and Krishna Chaitanya Kosaraju for their fruitful collaboration.

I wish to give my very special thanks to Dr. Navdeep M Singh who has been a constant source of support and encouragement for me from the beginning of my studies at ISU and also for introducing me to the show-stopper (Brayton-Moser form & Passivity) of the dissertation.

Special thanks to all my friends Deepak Tiwari, Amit Diwadkar, Sai Pushpak, Shikha Sharma, Alok Bharati, Amar, Srikant, Animesh Biswas, Subhrajit Sinha for making my stay in Ames a memorable one.

I wish to thank my entire family: parents, wife, sisters, brothers-in-law who gave me their unconditional love and support during all these years. Sorry to have missed many good times with you all during festivals.

ABSTRACT

Building energy sector is one of the important sources of energy consumption and especially in the United States, it accounts for approximately 40% of the total energy consumption. Besides energy consumption, it also contributes to CO_2 emissions due to the combustion of fossil fuels for building operation. Preventive measures have to be taken in order to limit the greenhouse gas emission and meet the increasing load demand, energy efficiency and savings have been the primary objective globally. Heating, Ventilation, and air-conditioning (HVAC) system is a major source of energy consumption in buildings and is the principal building system of interest. These energy systems comprising of many subsystems with local information and heterogeneous preferences demand the need for coordination in order to perform optimally. The performance required by a typical airside HVAC system involving a large number of zones are multifaceted, involves attainment of various objectives (such as optimal supply air temperature) which requires coordination among zones. The required performance demands the need for accurate models (especially zones), control design at the individual (local-VAV (Variable Air Volume)) subsystems and a supervisory control (AHU (Air Handling Unit) level) to coordinate the individual controllers.

In this dissertation, an airside HVAC system is studied and the following considerations are addressed: a) A comparative evaluation among representative methods of different classes of models, such as physics-based (e.g., lumped parameter autoregressive models using simple physical relationships), data-driven (e.g., artificial neural networks, Gaussian processes) and hybrid (e.g., semi-parametric) methods for different physical zone locations; b) A framework for control of building HVAC systems using a methodology based on power shaping paradigm that exploits the passivity property of a system. The system dynamics are expressed in the Brayton-Moser (BM) form which exhibits a gradient structure with the mixed-potential function, which has the units of power. The power shaping technique is used to synthesize the controller by assigning a desired

power function to the closed loop dynamics so as to make the equilibrium point asymptotically stable and c) The BM framework and the passivity tools are further utilized for stability analysis of constrained optimization dynamics using the compositional property of passivity, illustrated with energy management problem in buildings. Also, distributed optimization (such as subgradient) techniques are used to generate the optimal setpoints for the individual local controllers and this framework is realized on a distributed control platform VOLTTRON^{TM}, developed by the Pacific Northwest National Laboratory (PNNL).

CHAPTER 1. INTRODUCTION

1.1 Background & Motivation

Building sector accounts for 41% (residential 22% and commercial 19%) of total energy use in the United States Book (2011). The details on the percentage share of energy consumption in buildings are shown in Fig. 1.1. Apart from energy consumption, the building sector also contributes to CO_2 emissions due to the combustion of fossil fuels for building operation. In order to meet the targets of greenhouse gas emission reduction and increasing load demand, energy efficiency and savings have been a primary objective globally. HVAC (heating, ventilation, and air-conditioning) systems are the major source of energy consumption in buildings and are designed to provide occupants a safe and comfortable environment. Although energy consumption in buildings can be improved by retrofitting existing buildings in terms of the building envelope and HVAC design, it involves huge labor costs and is economically not a feasible solution whereas, improving control algorithms to operate HVAC systems efficiently is an cost effective solution. Control algorithms for such systems to have an optimal balance between comfort and energy usage have been targeted by many researchers.

Buildings are major stakeholders for power markets and with the increasing load demand and rapid penetration of distributed energy resources into the existing grid induces more uncertainties in maintaining the supply-demand balance. Traditionally, conventional generators are employed to meet the additional demand, while with the increasing demand-side management programs, utilities provide incentives to consumers for lowering the overall power demand and motivates to reduce load during the time when prices are high. These programs have led to the process which involves both supply-side and demand-side resources to minimize the overall cost of utilities and consumers. Demand-side management programs include usage of energy efficient appliances and adoption of variable pricing strategies. Managing the demand based on pricing opens new

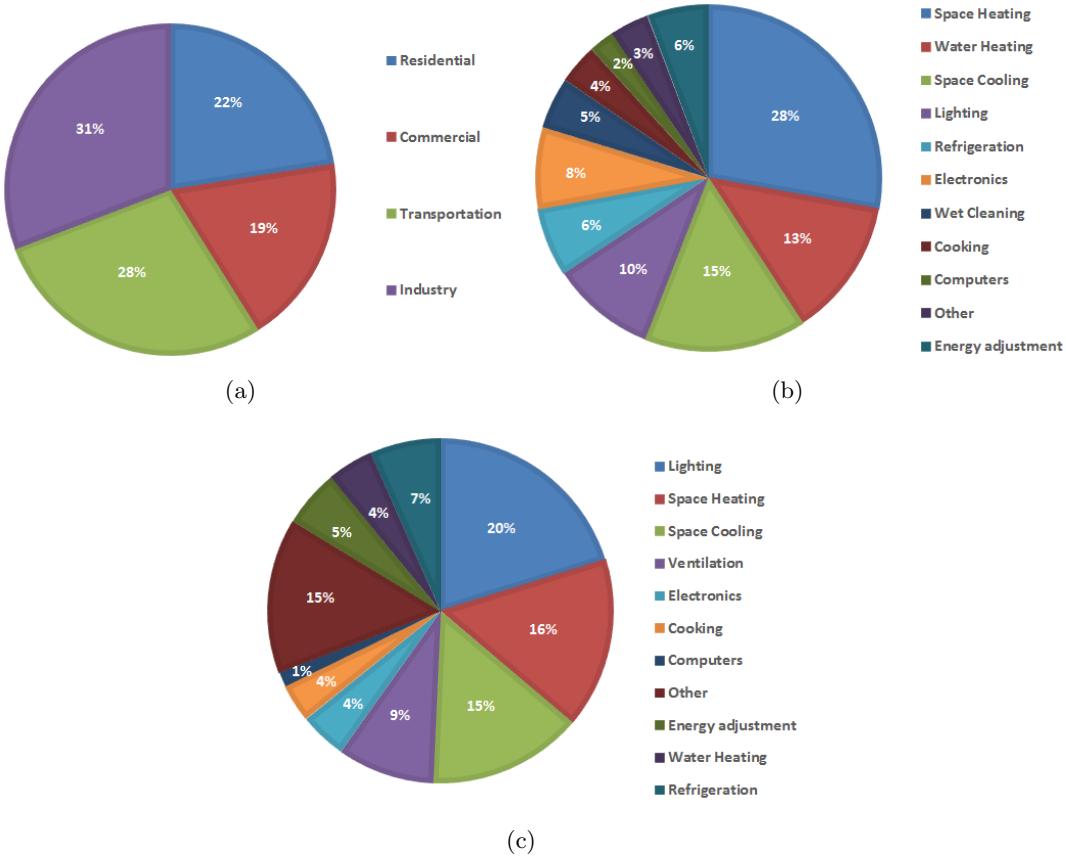

Figure 1.1 Energy Usage statistics (2010): (a) U.S; (b) Residential; (c) Commercial.

possibilities for energy management in buildings. Buildings are the strong contender for providing ancillary services to the grid and with the development of smart grid, which provides sophistication to the consumers and providers to schedule supply and demand at regular intervals.

Given the above considerations for improving energy efficiency as well as managing the load and also the vast amount of literature on the above two aspects, it is important to have a unified framework for modeling of building systems which facilitates for control and optimization. One of the main drivers for this framework is that building energy system, a complex entity, can be viewed as a set of interconnected subsystems such as heat exchangers, thermal zones etc. These subsystems which exchange power through their mutual interconnection and the external environment, it seems natural to take the system's power as the key component for the analysis. In Willems (2007), a

methodology is presented for modeling interconnected systems, called tearing, zooming, and linking. Although Willems (2007) details the thinking of a dynamical system as a behavior Willems and Polderman (2013), the systemic procedure helps in borrowing tools and framework for dynamical system analysis. A schematic showing the subsystem representation of whole building systems is shown in Fig. 1.2. One of the key subsystems is the thermal zone system where the occupant change setpoints to manage their comfort and drives the equipment accordingly. The thermal dynamics of a multi-zone building is constructed from energy and mass balance equations.

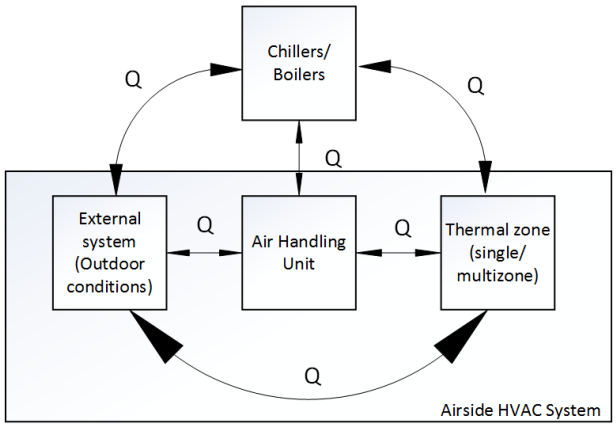

(a)

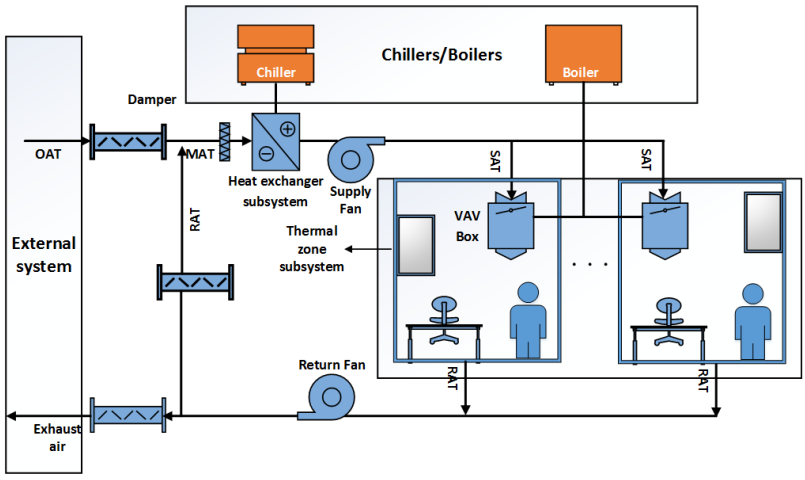

(b)

Figure 1.2 Building systems: (a) Interconnection of subsystems; (b) Individual components.

Capturing all the relevant phenomenon of heat transfer mechanisms lead to a coupled partial differential equations. These high fidelity models provide detailed indoor airflow information but remain computationally intractable for real-time control design. However, resistor-capacitor networks are commonly used for modeling thermal zones and other subsystems due to their simplicity and computational efficiency. Once the subsystem dynamics are represented as an electrical network, one can use various tools from network theory (e.g., passivity-based methods) to devise control approaches to attain the stable behavior of dynamical systems.

Passivity is an input-output property having roots in circuit theory and is widely used for control of engineering systems. This property later became a feedback design tool Arcak (2006) for group coordination problems with wider applications in sensor networks, robotics etc. In circuit theory, Tellegen's theorem has an important stance as it implies total power in the circuit is preserved and applies to electric networks that obey Kirchoff's laws. Passivity of electrical networks is established using port variables such as voltage and currents with storage function as the total energy of the system. In a seminal paper by Brayton and Moser (1964), where the content and co-content functions of the resistors are used for finding the storage function also called as the mixed potential function is used to prove the stability of equilibrium points. The mixed potential function has the units of power and also paves a new passivity property by differentiating one of the port variables. This new passivity property is attractive for control design purpose commonly called as power shaping control Ortega et al. (2003) and is found successful for control of systems such as electrical, mechanical Jeltsema and Scherpen (2007), electromechanical García-Canseco et al. (2010) and chemical reaction networks Favache and Dochain (2010). Systems possessing this property have additional features such as interconnection of them either in parallel or feedback is also passive. The composition property is useful for analysis of large-scale interconnected systems which consists of several passive subsystems.

Using the interconnected structure of buildings subsystems which exchange power through their mutual interconnections can be rendered passive by exploiting the input-output property. This compositional property makes the overall system passive and provides a viable solution for the

whole building energy analysis. Considering the applicability of building RC networks to the existing power shaping control that originated from RLC network theories motivates to model HVAC systems in the form of Brayton-Moser form by exploiting inherently passive nature of the system and provides a powerful framework for control of such systems. This is a new application of BM framework along with the passivity tool opens up new possibilities such as stability analysis of constrained optimization dynamics using the compositional property of passivity (application: energy management problem in buildings).

1.2 Literature Review

1.2.1 Thermal modeling of building systems

Given the importance of HVAC system in energy consumption of buildings, it is necessary to have good machinery (models, control actions etc.,) to obtain optimal operation of HVAC system. In this regard, the performance of model-based control strategies (such as Model Predictive Control (MPC)) is highly dependent on the thermal dynamics of buildings, which is a heat balance equation modeling the internal temperature within a building affected by various heat transfer mechanisms. There is a hierarchical structure of approaches for modeling thermal dynamics of buildings. A complete and holistic overview (for ex., advantages/disadvantages) of different approaches for the control-oriented modeling is discussed in Atam and Helsen (2016). Another important note highlighted in Atam and Helsen (2016) is that there are several points to be considered such as prediction accuracy, scalability, sensitivity to parameters, etc., during the development of control-oriented models which present challenges for real-time predictive controller implementation. There are several software tools for simulating the thermal performance of buildings Doe (2012) which provide detailed information but are not suitable for control purpose. A state-of-the-art review of various software's used for energy efficient buildings along with the needed features for their use in model-based control design is discussed in Atam (2017). Given the vast amount of literature on developing building thermal models, in this section, we highlight the papers related to representa-

tive models in different classes of control-oriented models such as physics-based, data-driven and hybrid relevant to the dissertation.

Among various control-oriented zone temperature modeling approaches that use physics-based knowledge, R-C networks, and physics-based autoregressive models have been quite popular. In Goyal et al. (2011) RC networks are used to model both conduction and convection processes in a building. It discusses on two sub-problems on structure identification and parameter estimation, where the former deals with finding appropriate convection edges which result in a reduced order model and latter is associated with finding R and C values by minimizing the error between measured and predicted temperature. A full RC model includes modeling indoor air, envelope, ambient etc., and model selection is important in order to meet various needs such as meeting occupant comfort, energy performance. Different models have been evaluated in Bacher and Madsen (2011) and statistical tests (likelihood ratio) are used to arrive at a sufficient model which provides reasonable estimates. A study conducted in Fux et al. (2011) on comparing different lumped RC models of internal mass and outside walls to observe the influence of internal mass on the temperature distribution of building. It is observed 3R2C models have minimal error and are proposed to be used in MPC implementation. The use of physics to determine the optimal structure and order of regression models is detailed in Wu and Sun (2012b) and the resulting model is called as physics-based regression model and more information on the use of ARX/ARMAX models in the buildings see references therein of Wu and Sun (2012b).

Data-driven models such as artificial neural networks (ANNs) have been the most popular for predicting zone air temperatures considering nonlinearities and uncertainties into the building system. In Huang et al. (2012), the use of ANNs for predicting zone temperature in a commercial building is discussed. Mainly, the model is used for determination of convection between zones and improvements in prediction accuracy by using additional variables relating to conduction between zones. The use of ANNs are dependent on the model structure such as the number of neurons, input lags etc., genetic algorithms are used in Ruano et al. (2006) to determine the structure along with standard optimization algorithms for estimation of parameters. However, Gaussian Processes can

also be quite effective as it inherently quantifies model confidence. The uncertainty information in modeling process is incorporated in finding system controls in a computationally inexpensive way Yan and Malkawi (2012). Although the technique has mostly been used for building level energy usage prediction Burkhart et al. (2014); Srivastav et al. (2014), we explore its applicability for zone temperature modeling. Semi-parametric Aswani et al. (2012d,b) regression have been recently used where the parametric component uses physics-based knowledge (lumped parameter model of zone-level heat transfer) and the nonparametric component helps capture the uncertainties from measured data. The primary advantage of this method is that there is no need to explicitly model the heating load and it is estimated using only temperature measurements. This reduces difficulties of searching appropriate models to describe zone specific behaviors.

In terms of comparison between different classes of models, a qualitative comparison using data-driven and physics-based models illustrated on a commercial building is reported in Zhou et al. (2017). It is shown that the prediction accuracy of data-driven models in closed-loop are very close in comparison to physics-based models. Jimenez and Madsen (2008) discusses the comparison between linear and nonlinear models (they fall under the physics-based modeling category) using experimental data and also highlights that stochastic state space models provide a strong framework for modeling physical systems. With the increase in building size, the model order increases and poses challenges for real-time estimation and control applications. In order to handle this several model reduction methods such as using constrained optimization Gouda et al. (2002), aggregation Deng et al. (2014), balanced truncation Goyal and Barooah (2012) have been used to reduce the dimension of the state space for model-based control.

1.2.2 Control and optimization of building energy systems

Numerous approaches have been proposed for energy efficient operation of HVAC systems. A review of various control techniques for energy and comfort management in buildings is described in Dounis and Caraiscos (2009). Primarily, for zone temperature regulation, several control strategies have been proposed such as passivity-based control (Mukherjee et al. (2012); Wen et al. (2013);

Aranovskiy et al. (2015)), MPC (Ma et al. (2011); Ma (2012); Oldewurtel et al. (2012)), learning based control (Minakais et al. (2014); Aswani et al. (2012a)), rule-based control Mařík et al. (2011). In Mukherjee et al. (2012) the input/output system is shown to be strictly passive and a passive output feedback controller is designed to improve both transient and steady-state performance while maintaining stability. The similar setup is extended in Wen et al. (2013) to motivate the construction of adaptive feedforward control which lends to an inner-outer loop control architecture where inner loop takes care of stability and outer loop provides balancing between temperature specification and power consumption. Zone level control algorithms commonly use PI controllers for setpoint regulation which has drawbacks when working with wide operating regimes and hence, a robust PI controllers for nonlinear systems with uncertain parameters is proposed in Aranovskiy et al. (2015) with application to temperature regulation. Local control at individual zone level is provided by VAV terminal box to ensure comfort to the occupants which typically leads to high energy consumption due to disparate energy demands from individual zones. Optimal control strategies such as Model Predictive Control have been popular in building control community as an efficient methodology to minimize energy consumption while satisfying operation constraints. Given the weather and occupancy information, a distributed MPC is proposed in Ma et al. (2011) to achieve a balance between comfort and energy and is implemented using the sequential quadratic program and dual decomposition. As weather and occupancy information is unknown, a stochastic MPC approach is proposed using predictions of both weather and internal gains to increase the energy efficiency of buildings. The influence of occupancy information for energy efficient buildings is investigated in Oldewurtel et al. (2013); Goyal et al. (2012). Iterative learning control is used for reducing the impact of disturbances which are repeating in some sense given the diurnal weather patterns and can significantly improve the energy performance using the available historical data. This approach is used in conjunction with model-based and model-free approaches as proposed in Aswani et al. (2012a); Minakais et al. (2017) and results show improved performance over traditional controls (two-position control). Rule-based control is governed by rules and heuristics for computing various setpoints to reduce HVAC energy consumption and they yield sub-optimal solutions. They

can be effective and provide significant savings if properly implemented and needs expert knowledge for designing rules and a list of rule-based control strategies are listed in Mařík et al. (2011).

Apart from the need for having optimal HVAC operation, buildings have the potential to provide value to energy systems by providing ancillary services. Additionally, with rapid penetration of distributed energy resources into the existing grid demands the need for a large amount of ancillary services to maintain supply-demand balance in real time. There is a vast amount of literature on demand response (DR) strategies in maintaining an optimal balance between supply and demand at all times. An overview of the types of DR and taxonomy for demand-side management is described in Palensky and Dietrich (2011). Demand-side management programs include usage of energy efficient appliances and smart adaption of variable pricing strategies. Real-time pricing based DR application Mathieu et al. (2013) has been deployed in smart meters of residential homes to have direct control of loads such as air conditioners etc. Due to the increasing load in buildings and its significant contribution to peak demand leads to increased energy prices. Buildings can respond to these prices by control of active and passive thermal storage systems Braun (1990); Dincer (2002); Henze et al. (2004) and participation in demand response Henze (2005) programs which will lead to reduced energy costs. Buildings at low-cost have the flexibility to modulate their individual subsystem components such as fans (fast-time scale) Hao et al. (2014), chillers (slow-time scale) Lin et al. (2013) to provide regulation service to track a frequency regulation signal provided by grid operator. In Ma et al. (2016), primal-dual gradient method is used to solve the energy management problem in application to HVAC systems. A multi-agent based control strategy for optimal control of centralized air conditioning systems is proposed in Cai et al. (2015), where two distributed optimization algorithms have been formulated to minimize the energy consumption satisfying the constraints on the load. Recently, Cai et al. (2016) propose a multi-agent control based demand response strategy for multi-zone buildings. In Jiang et al. (2016), authors have proposed a modular optimization framework using Generalized Gossip for building energy systems that naturally generalizes to the entire spectrum of "complete disagreement" to "complete agreement (consensus)" which will be useful for handling multiple energy resources and

constraints. The use of VOLTTRON^{TM} platform (an agent-based distributed control platform) has been demonstrated in several applications Haack et al. (2013a,c) such as achieving the power consumption goal in a building while charging Electric Vehicle within user schedule, control of an electric bus for a local transit company and coordinating commercial building energy usage. In Khamphanchai et al. (2014, 2015) a low-cost, user-friendly building energy management platform has been built on the top of VOLTTRON^{TM} to facilitate improved sensing and control of equipment in small and medium-sized buildings.

1.3 Organization of the Dissertation

The dissertation is organized as follows. Chapter 1, provides an introduction to the energy usage statistics and interconnected structure in buildings followed by a literature review on modeling, control, and optimization pertaining to buildings. In Chapter 2, a brief review of mathematical preliminaries used in the developments of this dissertation are presented. In Chapter 3, a comparative evaluation in terms of qualitative and quantitative metrics of different building thermal modeling schemes are presented. The main contribution is presented in Chapter 4 where Brayton-Moser framework and passivity tool are used for control of HVAC subsystems. In Chapter 5, we address the stability analysis of constrained optimization dynamics using passivity and illustrate with building energy management application. In Chapter 6, deals the implementation of the distributed optimization algorithms in a real-time distributed control platform VOLTTRON^{TM}. In Chapter 7, we make concluding remarks and give possible directions for future research.

CHAPTER 2. PRELIMINARIES

In this chapter, we provide a brief review of some of the mathematical concepts that are needed to develop the results presented in this dissertation. We summarize the important results on Lyapunov stability, passive dynamical systems, continuous time optimization dynamics and Brayton-Moser (BM) formulation. For more details on stability and passivity we refer the reader to Sepulchre et al. (2012); Khalil and Grizzle (1996), for continuous time optimization dynamics Arrow et al. (1958); Wang and Elia (2011) and Jeltsema and Scherpen (2009); Ortega et al. (2003); García-Canseco et al. (2010) for BM.

2.1 Lyapunov Stability

Consider the time-invariant system

$$\dot{x} = f(x) \tag{2.1}$$

where $x \in \mathbb{R}^n$ and $f : \mathbb{R}^n \to \mathbb{R}^n$ is locally Lipschitz continuous. We state the theorems for the case when equilibrium point is the origin of $\mathbb{R}^n$, since any equilibrium point can be shifted to origin using change of coordinates.

Theorem 1 (Stability) *Let $x = 0$ be an equilibrium of (2.1) and suppose f is locally Lipschitz continuous. Let $V : \mathbb{R}^n \to \mathbb{R}^+$ be a $\mathcal{C}^1$ positive definite and radially unbounded ($V(x) \to \infty$ as $\|x\| \to \infty$) function $V(x)$ such that*

$$\dot{V} = \frac{\partial V}{\partial x}(x) f(x) \leq 0, \quad \forall x \in \mathbb{R}^n$$

Then $x = 0$ is globaly stable and all solutions of (2.1) converge to the set E where $\dot{V}(x) \equiv 0$. If $\dot{V}$ is negative definite, then $x = 0$ is globally asymptotically stable.

In order to state the LaSalle's invariance principle which is key step invoked and found in many papers for proving asymptotic stability (pendulum equation with friction is a classical example

(Example 4.4 of Khalil and Grizzle (1996)) which illustrates the idea) the following definition is needed.

Definition 2 *A set M is said to be invariant with respect to (2.1) if any solution $x(t)$ that belongs to M at some time t_1 belongs to M for all future and past time:*

$$x(t_1) \in M \Rightarrow x(t) \in M, \quad \forall t \in \mathbb{R}$$

A set P is positively invariant if this is true for all future time only:

$$x(t_1) \in P \Rightarrow x(t) \in P, \quad \forall t \geq t_1$$

Theorem 3 (LaSalle invariance principle) *Let Ω be a positively invariant set of (2.1). Suppose that every solution starting in Ω converges to a set $E \subset \Omega$ and let M be the largest invariant set contained in E. Then, every bounded solution starting in Ω converges to M as $t \to \infty$.*

Corollary 4 (Asymptotic stability) *Under the assumptions of (2.1), let $E = \{x \in \mathbb{R}^n \,|\dot{V}(x) = 0\}$. If no solution other than $x(t) \equiv 0$ can stay for all t in E, then the equilibrium $x = 0$ is globally asymptotically stable.*

2.2 Passive Dynamical Systems

One of ways to construct Lyapunov functions is using passivity approach which helps in stability analysis of physical systems (illustrated in Chapter 4 of the dissertation) as well as interconnected systems (illustrated in Chapter 5 of the dissertation).

Consider a dynamical system with state $x \in \mathbb{R}^n$, input $u \in \mathbb{R}^m$ and output $y \in \mathbb{R}^m$

$$\begin{aligned} \dot{x} &= f(x,u) \\ y &= h(x,u) \end{aligned} \tag{2.2}$$

where $f : \mathbb{R}^n \times \mathbb{R}^m \to \mathbb{R}^n$ isl locally Lipschitz and $h : \mathbb{R}^n \times \mathbb{R}^m \to \mathbb{R}^m$ is continuous, we assume the equilibrium conditions are $f(0,0) = 0$, $h(0,0) = 0$. Note, we assume the system has same number of inputs and outputs.

Definition 5 (Passive system) *The system (2.2) is said to be passive if there exists a $\mathcal{C}^1$ positive semidefinite function $S(x)$ called as the storage function such that*

$$\dot{S} = \frac{\partial S}{\partial x} f(x,u) \leq u^T y, \quad \forall (x,u) \in \mathbb{R}^n \times \mathbb{R}^m$$

Additionally, the system is said to be strictly passive

$$\dot{S} \leq u^T y - \psi(x), \quad \forall (x,u) \in \mathbb{R}^n \times \mathbb{R}^m$$

for some positive definite function ψ.

In order for the passivity to imply Lyapunov stability, we need the following notions of zero-state detectability and observability.

Definition 6 (Zero-state detectability and observability) *Consider the system (2.2) with zero input, that is $\dot{x} = f(x,0)$, $y = h(x,0)$, and let $Z \subset \mathbb{R}^n$ be its largest positively invariant set contained in $\{x \in \mathbb{R}^n \mid y = h(x,0) = 0\}$. We say that system (2.2) is zero-state detectable (ZSD) if $x = 0$ is asymptotically stable conditionally to Z. If $Z = \{0\}$, we say that system PDS is zero-state observable.*

Theorem 7 (Passivity and stability) *let the system (2.2) be passive with a $\mathcal{C}^1$ storage function S and $h(x,u)$ be $\mathcal{C}^1$ in u for all x. Then the following properties hold:*

- *If S is positive definite, then the equilibrium $x = 0$ of system (2.2) with $u = 0$ is stable.*
- *If the system (2.2) is ZSD, then the equilibrium $x = 0$ of system (2.2) with $u = 0$ is stable.*
- *When there is no throughput, $y = h(x)$, then the feedback $u = -y$ achieves asymptotic stability of $x = 0$ if and only if system (2.2) is ZSD.*

Passivity is an important tool which is used for stability analysis of physical systems as well as analyzing large complex systems which has interconnected nature of subsystems.

Consider the feedback connection of two systems as shown in Fig. 2.1

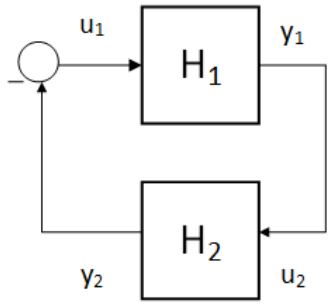

Figure 2.1 Negative feedback interconnection of two systems

where each of the feedback components H_1 and H_2 is given by

$$\begin{aligned} \dot{x}_i &= f(x_i, u_i) \\ y_i &= h(x_i, u_i) \end{aligned}$$

for $i = 1, 2$. The closed loop state model of the interconnected dynamical systems

$$\begin{aligned} \dot{x} &= f(x, u) \\ y &= h(x, u) \end{aligned}$$

where $x = (x_1, x_2)^T$, $u = (u_1, u_2)^T$ and $y = (y_1, y_2)^T$. We assume that f is locally Lipschitz, h is continuous, $f(0, 0) = 0$, and $h(0, 0) = 0$. Then the fundamental property used for analysis of interconnected systems is stated below:

Theorem 8 *Negative feedback connection of two passive systems is passive.*

The main idea for the proof is to use the sum of individual Lyapunov functions as the Lyapunov function for the closed loop system.

2.3 Brayton-Moser Formulation

Brayton-Moser (BM) systems are a class of systems which lie at the intersection of Hamiltonian and gradient systems van der Schaft (2011). For a more detailed description on the origin of Brayton-Moser equations as well as its connection with Lagrangian and Hamiltonian formulations,

the reader is referred to Jeltsema and Scherpen (2009). The key ingredient of the BM equation is the existence of a function called the mixed potential function. This function consists of the difference between the content and co-content functions plus an additional term reflecting power transfer between subsystems and since the circuit is a mix of three different functions hence the name mixed potential function. The mixed potential function has the units of power and hence BM equations refer to power based modeling framework. The mixed potential function can be used as a candidate Lyapunov function for stability analysis which the originators initially used for investigating stability for the tunnel diode circuit. The theory was initially generalized to the class of topologically complete circuits and we provide brief details on it with respect to RLC circuits.

A circuit is topologically complete if each branch of the circuit can be expressed either in terms of the inductor currents I, or the capacitor voltages V, or both, and the entire circuit can be partitioned into subcircuits with $\sum_1$ contains the current-controlled inductors and resistors and $\sum_2$ containing voltage controlled capacitors and resistors. The mixed potential function for such a circuit has the form

$$\mathcal{P}(I,V) = \mathcal{C}(I) - \mathcal{C}^*(V) + V^T N I,$$

where $\mathcal{C}(I)$, $\mathcal{C}^*(V)$ represents the resistive content and co-content functions. The term $V^T N I$ represents instantaneous power transfer from $\sum_1$ to $\sum_2$. The matrix N have entries $\pm 1, 0$, obtained from applying Krichhoff's laws. A generic representation of the dynamics of nonlinear RLC circuit is given as

$$Q(x)\dot{x} = \nabla_x \mathcal{P}(x), \tag{2.3}$$

with $x = (I,V)^T$ and

$$Q(x) = \begin{bmatrix} -L(I) & 0 \\ 0 & C(V) \end{bmatrix}$$

The system of equations (2.3) are referred to as BM equations. The primary purpose of mixed potential function is in its use as a Lyapunov function for stability analysis. Considering $\mathcal{P}$ as

Lyapunov function and taking derivative gives

$$\begin{aligned}\dot{\mathcal{P}}(x) &= \nabla_x \mathcal{P}(x)^T \dot{x} \\ &= \dot{x}^T Q(x) \dot{x}\end{aligned}$$

For circuits involving only resistors and capacitors (for example: Building subsystems discussed in detail in Chapter 4), we have $Q(V) = C(V)$, $\mathcal{P}(V) = -\mathcal{C}^*(V)$. Since capacitor values being non-negative and rearranging $(-)$ sign yields $\dot{\mathcal{P}}(V) \leq 0$, which upon using LaSalle's theorem implies V approaches the equilibrium. However, for the case of RLC circuits the symmetric part of $Q(x)$ is indefinite. The key strategy developed by BM is to generate another admissible pair $\{\tilde{Q}, \tilde{P}\}$ such that the symmetric part of $\tilde{Q}$ is negative definite and also represent the dynamics, that is

$$\tilde{Q}(x)\dot{x} = \nabla_x \tilde{\mathcal{P}}(x),$$

A more constructive procedure to generate admissible pairs is deatiled in Ortega et al. (2003). For all $\lambda \in \mathbb{R}$, and symmetric matrix functions $M(x)$, the pair

$$\begin{aligned}\tilde{\mathcal{P}}(x) &= \lambda \mathcal{P}(x) + \frac{1}{2} \nabla_x^T \mathcal{P}(x) M \nabla_x \mathcal{P}(x) \\ \tilde{Q}(x) &= \lambda Q(x) + \frac{1}{2} \nabla_x^2 \mathcal{P}(x) M Q(x)\end{aligned}$$

is admissible.

2.4 Continuous-Time Optimization Dynamics

The early work done by economists Arrow et al. (1958) in the optimization field shows that for a class of optimization problems (strictly convex) there exists a natural continuous time optimization dynamics (also called primal-dual dynamics). These dynamics are shown to converge to the optimal solution of the optimization problem under mild conditions. This natural connection between optimization problem and optimization dynamics opens up a control theoretic viewpoint for analysis and provides new insights into optimization research. In this regard, a report Nikolova and Nikolova (2003) discusses a connection between optimization and control using gradient method

and Lyapunov functions. A general introduction to control perspective for solving centralized and distributed optimization problems is reported in Wang and Elia (2011). In the following, the equality constrained optimization problem is considered to illustrate the equivalent dynamical system.

Consider the constrained optimization problem with equality constraints

$$\begin{aligned} \underset{x\in\mathbb{R}^n}{\text{minimize}} \quad & f(x) \\ \text{subject to} \quad & Ax = b \end{aligned} \tag{2.4}$$

where $A \in \mathbb{R}^{r\times n}$ with $r \leq n$, and $b \in \mathbb{R}^r$. We assume $f : \mathbb{R}^n \to \mathbb{R}$ is continuously differentiable and strictly convex, A has full row rank. Under the assumptions the problem (2.4) is a convex optimization problem; has a finite optimum, the constraints are strictly feasible, and (2.4) may be equivalently studied through its Lagrange dual with zero duality gap Boyd and Vandenberghe (2004).

The Lagrangian of (2.4) is given by

$$\mathcal{L}(x,\lambda) = f(x) + \lambda^T(Ax - b) \tag{2.5}$$

where λ is a vector of Lagrange multipliers. By strong duality, the KKT conditions are given by

$$\nabla f(x^*) + A^T\lambda^* = 0 \tag{2.6}$$

$$Ax^* - b = 0 \tag{2.7}$$

which are necessary and sufficient conditions for optimality. Then the Lagrangian (2.5) reduces to the following primal- dual dynamics to calculate the optimizer (x^*, λ^*) given by

$$\begin{aligned} \tau_x\dot{x} &= -\nabla f(x) - A^T\lambda \\ \tau_\lambda\dot{\lambda} &= Ax - b \end{aligned} \tag{2.8}$$

where τ_x, τ_λ are positive definite matrices of time constants. The steady state values of (2.8) converges to the optimal solution under given assumptions.

CHAPTER 3. COMPARATIVE EVALUATION OF CONTROL-ORIENTED BUILDING ZONE THERMAL MODELING APPROACHES

3.1 Background: Control Oriented Building Thermal Modeling

Energy efficiency in buildings is significantly impacted by the performance of a dynamic model of building thermal zone. The predictions obtained from the model are crucial for control design purpose and their impact is studied in Privara et al. (2013). The assessment of building performance needs accurate control-oriented models which are either physics/data-driven/hybrid models that can accurately capture the dynamics and uncertainties in the system. A case study using the Modelica Building System Library is presented in Eisenhower et al. (2012). Low-order control-oriented models using the data obtained from TRNSYS model for the model predictive control in buildings is reported in Li et al. (2013). An investigation into the complexity of model structure, model calibration for control-oriented modeling and the kind of sensors need for the model-based control is discussed in Lin et al. (2012). Behl et al. (2013) discusses the sources of uncertainty in modeling and the need for a reliable temperature prediction which has significant impact on zone comfort and energy efficiency. There are several modeling approaches used in the literature, firstly the use of building energy simulation programs such as EnergyPlus, TRNSYS etc., which obeys physical laws and uses physical properties of the building. The disadvantage associated with these models are the computational and set up costs for these models are significant and they are not suitable for on-line implementation by which they are not classified as control oriented modeling approaches. Similarly Computational Fluid Dynamics (CFD) is used as a common tool for modeling the heat transfer in buildings Chen (2009); Chen and Zhai (2004). These models have high fidelity in terms of providing detailed indoor airflow data in the domain of interest and are highly influenced by complex boundary conditions which makes them computationally intractable for real-time control design. The reliability issues related to the use of CFD in the

ventilation of buildings is discussed in Horan and Finn (2005). Given the complexity of buildings, due to large number of zones either the energy simulation programs or the CFD based analysis are not best suited for online implementation and also the engineering practices require a systematic approach with low labor cost. Alternatively, there are several other models which come under different classes of control-oriented models such as Physics-based, Data-driven, and Hybrid which have explicit form and are associated with their own advantages/disadvantages. The main goal is to evaluate and compare representative models from these classes which provides an intuition into which models are suitable for varied objectives. Among the physics-based models, physics-based ARX/ARMAX models are chosen which are simple, easily deployed for online implementation. The use of thermodynamic structure into the model is to provide physics-based understanding of the dynamics and is recently proposed in literature Wu and Sun (2012b). Similarly among data-driven, Artificial Neural Network (ANN) and Gaussian Process (GP) are chosen as they establish input-output relationships based on available data such that they don't specifically consider the physics of thermal zones. Especially, GP is used for uncertainty quantification which is the major component in the zone thermal model due to the building load (lighting, occupancy, solar radiation). Since the zone thermal model has the need for both parametric and non-parametric components, Semiparametric model is best suited and has the ability to estimate the non-parametric component only based on the temperature measurements.

3.2 Overview of Modeling Schemes

In this section, we discus representative models from different modeling approaches. The testbed considered for analysis consists of single zones separated by near adiabatic walls (as found in ERS test bed IEC (2010)), physics based parametric models such as ARX and ARMAX models are chosen for evaluation. Among purely data-driven tools, Artificial Neural Networks and Gaussian Processes have been the most popular and is used for analysis. Semi-parametric modeling has been used where the parametric component uses physics based knowledge (lumped parameter model of zone-level heat transfer) and the nonparametric component helps capture the uncertainties from

measured data and hence we categorize it as hybrid modeling technique. Brief description of each of the modeling scheme is presented below:

Autoregressive models with Physics-based knowledge embedding: These models are composed of an autoregressive part (in ARX) and/or a moving average part (in ARMAX) and exogenous disturbances ($d(n)$). The memory is incorporated in the autoregressive part and moving average models are so called random shock terms. The exogenous variables are building load due to occupancy and solar radiation. The generic (discrete-time) model is described as:

$$T(n+1) = \sum_{i=0}^{n_a} a_i T(n-i) + \sum_{j=0}^{n_b} b_j T_{oa}(n-j) + c\dot{m}(n)\left(T_s(n) - T(n)\right) + d(n) \tag{3.1}$$

where $T(n), T_s(n)$ and $T_{oa}(n)$ denote zone temperature, supply air temperature and outside air temperature respectively as functions of time; a_i, b_j, c are constants and $\dot{m}(n)$ is the mass flow rate; n_a, n_b denote the auto regressive orders for zone temperature and outside air temperature. Note, for an ARX model $n_b = 0$. A direct comparison of the ability of both ARX and ARMAX models to predict zone temperature is studied in Ríos-Moreno et al. (2007), Afram and Janabi-Sharifi (2014).

Artificial Neural Networks (ANN): These are purely data-driven black box models and have been extensively used as nonlinear input-output maps in various problems. The most common neural network structure is the Multi-Layer-Perceptron (MLP) trained using the back-propagation algorithm. The neural networks are trained based on standard nonlinear autoregressive models with exogenous inputs (NARX) Huang et al. (2013). The back-propagation algorithm is an iterative gradient based algorithm designed to minimize the mean square error between the actual and desired output. In Huang et al. (2013) ANNs are used to predict the future temperature in a single zone, multiple zones, and the effects of thermal coupling. The perceptron computes a single output from multiple real-valued inputs by forming a linear combination according to its input weights and then possibly putting the output through some nonlinear activation function. Mathematically this can be expressed as

$$y = \sum_{j=1}^{n_h} W_j f\left(\sum_{i=1}^{n_u} w_{ij} x_i + b_j\right) + B_1$$

where W_j and w_{ij} are the weights of the ANN to be estimated for the output and hidden layer

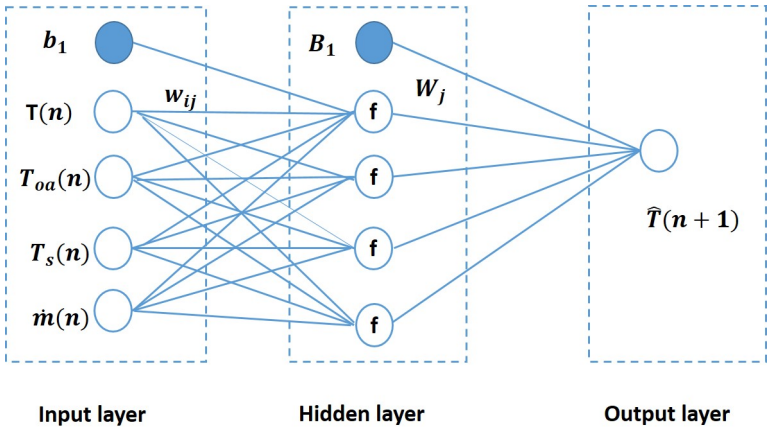

Figure 3.1 Neural Network architecture

respectively, and also b_j, B_1 are the weights for the bias connection with the hidden and output layers respectively. The inputs x_i are the actual temperature T, outside air temperature T_{oa}, supply air temperature T_s and mass flow rate $\dot{m}$, all are indexed by time and schematic representing all the three layers with different components is shown in Fig. 3.1. n_h and n_u representing the number of neurons, inputs in the hidden and input layer respectively. The hidden layer uses a logistic sigmoid function f as the activation function and the weights and bias of that layer were initialized using the Nguyen-Widrow method to ensure a more consistent result and the inputs of the model were normalized and prepared with a time delay of two to be consistent with the other models. Lastly, the training is halted as soon as the target mean squared error reached in order to keep the network from becoming over-trained.

Gaussian Process (GP): GP Heo and Zavala (2012), Rasmussen (2006) is a powerful and flexible uncertainty quantification and data modeling technique that enables the construction of complex models without the need of specifying algebraic relationships between variables by assigning a structure for the covariance matrix of input variables to compute predictions of output variables. It is derived from the Bayesian framework which naturally provides predictive probability distributions. As a result, GP models can capture complex nonlinear relationships between multiple input and output variables and can provide mean predictions and associated uncertainty levels.

Hence, effects of uncertainties in sensor data (due to weather, occupancy and solar radiation) can be captured using GP models. GP is characterized using the mean and covariance functions given by

$$f(x) \sim GP(m(x), \kappa(x, x^{'})),$$

where

$$m(x) = \mathbb{E}[f(x)]$$

$$\kappa(x, x^{'}) = \mathbb{E}[(f(x) - m(x))(f(x^{'}) - m(x^{'}))^{T}]$$

The training input data has 7 dimensions which includes regressors of actual temperatures, outside air temperatures and the heat transfer rate into the room, x and $x^{'}$ belong to the training set and output is the vector of training target temperatures. For the simulation purpose, we have considered composite mean function and squared exponential covariance function which is commonly used and is given by

$$\kappa(x, x^{'}) = \sigma_0^2 \exp\left(\frac{-(x - x^{'})^2}{2\lambda^2}\right)$$

the hyperparameters in the mean and covariance (λ, σ_0) functions are found by minimizing the log marginal likelihood Rasmussen and Nickisch (2010).

Semiparametric: Recently, this statistical approach has been used Aswani et al. (2012d) in the context of building systems for identifying models which are suitable for control design. Zone model is influenced by both parametric and non-parametric (building load) components. Therefore, it can be modeled using semi-parametric regression. The accuracy of zone model is largely affected by the building load due to occupancy, equipment and solar impact. An example dynamic model of a zone is given by partial linear model described below, which is similar to the (3.1) and the key difference is the presence of non-parametric part.

$$T(n+1) = \sum_{i=0}^{n_a} a_i T(n-i) + \sum_{j=0}^{n_b} b_j T_{oa}(n-j) + q(n) + c\dot{m}(n)\left(T_s(n) - T(n)\right) + \epsilon(n)$$

where $q(n)$ is the building load and has stochastic nature, $\epsilon(n)$ is assumed to be IID with zero mean and constant variance that is conditionally independent on the variables of model. The parametric

and non-parametric components are estimated using ordinary least squares and kernel regression method. For more details see Aswani et al. (2012d).

3.3 ERS Building Test Bed

To illustrate and compare the effectiveness of different methods in terms of various metrics, we have used real data form the Iowa Energy Center′s Energy Resource Station (ERS) test bed. The test bed consists of eight zones distributed in four directions, East, South, West, and North, respectively. All the test zones within the ERS are intended to simulate a typical office space and each zone has approximately 266 sq.ft of floor space. All zone and air handling system controls uses a modern programmable commercial-grade Direct Digital Control (DDC) system - Distech Controls' EC-NetAX™ Building Management System. The DDC system controls all air distribution equipment. The DDC system is fully equipped with instrumentations and sensors required for various building energy efficiency related research. Overall there are over 1,200 monitoring and control points with 600 of them the data are collected every minute. Note that the zones in north direction are also interior as they have no windows and the zones in other directions have exterior windows, hence they are perimeter zones. In each direction, two constructed zones marked A and B have identical exposures yielding identical external thermal loads and may have identical internal thermal loads thereby allowing simultaneous, side-by-side comparison testing of many types of HVAC systems and control schemes. For example, in B zones there are fan coil units in addition to variable air volume (VAV) boxes to heat the zone if necessary. However, the fan coil units were always off during data collection time windows such that conditions for zones A and B are completely identical. The schematic diagram is shown in Fig. 3.2. Some zones are connected with other offices and spaces. However, the effects caused by the connection with other offices and spaces were ignored due to strict separation steps taken during data collection times. Also, the test zones have some other equipment, such as computers and lighting facilities. They were always off such that we need not consider their effect either. Evidently, interior zones do not receive no solar radiation due to the absence of windows. On the other hand, zones located in other three directions

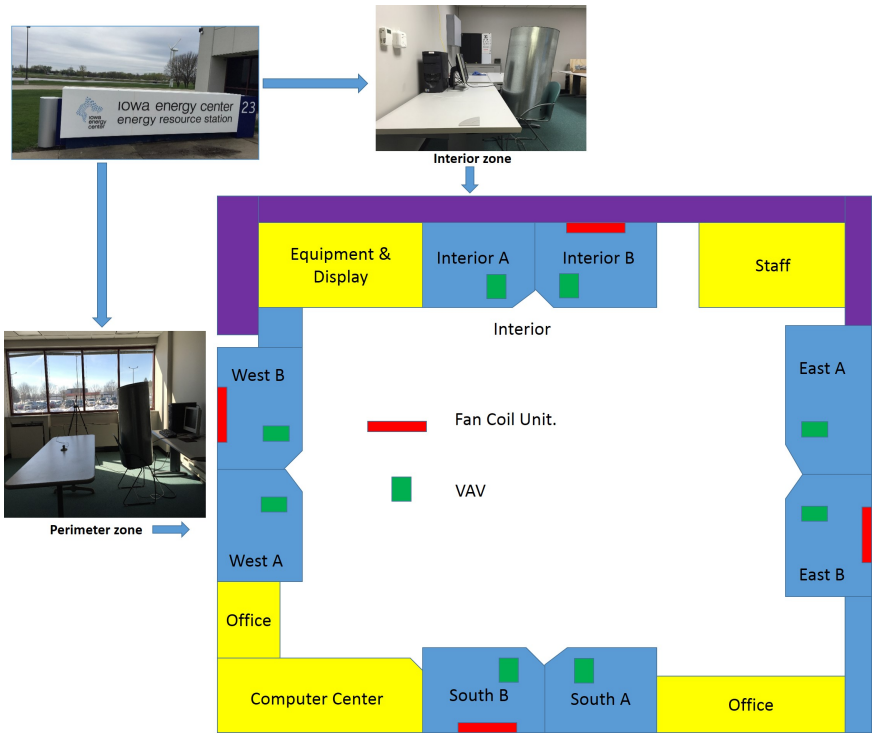

Figure 3.2 ERS Test bed : case study (1) - interior zone; case study (2) - perimeter zone

receive solar radiation through windows during the day time and the disparity in the interior and perimeter zones can be observed from the Fig. 3.2. In each zone, there are several sensors installed to measure variables, e.g., zone temperature, air volumetric flow rate, and discharge air temperature from VAV boxes which are used to train the different models described in the modeling section. Note, due to the availability of real historical data, we did not perform any functional test to generate data for model learning.

3.4 Performance Evaluation Using Different Zone Types

Zone temperature models are highly dependent on the physical location of zones such as interior and perimeter zones, which makes it important to investigate how the performance of these models are effected due to these changes. The perimeter zones which are exposed to the outside environment through windows are largely effected by the solar load compared to the interior zones. In this

section, we provide modeling and detailed analysis in terms of qualitative and quantitative metrics of the interior and perimeter zone behavior.

3.4.1 Modeling and analysis of interior zone behavior

A detailed performance comparison of the different methods on various aspects such as accuracy, computation time, memory requirement, robustness and cost of commissioning which are necessary for having a reliable model in terms of control design and analysis is shown in Table 3.1 and Table 3.3. Most quantitative results are based on training data consisting of 720 samples picked from a window of two weeks (from April 2011) in order to take into account different zone temperature characteristics and six days of validation data (from April 2011) unless otherwise mentioned. Also, the comparative analysis presented in the tables primarily uses one interior zone behavior over the six validation days. The models are simulated on a 3.30GHz Intel(R) Xeon(R) processor in the MATLAB R2014a environment. The model predictions are done in near-real time (change of Value (COV) from the historical data is 0.05°F), the sampling rate of prediction is 1min and the information used are the initial temperature values and the inputs. Typically, different zones in a building has different characteristics based on the solar load and other uncertainties. Fig. 3.3 shows zone temperature prediction performances of all the modeling schemes on the consecutive six day testing period. In the sequel, we focus on a particular testing day and evaluate each method separately. In order to show the effectiveness of these models for different scenarios, we have also considered a zone (east) which is affected largely by uncertain solar load. Similarly, a time window which is at the end of the season (during May 2011, end of Spring) is also chosen for evaluation of the modeling schemes under slight seasonal variations.

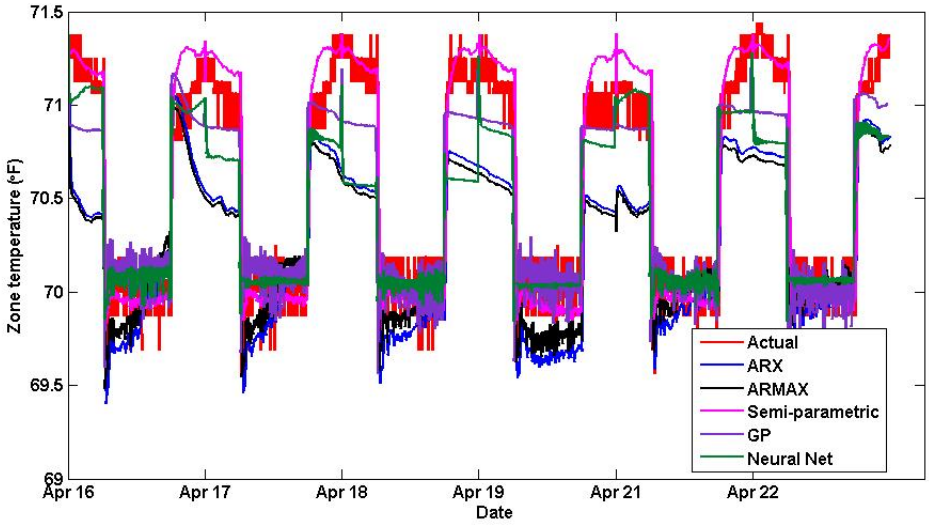

Figure 3.3 Zone temperature prediction for six validation days using different methods

3.4.1.1 ARX/ARMAX:

ARX/ARMAX are linear parametric models that use physics based relationships, such as heat transfer from the HVAC unit (VAV) significantly in order to predict zone temperature. Presence of control variables such as air flow rate and discharge air temperature enables us to use this type of models for controller design purpose. Furthermore, the weather characteristics can be included in discrete form and the dynamic zone model can be obtained by means of linear autoregressive techniques relating input and output of the system. The results using both ARX and ARMAX methods are shown in Fig. 3.4 and Fig. 3.5 respectively. As the plots show, both methods predict zone temperature conditions reasonably well during the occupied hours (when the HVAC is active) with a maximum error of about 1°F and suffer during the time when the HVAC is off. This can be explained by the fact that since these models use physics based relationships, therefore, without active heat transfer to the zone, they do not perform that well as they are unlikely to capture the building load dynamics effectively. ARMAX is slightly more effective compared to ARX in predicting zone temperature with relatively smaller prediction errors.

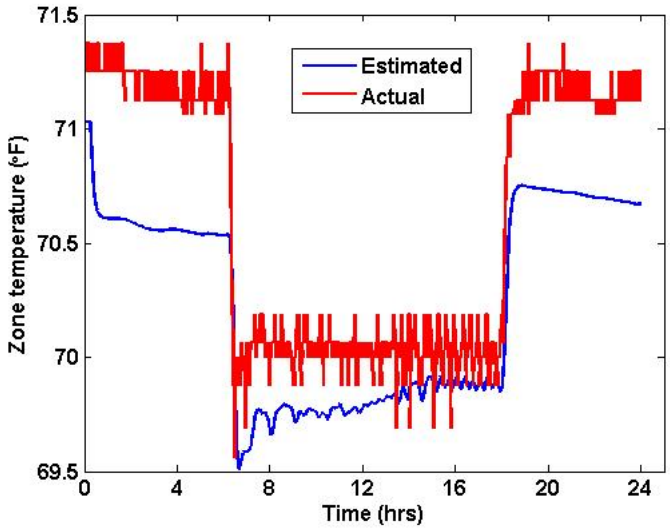

Figure 3.4 Zone temperature prediction ARX model

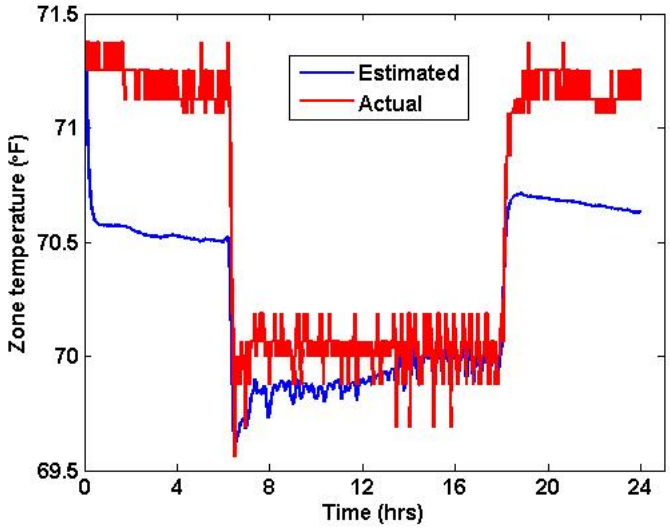

Figure 3.5 Zone temperature prediction using ARMAX model

On a more qualitative note, several observations related to the usability of the models can also be made in terms of ease and cost of implementation, robustness and time complexity. These models are easily implemented (due to the small number of hyper-parameters) and use the available data very efficiently in order to accurately update the models. The training time is quick (less than a second with 720 samples of training data) since the model complexity is quite low and they use a great deal of prior knowledge based on physics.

3.4.1.2 Artificial Neural Network:

The multilayered neural network is probably one of the most frequently used types of ANN structure in practical applications. The architecture of the network includes an input layer, one or more hidden layers, and an output layer. Fig. 3.6 shows the prediction capability of the ANN

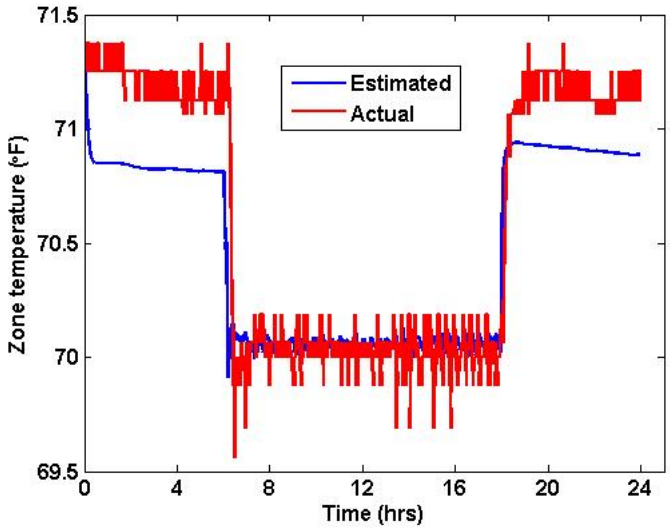

Figure 3.6 Zone temperature prediction using Artificial Neural Network model

model, the validation day was very similar to that of training days. Due to similar characteristics of the Training and Validation days, the weights and biases of the ANN are properly trained to give better performance. The prediction accuracy is slightly better compared to ARX/ARMAX models and especially during the occupied hours.

3.4.1.3 Gaussian Process:

GP is one of the non-parametric machine learning approaches that avoids the model specification problem and learns directly from the available data. For Gaussian process simulation, we have used a squared exponential covariance function and a composite mean function and all hyper parameters have zero initial conditions. The output of validated GP model is shown in Fig. 3.7. Mean prediction along with model confidence bound (two sigma) are presented. Note, localized confidence bounds in this case signify availability of training data in a particular region. Hence, in the case there is lack of training data for a certain region in the data space, GP automatically detects it with a larger variance. We can see that the zone temperature lies within the 95%

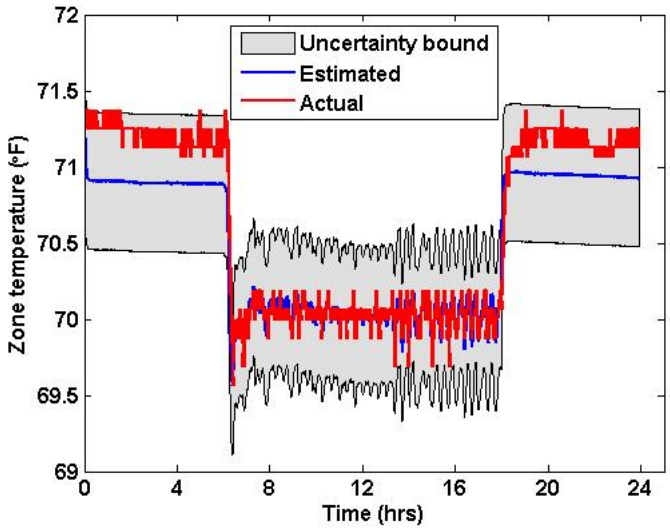

Figure 3.7 Zone temperature prediction using Gaussian process model

measure (2 sigma bound) of confidence interval. The model performs significantly better in both occupied and unoccupied hours compared to other physics and data driven models, the error is less than $0.5°F$ during unoccupied hours and even less during occupied hours.

The primary disadvantage associated with the GP model is the high computational burden, associated with learning of hyper-parameters. As the training data size and the number of hyper-parameters increases, the training time increases and requires a large amount of training data to

cover the entire data space. Therefore, GP-based modeling can be a good choice for initial off-line modeling, but may not be ideal for online adaptation purposes. The results can be potentially improved by using prior knowledge of hyper-parameters and also by incorporating local model (linear/nonlinear) into GP.

3.4.1.4 Semiparametric:

In general, zone temperature model is a blend of both parametric and non-parametric components. The primary non-parametric component in zone temperature modeling is the building load due to solar radiation, equipment and occupancy. In this model, the building load is identified only using temperature measurements Aswani et al. (2012d), which makes the model simpler and is readily used for controller design purpose. The average building load during the training phase is used for validation purpose.Temperature dynamics can be accurately predicted if the non-parametric component is accurate enough. As shown in Fig. 3.8, semiparametric model performs well both in occupied and unoccupied hours compared to other methods in terms of accuracy. Although the zone is an interior zone, where the building load is comparatively smaller this method performs the best. The advantage of this model is it doesn't require any additional sensors to

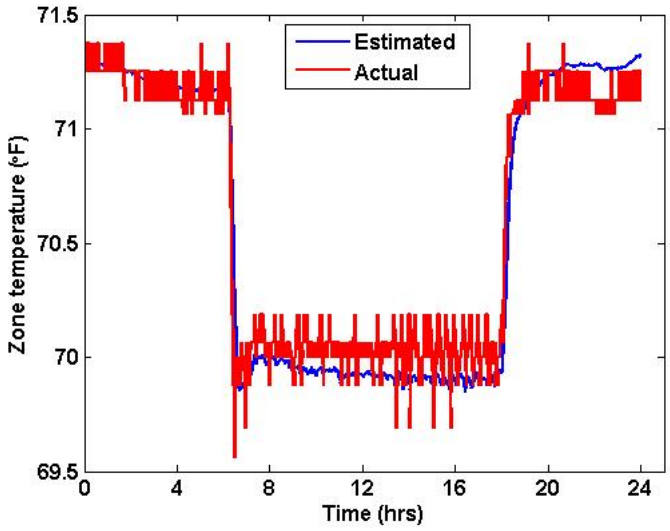

Figure 3.8 Zone temperature prediction using Semi-parametric model

measure building load and it is used for quantifying energy consumption in terms of several factors such as the outside air temperature (OAT) and other factors Aswani et al. (2012c). This method has been successfully tested on various test beds Aswani et al. (2012d). This model has been effectively used for several examples with increased complexity, several nonlinearities and input-output noise. These models can be easily deployed and has the same memory complexity as compared to ARX/ARMAX models. In terms of robustness, they are quite robust in predicting temperature in the same season which the training data belongs to.

3.4.1.5 Impact of worst-case uncertainty:

In order to evaluate the models for rather difficult (or, worst-case uncertainty) scenarios, a perimeter zone (east) is considered, which shares a large window with the outdoors and largely affected by the solar load. Furthermore, a daily temperature profile is chosen that has a significantly different pattern compared to the training patterns. Fig. 3.9 shows comparison of different methods in predicting the zone temperature under that condition. The result with the ARX/ARMAX model captures the trend in the initial hours of the day and also the abrupt change in the morning hours when the building load starts to increase due to solar load and typically the error is of the order of maximum 3°F. The performance of purely data-driven models (ANN and GP) degrades significantly compared to other methods in terms of accuracy. As typically in the morning hours, building load becomes large due to which it captures the jump during the initial occupied hours and later it tries to capture the nearly constant dynamics and the comparison in terms of different metrics is listed in Table. 3.1. For the Semiparametric model, the average of all the training days building load is used to validate on different days. In Fig. 3.9, the model performs well in occupied hours compared to all the other methods, which is typically when the building load is large. During the rest of the day, there is a error less than 3°F due to the fact that the test day shows a quite different characteristics in terms of small building load during the unoccupied hours. Adding constraints on the coefficients or using regularization, the coefficients can be tuned accordingly to physically represent the system and improved accuracy can be obtained. Errors for

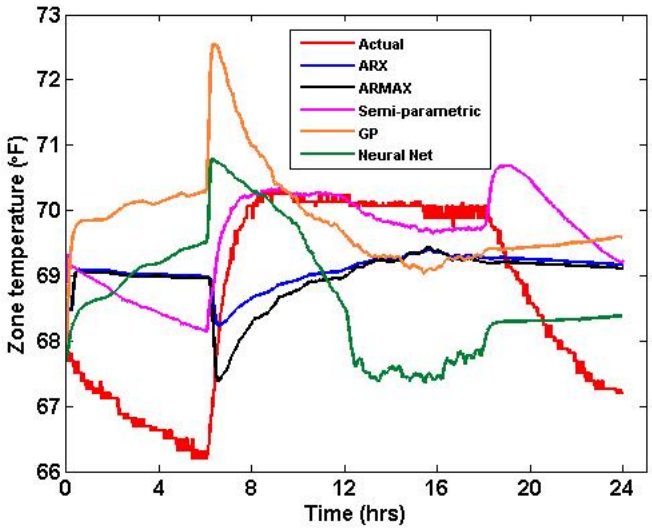

Figure 3.9 Zone temperature prediction accuracy using different methods for perimeter zone

ARX/ARMAX are around 3°F. The drawbacks associated with these models are that they are not good at estimating the building load on the zone and provide crude approximations of the actual system dynamics. However, they are better in terms of performance compared to other methods, since these methods are driven by physical laws.

3.4.1.6 Analysis of an end of season day:

In order to evaluate the model performances under slight seasonal variations and to show the robustness of modeling schemes, we have considered a day towards the end of the season (May 30^{th} 2011, end of spring) for the interior zone. The result is shown in Fig. 3.10 and it can be seen that the GP model is able to capture the abrupt changes in the initial occupied hours and the associated trend during that period, the performance degrades during the period when the HVAC is off. Note that there is no solar radiation and the change in the temperature is only due to outside air which is significantly different during the test day compared to that during the training days. Using ANN, the performance is better compared to all the other methods in the occupied hours and the error is large during rest since the AHU is off during those times and largely depends

on the outside air temperature. The performance degradation of ANN, GP is because of change in data distribution due to seasonal variation and this shows the lack of extrapolation ability of purely data-driven methods. The results using Semiparametric model are better compared

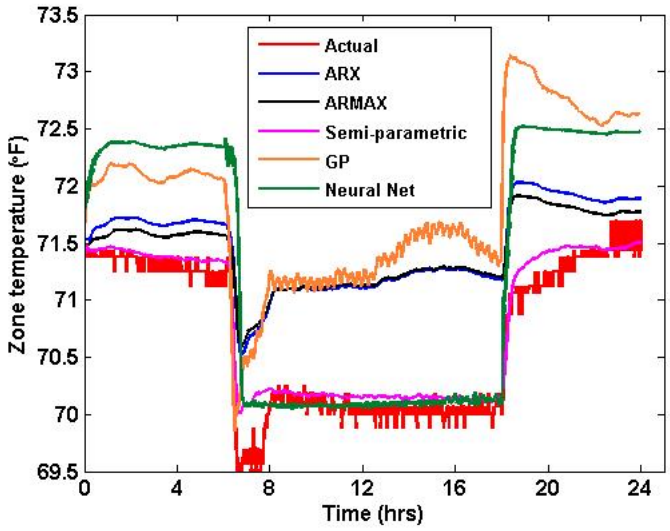

Figure 3.10 Zone temperature prediction accuracy using different methods for end of season day

to other methods in terms of accuracy. Since, it is tested on the same season and the estimated building load approximately matches with the actual building load and this model can become worse compared to others when tested on other season days, the disadvantage of this model is that it is highly dependent on building load and the results can be worse, if the temperature characteristics are highly different from that of training data. For ARX/ARMAX, the error is greater with the maximum error being less that 1.5°F. This suggests, that such a model does not have to be re-trained as often as some other models would require. ARX/ARMAX and Semiparametric perform better compared to purely data-driven as they have slightly better extrapolation capability due to the involvement of physics-based relationships.

3.4.1.7 Analysis of short-term prediction capabilities:

It is evident that the performance of the models can be improved by updating the estimated temperature to actual temperature after certain fast time windows (15 minutes). This can be quite feasible as the supervisory control schemes typically work in a slower time scale and often allow update of initial conditions periodically (such as in receding horizon schemes). For example, we have considered the worst-case uncertainty data and the performance of ARX using 15 minute update after smoothing is shown in Fig. 3.11. As expected, error is greatly reduced by updating

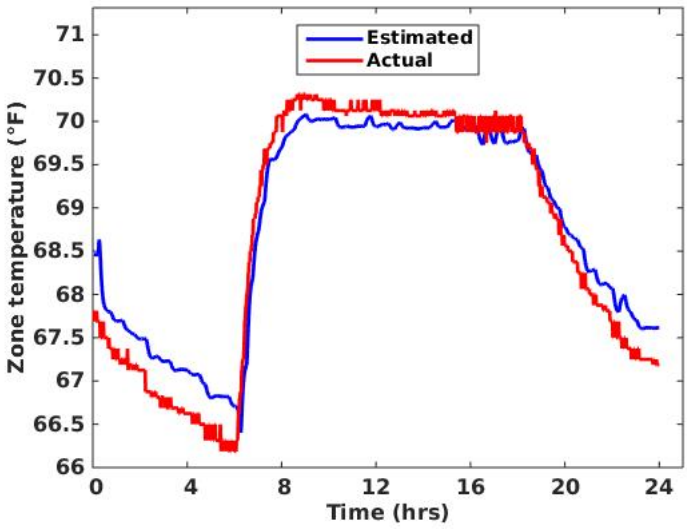

Figure 3.11 Zone temperature prediction accuracy using ARX for 15 min update after smoothing

the temperature to actual values. The maximum error goes down to 1°F as shown in Fig. 3.11 compared to 3°F in Fig. 3.9. The improved performance using the update for different methods is shown in Table. 3.1.

3.4.2 Modeling and analysis of perimeter zone behaviour

In order to account for variability in the model performance to physical location of zones, we provide a quantitative performance comparison of various models for the perimeter zone listed in Table 3.2. These results are based on the training data consisting of 260 samples picked from five

Table 3.1 Comparative evaluation of zone temperature prediction using different methods (interior zone)

Method	Training (MSE)	Validation (MSE)	Training time (720 samples) (sec)	Parameter space	Worst-case uncertainty (MSE)	Sensitivity to end of season day (MSE)	Prediction error with 15 min reset for worst-case uncertainty(MSE)
ARX	0.1734	0.1630	0.0827	Small	2.0512	0.7589	0.0679
ARMAX	0.2104	0.1671	0.0577	Small	2.2567	0.7304	0.0734
Semiparametric	0.0364	0.0157	0.5955	Medium	1.7188	0.0410	1.4302
Gaussian process	0.1426	0.0367	5.7821	Medium	4.2413	1.5212	2.6280
Neural Net	0.4919	0.0710	1.8941	Large	2.2428	0.9789	2.0671

days in the months of August and September 2014 in order to account for the variability of the zone temperature characteristics and three validation days are considered in the similar months which are different from the training days. The comparative analysis presented in the Table 3.2 primarily uses one exterior zone behaviour over three validation days. We presents the results for a particular testing day and the performance of these methods are described separately.

3.4.2.1 ARX/ARMAX:

These methods are linear auto regressive models with are widely used for various applications. In addition to that we use thermodynamic equations in the models which makes physics-based regression models. A novel contribution into the pbARMAX is provided in Wu and Sun (2012b,a). Fig. 3.12 and 3.13 shows the results using ARX and ARMAX models. The results shows that the models are able to reasonably follow the trend and capture the jump during the occupied hours i.e when HVAC is active, and the performance will improve if enough data is available to learn the characteristics during the occupied hours which can be seen during the Spring season. Compared to other data-driven and hybrid models these models does not capture accurate enough the uncertainty due to the building load. This is attributed to deviation in the response during the occupied hours. These models are simple in structure, computation and easily deployable which makes them widely used for diverse applications.

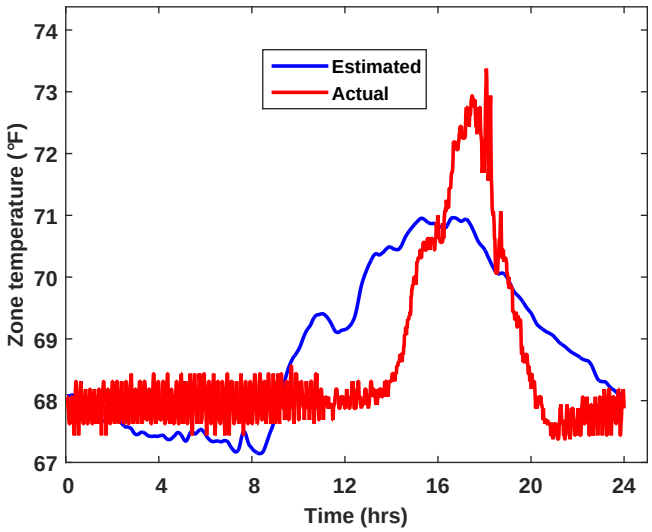

Figure 3.12 Zone temperature prediction ARX model

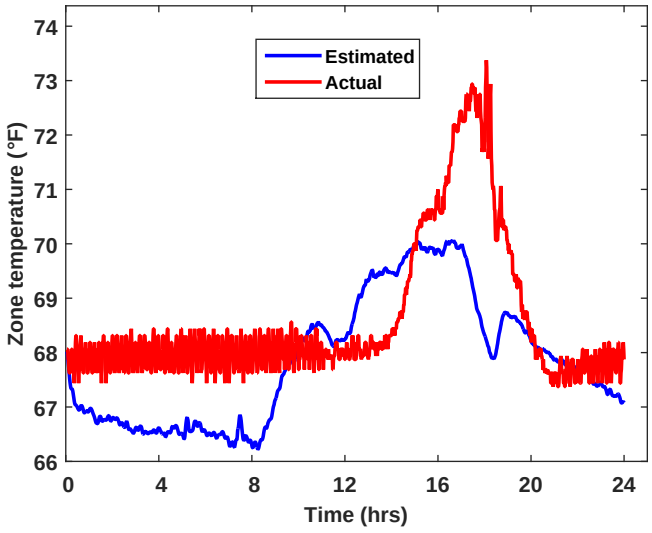

Figure 3.13 Zone temperature prediction ARMAX model

3.4.2.2 Artificial Neural Network:

ANN are black box models which requires no detailed information about the system. Given the input and output data they try to learn the relationships which are used for prediction purpose. The

information acquired through training is stored in the weights and biases. The ANN architecture used is same as the one described in the section 3.4. Fig. 3.14 shows the temperature prediction behaviour using ANN which has better prediction capability compared to physics based and GP. The reason is two fold, one the weights and biases are properly trained and the training time is slightly larger compared to other methods and the other is the validation and training days are in the same season.

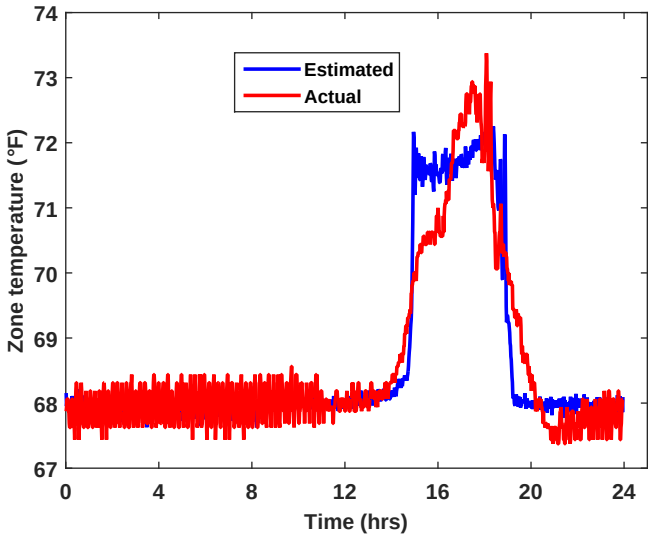

Figure 3.14 Zone temperature prediction using Artificial Neural Network model

3.4.2.3 Gaussian Process:

GP belongs to class of non-parametric learning methods and has the ability to learn the features from the available data. Similar to the interior zone model, here also we used the squared exponential covariance function and composite mean function with non zero initial conditions. The result using the GP method is shown in Fig. 3.15. The zone temperature lies within the 2 sigma bound of confidence interval. GP performs better compared to physics based ARX/ARMAX models during the entire region. In the case of more training data, the GP performance will be improved but it also suffers from the computational burden associated with it.

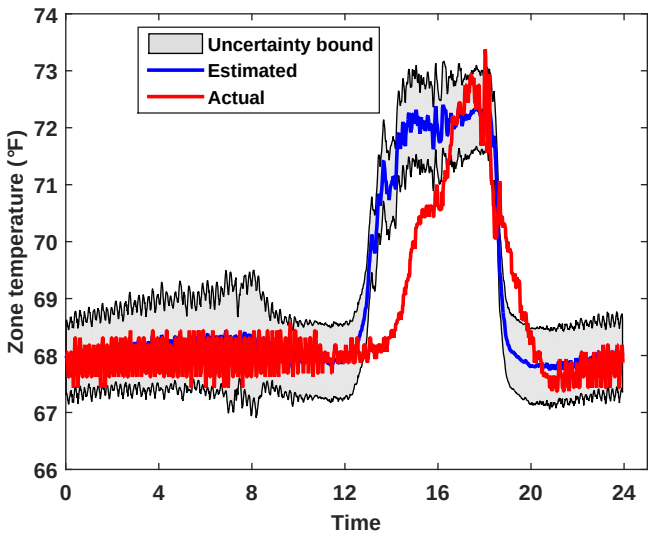

Figure 3.15 Zone temperature prediction using Gaussian process model

3.4.2.4 Semiparametric:

As described in section 3.4, the main feature of semiparametric is to capture the non-parametric component in the zone temperature modeling. As the test case zone is perimeter zone the building load plays an important role. Similar to the interior zone model, the average building load during the training phase is used for validation purpose. As shown in Fig. 3.16 semiparametric performs reasonably well during the unoccupied hours and during the occupied hours although it captures the trend associated, the slight deviation may be attributed to the lack of training data which is essential to capture the dynamics accurate enough.

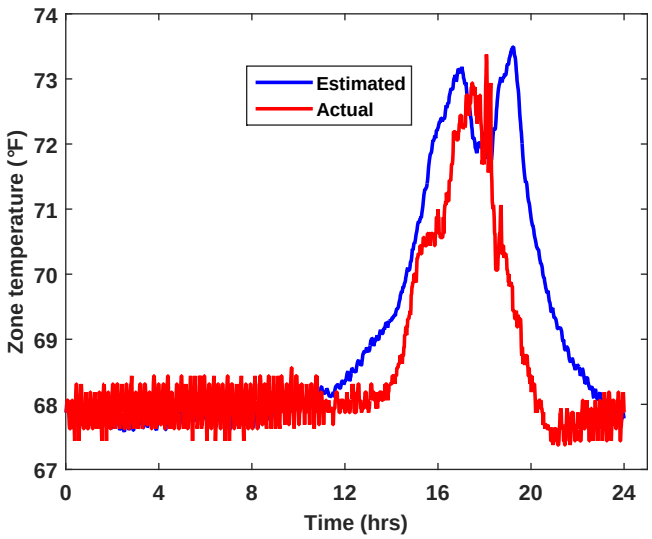

Figure 3.16 Zone temperature prediction using Semi-parametric model

Table 3.2 Comparative evaluation of zone temperature prediction using different methods (perimeter zone)

Method	Training (MSE)	Validation (MSE)	Validation time (sec)	Training time (sec)	Parameter space
ARX	0.0300	1.1846	0.1155	0.0434	Small
ARMAX	0.0295	1.9517	0.0857	0.0270	Small
Semiparametric	0.0123	0.7794	0.1741	0.1344	Medium
Gaussian process	0.0257	1.3244	4.6841	1.0208	Medium
Neural Net	0.1710	0.7994	0.4777	1.2852	Large

3.4.3 Discussion

A comparative evaluation of different modeling techniques in terms of both quantitative and qualitative metrics is presented in Tables 3.1, 3.2 and 3.3. Specifically for Table 3.3, we discuss

Table 3.3 Qualitative evaluation using different methods

Method	Handling Uncertainty	Cost of commissioning
ARX	Captures minimally	Low
ARMAX	Captures minimally	Low
Semiparametric	Captures significantly	Low
Gaussian process	Captures significantly and quantifies uncertanity	High
Neural Net	Captures significantly	Medium

the qualitative metrics such as the ability to handle uncertainty by a modeling scheme and cost of commissioning/deployment. Brief descriptions of these two qualitative terms is described as follows:

Handling uncertainty: This is a key modeling requirement due to the various inherent uncertainties (e.g., solar radiation, occupant behavior) present in the zone temperature prediction problem. This qualitative characteristics is evaluated by the inherent properties (such as deterministic or stochastic) of modeling schemes and their outputs (such as only predicted value or predicted value with uncertainty bounds).

Cost of Commissioning: For embedded computing, the time and man-hour need to be accounted for training and tuning the models. This qualitative characteristics is evaluated based on the typical effort requirements by the modeling schemes as reported in literature as well as specific time taken for various modeling steps in this case study.

GP has the ability to quantify the uncertainty arising from the noisy training data and performs well compared to other methods in terms of accuracy. At the same time, it provides uncertainty bound (or model confidence) around the mean prediction. However, it suffers from larger training and validation time compared to ARX/ARMAX and Semiparametric models due to its iterative nature and similar time complexity can be observed for ANN, therefore they may not be ideal for fast online adaption purposes. ANN performs reasonably well and it shows a bias error that can be attributed to the overfitting issue. ANN, GP can perform well for off-line studies given enough data available for training purpose and since they are come under the class of nonparametric methods they have the ability to capture the uncertainty in the temperature prediction. These

nonparametric models have many parameters to be identified using the training data, especially GP depends on the dimension of the input training data, the number of parameters increases as the dimension increases and similarly for ANN the weights and bias in the hidden layer and output layers count on this. ARX/ARMAX are easily implemented with the data available compared to other methods since they obey physical laws and errors can be reduced by applying the periodic reinitialization with actual measured values. These models are simple, which gives an edge over other methods in terms of control implementation and using these models it is difficult to capture the uncertain component which is the building load on the building zone temperature prediction by which the validation MSE are higher compared to other mehtods. Due to the simplicity of model structure, the number of parameters to be identified is less compared to all the other methods in different classes. Semiparametric performs the best compared to other methods when the training and validation days are in the same season due to the building load approximation (component in building zone model, which is highly time varying) being accurate enough and can be used for online adaptation. Compared to ARX/ARMAX, semiparametric method has an additional nonparametric part which needs to be identified separately using kernel regression methods, due to which the parameter space lies in between physics based methods and nonparametric methods. It was pretty robust too in all the weird conditions. A model comprising, blend of parametric and nonparametric components is well suited for building thermal modeling.

3.5 Summary and Conclusions

In this chapter, representative methods from different classes of control-oriented zone modeling techniques are reviewed and compared. Three main classes are identified which includes physics-based, purely data-driven and hybrid methods. Data-driven methods completely rely on the measurement data of the input and output variables and learned functions to approximate the behavior of the system as closely as possible. These models include well-established techniques such as Artificial Neural Networks and Gaussian Process. Another classification of models, which are physics based (ARX, ARMAX) they completely rely on the knowledge and the physical laws gov-

erning this process. The models built using physics-based rules represent the system more closely and have better extrapolation capabilities. Purely, data-driven methods typically need a comparatively larger amount of data to train the models. Another modeling technique which is a blend of physics-based and data-driven models. Hybrid models use physical laws to define the parametric part of the models and use measured data to find the function approximation of the nonparametric parts. For parameter identification, several optimization techniques such as least squares, gradient descent etc., can be used. Semiparametric model comes under this category.

Based on the discussion provided regarding the comparison, many crucial advantages, disadvantages and insights are explored that can be significant for the building controls community and they can be used as guidelines for choosing modeling scheme in an appropriate manner for various applications. There are many future directions in terms of using these control-oriented models, such as designing controls to stabilize at a given set point temperature, devising cost functions which involve both energy and occupant comfort to achieve respective objectives. If the model is accurate enough, it can be used to test the fault detection and diagnostics algorithms. Models can be developed which can deal with prediction of both temperature and relative humidity. The case study presented here discuss the analysis of zone temperature prediction of forced air system using different methods, however in other types of airside systems such as radiant floor or ceiling, natural ventilation; purely data-driven and hybrid models can also be directly useful whereas the physics driven models such as ARX/ARMAX, needs to be appropriately modified with relevant physics based relationships.

CHAPTER 4. A PASSIVITY-BASED APPROACH TO CONTROL OF BUILDING HVAC SYSTEMS

Traditionally controllers for building HVAC systems at the zone (local) level are operated by PI controllers for regulation tasks. Tuning of such gains is a difficult task for a wide range of operating regions. However, HVAC systems obey physical laws and hence energy/co-energy(power) based methods for setpoint regulation serves as an alternative to PI controllers Zhang et al. (2017). Building subsystems exchange power through their mutual interaction and hence it is natural to employ power-based methods which can be used for analysis and later to control the system by shaping the power to obtain the desired behaviour. The power-based framework known as Brayton-Moser framework has the practical advantage of expressing system variables in terms of easily measurable quantities, such as temperature, pressure. There is difficulty associated with controller design for finding the desired potential function which involves solving PDEs García-Canseco et al. (2010). This can be obviated by finding new passive maps ('add a differentiation' to the output port-variable) motivated by energy shaping methods Donaire et al. (2016b). As details on modeling of thermal zone subsystem is covered in Chapter 3, this chapter focuses on the controller design of HVAC subsystems.

4.1 Power Shaping Approach

In passivity theory, identifying storage functions that result in desired passive port variables is crucial. In this context, we use power shaping methodology, where a power like function is considered as storage function instead of energy. This storage function is alternatively called as the mixed potential function which has its roots in Brayton-Moser framework. Moreover, the power like storage function results in port variables that has a differentiation at the output. Therefore,

we refer to them as power shaping port variables. This section describes the underlying idea of power shaping.

4.1.1 Brayton-Moser form

In early sixties Brayton and Moser (1964), Brayton-Moser showed that the dynamics of a class of (topologically complete) nonlinear RLC circuit can be written in gradient form using a power like function called the mixed potential function. It is a scalar function of a state which has the units of power, is the combination of content and co-content functions and the power transfer between the capacitor and inductor subsystems Jeltsema and Scherpen (2009). This formulation was later used for power shaping, where the storage functions for open loop system are constructed using the mixed potential function.

Consider the standard representation of a system in Brayton-Moser formulation

$$Q(x)\dot{x} = \nabla_x P(x) + G(x)u \tag{4.1}$$

the system state vector $x \in \mathbb{R}^n$ and the input vector $u \in \mathbb{R}^m$ $(m \leq n)$. $P : \mathbb{R}^n \to \mathbb{R}$ is the mixed potential function, $Q(x) : \mathbb{R}^n \to \mathbb{R}^n \times \mathbb{R}^n$ and $G(x) : \mathbb{R}^n \to \mathbb{R}^n \times \mathbb{R}^m$. The time derivative of the mixed potential functional is

$$\begin{aligned} \frac{d}{dt}P(x) &= (\nabla_x P)^\top \dot{x} \\ &= (Q\dot{x} - G(x)u)^\top \dot{x} \\ &= \dot{x}^\top Q\dot{x} - u^\top G(x)^\top \dot{x} \end{aligned}$$

This suggests that if $P(x) \geq 0$ and $Q(x) \leq 0$, the system (4.1) is passive with storage function $P(x)$ and port power variables are input u, output $y = -G(x)^\top \dot{x}$.

But, in general $P(x)$ and $Q(x)$ can be indefinite Ortega et al. (2003).

Assumption 9 *For the given system, there exists* $\tilde{P}(x) \geq 0$ *and* $\tilde{Q}(x) \leq 0$ *and*

$$\tilde{Q}(x)\dot{x} = \nabla_x \tilde{P}(x) + \tilde{G}(x)u \tag{4.2}$$

describe the dynamics (4.1) *(procedure for finding such pair is given in Brayton and Moser (1964)). Such* $\tilde{P}$ *and* $\tilde{Q}$ *are called* admissible pairs *for* (4.1).

This assumption leads to new passive map with "differentiation" on output port-variable.

Proposition 10 *Consider the system (*(4.1)*) in BM form* (4.2) *satisfying Assumption 9. Then the system is passive with input* u*, output given by* $y_{PB} = -\tilde{G}(x)^T\dot{x}$ *and storage function* $\tilde{P}$*.*

Proof. *Time differential of* $\tilde{P}$ *is given by*

$$\begin{aligned}\dot{\tilde{P}} &= (\nabla_x \tilde{P})^\top \dot{x} \\ &= \dot{x}^\top \tilde{Q}\dot{x} + u^\top y_{PB} \\ &\leq u^\top y_{PB}, \end{aligned} \tag{4.3}$$

where y_{PB} *is given by*

$$y_{PB} = -\tilde{G}(x)^T\dot{x} \tag{4.4}$$

which is referred as power balancing (shaping) output Ortega et al. (2003). ■

The control objective is to stabilize the system at the equilibrium point (x^*, u^*) satisfying

$$\nabla_x \tilde{P}(x^*) + \tilde{G}(x^*)u^* = 0 \tag{4.5}$$

To achieve the control objective, the usual approach is to assign a closed loop storage function P_d of the closed loop system such that

$$\tilde{Q}\dot{x} = \nabla_x P_d \quad \text{and} \quad x^* = \arg\min_x P_d \tag{4.6}$$

where,

$$P_d = \tilde{P} + P_c \tag{4.7}$$

P_c is the power supplied by the controller. In García-Canseco et al. (2010), the power supplied by controller is found by solving PDE's and satisfies the constraint of preserving gradient structure (4.6) in closed-loop. The desired potential function P_d is obtained by shaping the actual potential function $(\tilde{P})$ using P_c and hence the approach is called as power shaping. In the context of energy

shaping, the difficulty in solving PDE's is obviated by relaxing the structure preserving constraint and the energy shaping is obtained by using passive outputs of the system Gogte et al. (2012); Satpute et al. (2014); Donaire et al. (2016a). Recently, a similar idea is pursued for systems in port-Hamiltonian form Borja et al. (2016). Here, we relax the structure preserving constraint and present a procedure of finding P_d using the power balancing outputs of the system. The desire is to find a closed loop storage function P_d satisfying

$$\dot{P}_d \leq 0 \quad \text{and} \quad x^* = \arg\min_x P_d \tag{4.8}$$

The conditions imposed on the power balancing output boils down to a classical integrability condition of some computable vector fields.

Definition 11 (Integrable) *Consider $x \in \mathbb{R}^n$ and $g(x) \in \mathbb{R}^{n\times m}$. Let $g_k(x)$ be the k^{th} column of $g(x)$ and $g_{kl}(x)$ denoted the l^{th} element of $g_k(x)$ where, $k \in \{1, 2, \ldots, n\}$ and $l \in \{1, 2, \ldots, m\}$. Denote $g^k(x) \triangleq \sum_{l=1}^{m} g_{kl} dx^l, k \in \{1, 2, \ldots, n\}$. We call the matrix $g(x)$ integrable if 1-forms $g^k(x), \forall k \in \{1, 2, \ldots, n\}$ are closed. This is equivalent to the following: the matrix $g(x)$ is integrable if $\nabla_x g_k(x) = (\nabla_x g_k(x))^\top, \forall k \in \{1, 2, \ldots, n\}$.*

Lemma 12 (Poincaré Lemma) *Given $f : \mathbb{R}^n \to \mathbb{R}^n, f \in \mathcal{C}'$. There exists $\varphi : \mathbb{R}^n \to \mathbb{R}$ such that $\nabla\varphi = f$ if and only if $\nabla f = (\nabla f)^\top$ (The reader can refer to Spivak (1979) for the Poincaré lemma in differential form).*

Assumption 13 *Input matrix $\tilde{G}(x)$ is Integrable.*

Proposition 14 *The power balancing output y_{PB} given in (4.4) is integrable.*

Proof. *From Assumption 13, we have that $\tilde{G}(x)$ is integrable, Poincaré's Lemma ensures the existence of a function $\Gamma(x) : \mathbb{R}^n \to \mathbb{R}^m$ such that*

$$\dot{\Gamma} = -\tilde{G}(x)^\top \dot{x} \tag{4.9}$$

using (4.4) we conclude the proof. ∎

By using Assumption 13, the power balancing output is integrable from Proposition 14. Using this the desired closed loop potential function P_d is constructed in the following way

$$P_d = k\tilde{P} + \frac{1}{2}||\Gamma(x) + a||^2_{k_I} \tag{4.10}$$

where $k > 0$, $a \in \mathbb{R}^m$, $k_I \in \mathbb{R}^{m\times m}$ with $k_I > 0$. And further a is chosen such that (4.8) is satisfied, which implies

$$\nabla_x P_d(x^*) = 0 \qquad \nabla^2_x P_d(x^*) \geq 0 \tag{4.11}$$

which upon solving gives

$$a := kk_I^{-1}\tilde{G}^\dagger(x^*)\nabla_x\tilde{P}(x^*) - \Gamma(x^*) \tag{4.12}$$

where $\tilde{G}^\dagger$ represents pseudoinverse of $\tilde{G}$.

Proposition 15 *Consider the system (4.1) satisfying the Assumptions 9 and 13. We define the mapping* $u : \mathbb{R}^n \to \mathbb{R}^m$

$$u := \frac{1}{k}\left(v + \alpha\tilde{G}^\top\dot{x} - k_I(\Gamma(x) + a)\right). \tag{4.13}$$

where $\alpha > 0$, $\nabla\Gamma(x) := -\tilde{G}(x)$. *Then system (4.1) in closed loop is passive with storage function* P_d *(4.10) satisfying (4.11), input* v *and output* y_{PB}. *Further with* $v = 0$ *the system (4.1) is stable with Lyapunov function* $P_d(x)$ *and* x^* *as stable equilibrium point. Furthermore, if* $y_{PB} = 0 \implies \lim_{t\to\infty} x(t) \to x^*$, *then* x^* *is asymptotically stable.*

Proof. *The time derivative of closed loop potential function (4.10) is*

$$\begin{aligned}
\dot{P}_d &= k\dot{\tilde{P}} + y_{PB}^\top k_I(\Gamma(x) + a) \\
&\leq y_{PB}^\top\left(ku + k_I(\Gamma(x) + a)\right) \\
&= y_{PB}^\top(v - \alpha y_{PB}) \\
&\leq y_{PB}^\top v - \alpha y_{PB}^\top y_{PB} \\
&\leq y_{PB}^\top v,
\end{aligned}$$

where we used equations (4.3), (4.4), (4.13) in arriving at the result. This proves that the closed loop is passive with storage function P_d *(4.10), input* v *and output* y_{PB}. *Further for* $v = 0$ *we have*

$$\dot{P}_d \leq -\alpha y_{PB}^\top y_{PB}$$

and at equilibrium

$$u^* = -\frac{k_I}{k}\left(\Gamma(x^*) + a\right). \tag{4.14}$$

Finally from (4.12) *and* (4.14) *we can show that* (x^*, u^*) *satisfy* (4.5)*. This concludes the system* (4.1) *is Lyapunov stable with Lyapunov function* P_d *and* x^* *as equilibrium point Khalil and Grizzle (1996). Furthermore, if* $\dot{P}_d = 0 \Rightarrow y_{PB} = 0 \Rightarrow \lim_{t\to\infty} x(t) \to x^*$*. Finally, we conclude the proof by invoking LaSalle's invariance principle.* ■

Remark 16 *The choice of closed loop potential function is obviously not unique. Instead of* (4.10) *we can have* P_d *in the following way:*

$$P_d(x) = k\tilde{P}(x) + f(\Gamma) \tag{4.15}$$

where $f(\Gamma) : \mathbb{R}^m \to \mathbb{R}$ *has to be chosen such that* (4.11) *is satisfied. One such choice for* $f(\Gamma)$ *is* $\frac{1}{2}||\Gamma(x) + a||^2_{k_I}$*. For general* P_d *of the form* (4.15)*, the control* u *in* (4.13) *will take the form*

$$u = \frac{1}{k}\left(v + \alpha\tilde{G}^\top\dot{x} - \nabla_\Gamma f(\Gamma)\right). \tag{4.16}$$

Further one can choose $f(\Gamma)$ *such that the controller gives the desired performance.*

4.1.2 Disturbance rejection at input

In this subsection, we construct a new controller using (4.13) for constant disturbance rejection at input. Consider the system (4.1) satisfying Assumptions 9 and 13 with constant disturbance d at input, i.e.

$$Q\dot{x} = \nabla_x P(x) + G(x)(u - d) \tag{4.17}$$

Proposition 17 *The closed loop system* (4.17) *with power shaping plus integral control input*

$$u = \frac{1}{k}\left(\alpha\tilde{G}^\top\dot{x} - k_I(\Gamma(x) + a)\right) + u_d.$$

and integrator dynamics

$$\dot{u}_d = -k_s y_{PB}$$

with $k_s > 0$ is asymptotically stable.

Proof. *Consider the following Lyapunov function*

$$P_i = k\tilde{P} + \frac{1}{2}||\Gamma(x) + a||^2_{k_I} + \frac{1}{2}||u_d - d||^2_{k_s^{-1}}. \tag{4.18}$$

Using Proposition 3, the time derivative of P_i along the trajectories of the closed loop system is given by

$$\begin{aligned} \frac{d}{dt}P_i &\leq (u_d - d)^\top y_{PB} + (u_d - d)^\top k_s^{-1}\frac{du_d}{dt} \\ &= (u_d - d)^\top \left(y_{PB} + k_s^{-1}\frac{du_d}{dt}\right) \end{aligned}$$

Finally using $\dot{u}_d = -k_s y_{PB}$, we have $\dot{P}_i \leq 0$. Then by invoking Lasalle's invariance principle, asymptotic stability of x^* is achieved, implying that $(u_d - d)$ converges to zero. ■

4.2 Control of HVAC Subsystems

Building energy systems encompass HVAC water and air-distribution systems, where air-distribution systems provide conditioned air to maintain indoor air environment and have direct effect on occupant comfort. Water-distribution systems are responsible for heating/cooling the water at central place and transfer to air handling units where ventilation air is conditioned as needed and the process involves various heat exchanging operations. The main focus of this paper is on applying the proposed approach on air-distribution system which is responsible for providing user comfort. We neglect the dynamics of the ducts and AHUs and focus only on the zone thermal dynamics. For the validation of the proposed approach, we have considered an illustrative example emulating the Iowa Energy Center$'$s Energy Resource Station (ERS) test bed. This test bed is considered as a means to present the promising nature of the proposed approach to large scale systems and is a target for future validation.

4.2.1 Thermal zone

4.2.1.1 Simple two zone model

In order to illustrate the proposed idea of power based modeling and regulation of building systems, the dynamics of a two-zone building separated by a surface is used as a simplest example Deng et al. (2014), where the surface is modeled as a 3R2C network and is shown in Figure (4.1). A building zone model is constructed by combining lumped parameter models of thermal interaction between zones separated by a solid surface (e.g walls) Mukherjee et al. (2012). A lumped parameter model of combined heat flow across a surface is modeled as RC-network, with current and voltage being analogous of heat flow and temperature. In this modeling framework, the capacitances are used to model the total thermal capacity of the wall, and the resistances are used to represent the total resistance that the wall offers to the flow of heat from one side to other.

The thermal dynamics of a multi-zone building are given by:

$$C_i \dot{T}_i = \sum_{j \in \mathbb{N}_i} \frac{(T_j - T_i)}{R_{ij}} + u_i + \underbrace{\frac{(T_\infty - T_i)}{R_{i0}}}_{Q_i} \tag{4.19}$$

where $\mathbb{N}_i$ denotes all resistors connected to the ith capacitor (includes zone and surface capacitances), T_∞ is the ambient temperature. u_i is the heating/cooling generation input to the ith zone and Q_i is the external heat input due to ambient and is nonzero only for the zone nodes.

The dynamics of the system is given by

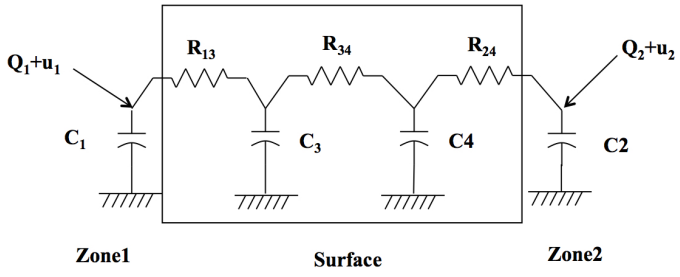

Figure 4.1 Two zones separated by surface and lumped RC network model.

$$\begin{aligned} C_1\dot{T}_1 &= \frac{T_3 - T_1}{R_{31}} + Q_1 + u_1 \\ C_2\dot{T}_2 &= \frac{T_4 - T_2}{R_{42}} + Q_2 + u_2 \\ C_3\dot{T}_3 &= \frac{T_1 - T_3}{R_{31}} + \frac{T_4 - T_3}{R_{34}} \\ C_4\dot{T}_4 &= \frac{T_2 - T_4}{R_{42}} + \frac{T_3 - T_4}{R_{34}} \end{aligned} \tag{4.20}$$

Here T_1, T_2 are zone temperatures and T_3, T_4 are surface temperatures.

The above system of equations (4.20) can be written in the Brayton-Moser form (4.2) with $x = \left[T_1, T_2, T_3, T_4\right]^\top$, and

$$\begin{aligned} P(x) &= \frac{(T_3 - T_1)^2}{2R_{31}} + \frac{(T_4 - T_2)^2}{2R_{42}} + \frac{(T_3 - T_4)^2}{2R_{34}} \\ &\quad + \frac{(T_\infty - T_1)^2}{2R_{10}} + \frac{(T_\infty - T_2)^2}{2R_{20}}. \\ Q(x) &= \text{diag}[-C_1, -C_2, -C_3, -C_4] \text{ and} \\ G(x) &= \begin{bmatrix} -1 & 0 & 0 & 0 \\ 0 & -1 & 0 & 0 \end{bmatrix}^\top. \end{aligned} \tag{4.21}$$

It is easily verified $P(x)$, $Q(x)$ and $G(x)$ defined in (4.21) satisfy Assumptions 9 and 13. From Proposition 10, system (4.20) is passive with input $u = [u_1, u_2]^\top$, power balancing output $y = [\dot{T}_1, \dot{T}_2]^\top$ and storage function $P(x)$, further from Proposition 14, we have $\Gamma(T) = [T_1, T_2]^\top$.

Control objective: The control objective is to stabilize a given equilibrium point $[T_1^*, T_2^*]$ satisfying (4.5) where

$$\begin{aligned} u_1^* &= -\left(\tfrac{(T_3^* - T_1^*)}{R_{31}} + \tfrac{(T_\infty - T_1^*)}{R_{10}}\right) \\ u_2^* &= -\left(\tfrac{(T_4^* - T_2^*)}{R_{42}} + \tfrac{(T_\infty - T_2^*)}{R_{20}}\right) \end{aligned} \tag{4.22}$$

4.2.1.2 Controller design

Proposition 18 *Consider the closed loop storage function defined in (4.10) with $k_I = diag(k_1, k_2)$ and $a = [a_1, a_2]^\top$. P_d defined in (4.10), takes the form*

$$P_d = kP + \frac{k_1}{2}(T_1 + a_1)^2 + \frac{k_2}{2}(T_2 + a_2)^2 \tag{4.23}$$

(a) for $a_1 = -\frac{k}{k_1}u_1^* - T_1^*$, $a_2 = -\frac{k}{k_1}u_2^* - T_2^*$, P_d *is positive definite and has a minimum at* $[T_1^*, T_2^*]$.

(b) further with the state feedback controller (4.13)

$$\begin{aligned} u_1 &= -\tfrac{\alpha}{k}\dot{T}_1 - \tfrac{k_1}{k}\left(T_1 - T_1^* - \tfrac{k}{k_1}u_1^*\right) \\ u_2 &= -\tfrac{\alpha}{k}\dot{T}_2 - \tfrac{k_2}{k}\left(T_2 - T_2^* - \tfrac{k}{k_2}u_2^*\right). \end{aligned} \tag{4.24}$$

If the tuning parameters α, k, k_1, k_2 *are nonnegative, then* $[T_1^*, T_2^*]$ *is asymptotically stable equilibrium of the closed loop system with* P_d *as Lyapunov function.*

Proof. *We need to choose a such that* $\nabla P_d(x^*) = 0$ *and* $\nabla^2 P_d(x^*) \geq 0$ *at the desired equilibrium. Therefore, proof of (a) directly follows from* (4.12) *and* (4.14). *The proof of* (*b*) *follows from Proposition 15. It can also be proved by taking the time differential of the Lyapunov functional* P_d *defined in* (4.23) *as shown below*

$$\begin{aligned} \dot{P}_d &= k\dot{P} + k_1(T_1 + a_1)\dot{T}_1 + k_2(T_2 + a_2)\dot{T}_2 \\ &= k(\dot{T}_1 u_1 + \dot{T}_2 u_2) + k_1(T_1 + a_1)\dot{T}_1 + k_2(T_2 + a_2)\dot{T}_2 \\ &= \dot{T}_1(ku_1 + k_1(T_1 + a_1)) + \dot{T}_2(ku_2 + k_2(T_2 + a_2)) \end{aligned} \tag{4.25}$$

Using u_1 *and* u_2 *from* (4.24) *the resulting equation* (4.25) *becomes*

$$\frac{d}{dt}P_d \leq -\alpha(\dot{T}_1^{\,2} + \dot{T}_2^{\,2}) \leq 0. \tag{4.26}$$

■

The controller obtained is a PI controller with respective to power balancing outputs. The controller needs model information to compute u^*, but the system attains stability for error in u^*. The analysis provided uses zone heating/cooling as input, but the proposed approach can be easily extended to more general model where the zone mass flow rate is the control variable Deng et al. (2014). Simulations were conducted on the simple two-zone model, in order to show the effectiveness of the proposed approach. Different operating conditions are considered, where the zones temperatures have same and different set points and with different outside air temperatures. The parameters

used for the simulation can be found in Deng et al. (2014). The objective is to regulate the zone temperatures such that $T_1 = T_1^*$, $T_2 = T_2^*$.

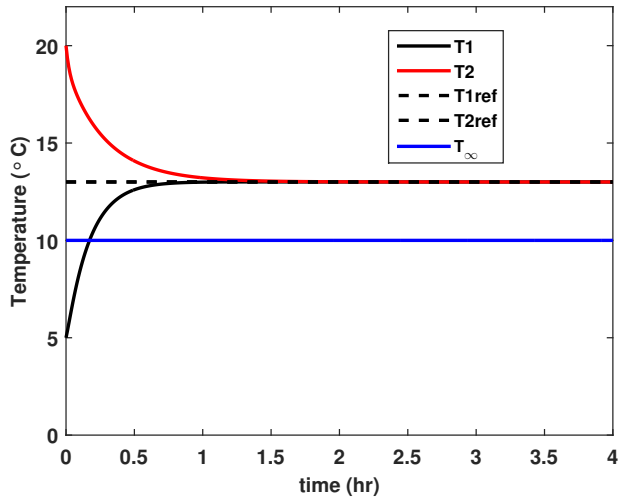

(a)

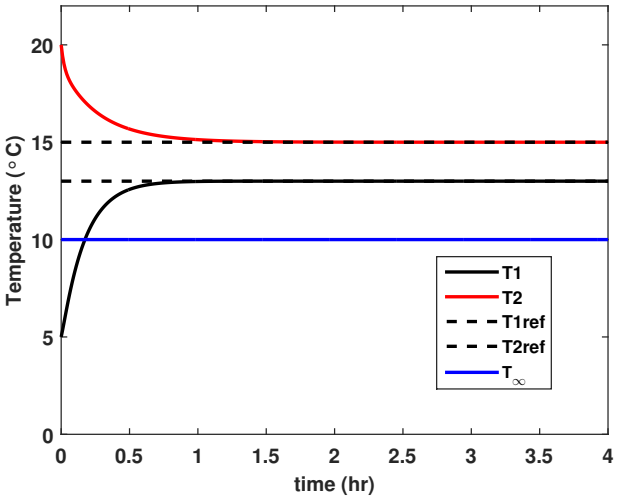

(b)

Figure 4.2 Zone temperature for constant ambient temperature a) Same setpoint b) Different setpoint.

Figure 4.2 shows the case where the individual zones are subjected to constant ambient temperature with same and different set points. The controller effectiveness in terms of transient and steady state performance is verified in regulating the zone temperatures to their corresponding set points. The important note is that there is no overshoot in the time response of states before settling to the target values, which shows the effectiveness of controller compared to energy based controllers.

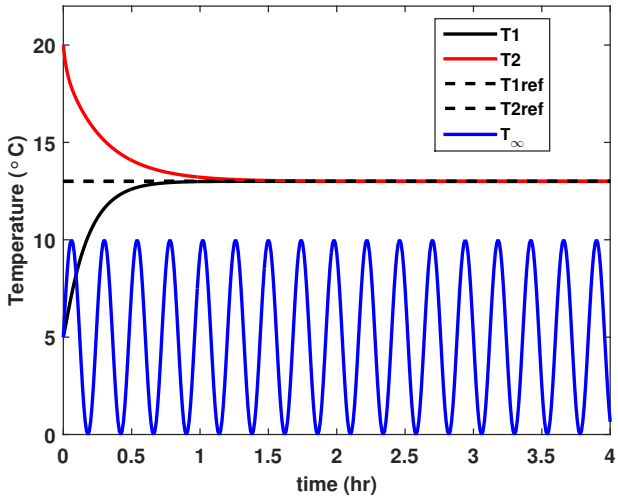

Figure 4.3 Zone temperature for varying ambient temperature with same setpoint

Figure 4.3 and 4.4 shows the case where the individual zones are subjected to time varying sinusoidal ambient temperature ($T_\infty = 5\sin(2\pi t/T) + 5°C, T = 24$hrs Mukherjee et al. (2012)) with same and different set points, the controller performs reliably under different ambient temperatures.

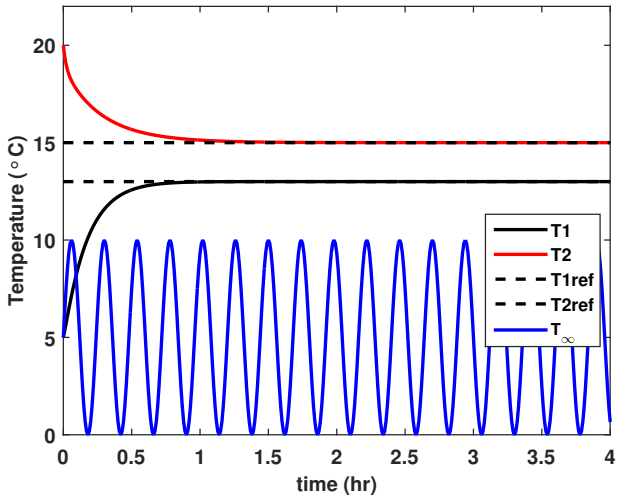

Figure 4.4 Zone temperature for varying ambient temperature with different setpoint

4.2.1.3 Medium-sized commercial building (ERS test bed)

In the subsection, we extend the proposed methodology on a simulated building model emulating the ERS test bed. This simulated model consists of two side-by-side independent and similar zones marked as A and B and distributed in four directions, East, South, West, and North, respectively. These zones are served using two air handling units (AHU) marked A and B, where each AHU will be serving four Variable Air Volume systems (AHU A serving 4 zones (A) in different directions). This model configuration reflects a medium-sized commercial building and each test zone has approximately 266 sq.ft of floor space. The model consists of three exterior zones and one interior zone (North). In each direction, two constructed zones have identical exposures yielding identical external thermal loads and may have identical internal thermal loads thereby allowing simultaneous, side-by-side comparison testing of many types of HVAC systems and control schemes. Some zones are connected with other offices and spaces.

The schematic diagram is shown in Fig. 4.5.

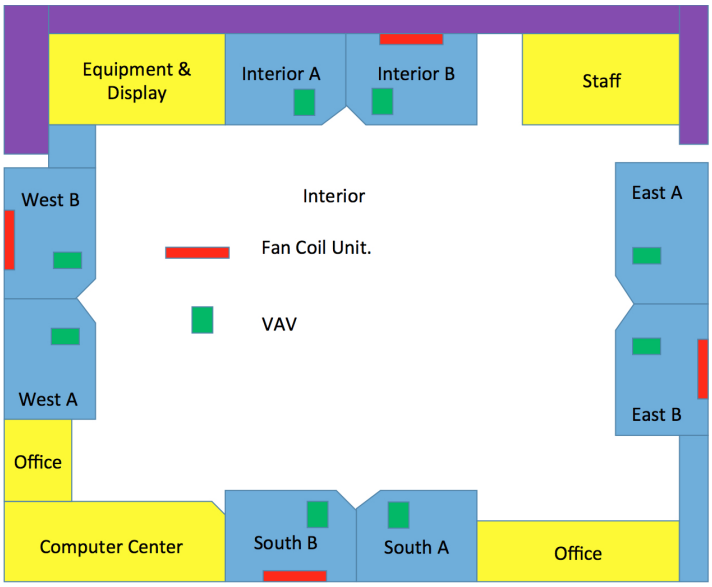

Figure 4.5 Schematic of the simulated building model

4.2.1.4 RC network model

Modeling building thermal zone dynamics can be classified into three categories Atam and Helsen (2016) white box, data-driven and hybrid models. There are several advantages/disadvantages associated with each of the methods in different classes; such as the computational fluid dynamics (CFD) approach which is based on the solution of partial differential equations can provide detailed occupant level micro-environment Gao and Niu (2004). However, it is not suitable for control design purpose due to the models being complex, together with large computation time. On the other hand, RC modeling Atam and Helsen (2016) belongs to the class of hybrid approach and there is an analogy between the electrical and thermal systems which helps in deriving the dynamic equations based on circuit theory and the parameters provide a physical interpretation of the governing system. Since the building is an interconnected system with individual zones as its subsystems, the heat transfer between these zones can occur due to conduction, convection and radiation. In this paper, we assume that the heat transfer occurs only through conduction, convection from the ambient and contribution due to radiation is negligible. The supplied air to the zone is modulated at the Variable Air Volume (VAV) boxes by changing the flow rate and temperature

of air through dampers. In this section, it is shown that the building zone thermal dynamics poses inherent gradient structure and can be represented in BM framework. A building zone model is

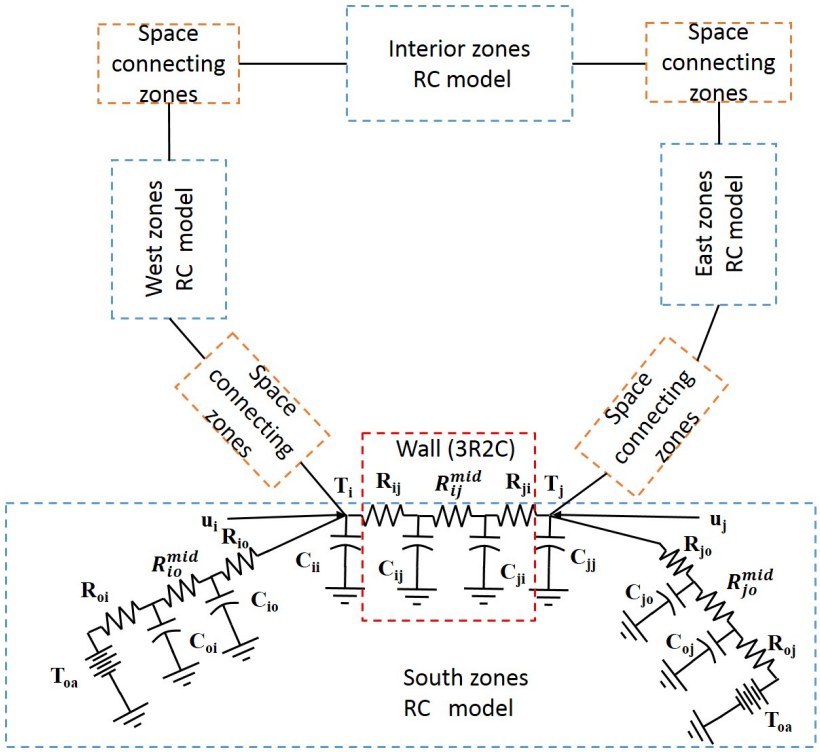

Figure 4.6 RC network schematic for the test bed

constructed Mukherjee et al. (2012) by combining lumped parameter models of thermal interaction between zones separated by a solid surface (e.g walls). A lumped parameter model of combined heat flow across a surface is modeled as RC-network, with current and voltage being analogous of heat flow and temperature. In this modeling framework, the capacitances are used to model the total thermal capacity of the wall, and the resistances are used to represent the total resistance that the wall offers to the flow of heat from one side to other.

The thermal dynamics of a multi-zone building are given by Mukherjee et al. (2012):

$$C_i\dot{T}_i = \sum_{j\in\mathbb{N}_i} \frac{(T_j - T_i)}{R_{ij}} + \dot{m}_i c_p (T_s - T_i) + \underbrace{\frac{(T_\infty - T_i)}{R_{i0}}}_{Q_i} \tag{4.27}$$

where $\mathbb{N}_i$ denotes all resistors connected to the i^{th} capacitor (includes zone and surface capacitances), T_∞ is the ambient temperature, Q_i is the external heat input due to ambient and is nonzero only for the zone nodes. The system (4.27) becomes nonlinear due to the presence of bilinear term $\dot{m}_i T_i$, where m_i is the mass flow rate of i^{th} room, which also acts a control input to the system and T_s is the supply air temperature and c_p is the specific heat capacitance of the supplied air at constant pressure.

RC network schematic of building testbed is shown in Fig. 4.6. Since the zones in different directions have the same characteristics, it can be seen that the RC network schematic for the zones located on the south side where the wall connecting south zones is modeled as 3R2C model and other direction zones has the same model. For our analysis the space connecting zones is modeled as a 3R2C model. The resulting interconnected RC network model can be represented as a undirected graph $G = (\mathbb{V}, \mathbb{E})$ where $\mathbb{V}(\mathbb{G}) := \{v_1, \ldots, v_{n+1}\}$ denotes the set of nodes in the graph, which represent temperature in the zones, walls, ambient and edge set $\mathbb{E} \subset \mathbb{V} \times \mathbb{V}$, where $\mathbb{E}(\mathbb{G}) = \{e_1, \cdots, e_m\}$. The nodes are re-indexed into zone nodes and wall nodes, the first r nodes are corresponding to zone nodes and $n - r$ nodes corresponds to wall nodes which represents temperatures internal to the walls and the ambient node is $n + 1$. The conductive effect between the zones is represented as a edge $(i, j) \in \mathbb{E}$ and is represented by the resistance R_{ij} connecting them. Since the graph is undirected, we have $R_{ij} = R_{ji}$. The states of the system are represented by the $T_1, \cdots, T_r, T_{r+1}, \cdots T_n$, where $T_1, \cdots T_r$ are the zone temperatures, $T_{r+1}, \cdots T_n$ are the wall temperatures. We assume the supply air temperature T_s is constant. If G has m edges its node-edge incidence matrix $\tilde{B}$ is given by

$$\tilde{B}_{ij} = \begin{cases} 1, & \text{if node } i \text{ starts link } j \\ -1, & \text{if node } i \text{ ends link } j \\ 0, & \text{otherwise.} \end{cases} \tag{4.28}$$

this results in incidence matrix $\tilde{B} \in \mathbb{R}^{n+1\times m}$ and $\tilde{B} = \begin{bmatrix} B & b_{n+1} \end{bmatrix}^\top$. Using the graph structure the compact representation of the dynamics (4.27) is given by

$$C\dot{T} = -BR^{-1}B^\top T + D_0 T_\infty + Du \tag{4.29}$$

where C, R are diagonal, positive definite matrices consisting of thermal capacitances of all the nodes except the ambient node and thermal resistances representing the thermal interaction between nodes. The nonzero elements of the vector $D_0 = -BR^{-1}b_{n+1}^\top$, where b_{n+1} is the row corresponding to the ambient node in the incidence matrix $\tilde{B}$ and represents the thermal conduction with the ambient.

The above system of equations (4.29) can be written in the Brayton-Moser form (4.2) with $x = [T_1, \cdots, T_n]^\top$ and

$$\begin{aligned} P(x) &= \frac{T^\top BR^{-1}B^\top T}{2} - T^\top D_0 T_\infty. \\ Q(x) &= \text{diag}[-C_1, -C_2, \cdots, -C_n] \text{ and} \\ G(x) &= \begin{bmatrix} -\text{diag}(c_p(T_s - T_i)) \\ 0_{n-r\times r} \end{bmatrix} \quad \text{for } i = 1, \cdots, r. \end{aligned} \tag{4.30}$$

It is easily verified $P(x)$, $Q(x)$ and $G(x)$ defined in (4.30) satisfy Assumption 9 and 13. From Proposition 10, system (4.29) is passive with input $u = [u_1, u_2, \cdots, u_r]^\top$, power balancing output $y = [c_p(T_s - T_1)\dot{T}_1, c_p(T_s - T_2)\dot{T}_2, \cdots, c_p(T_s - T_r)\dot{T}_r]^\top$ and storage function $P(x)$. Further from Proposition 14, we have $\Gamma(T) = [\frac{-1}{2}c_p(T_s - T_1)^2, \cdots, \frac{-1}{2}c_p(T_s - T_r)^2]^\top$.

Control objective: The control objective is to stabilize a given equilibrium point T^* satisfying (4.5) where

$$u^* = D^\dagger \left(BR^{-1}B^\top T^* - D_0 T_\infty\right) \tag{4.31}$$

where $D^\dagger$ represents pseudoinverse of D.

4.2.1.5 Controller design

Proposition 19 *Consider the closed loop storage function defined in (4.10) with* $k_I = diag(k_1, k_2, \cdots, k_r)$ *and* $a = [a_1, a_2, \cdots, a_r]^\top$. P_d *defined in (4.10), takes the form*

$$P_d = kP + ||\Gamma(T) + a||^2_{k_I} \tag{4.32}$$

(a) for $a = -kk_I^{-1}u^* - \Gamma(T)^*$, P_d *is positive definite and has a minimum at* $\tilde{T}^*$.

(b) further with the state feedback controller (4.13)

$$u = -\tfrac{\alpha}{k}\dot{\tilde{T}} - \tfrac{k_I}{k}\left(\Gamma(T) - \Gamma(T)^* - kk_I^{-1}u^*\right) \tag{4.33}$$

where, $\tilde{T} = [T_1, T_2, \cdots, T_r]^\top$. *If the tuning parameters* α, k, k_I *are nonnegative, then* $\tilde{T}^*$ *is asymptotically stable equilibrium of the closed loop system with* P_d *as Lyapunov function.*

Proof. *We need to choose a such that* $\nabla P_d(x^*) = 0$ *and* $\nabla^2 P_d(x^*) \geq 0$ *at the desired equilibrium. Therefore, proof of (a) directly follows from (4.12) and (4.14). The proof of (b) follows from Proposition 15. It can also be proved by taking the time differential of the Lyapunov functional* P_d *defined in (4.32) as shown below*

$$\begin{aligned} \dot{P}_d &= k\dot{P} + \dot{\tilde{T}}^\top k_I(\Gamma(T) + a) \\ &= k\dot{\tilde{T}}^\top u + \dot{\tilde{T}}^\top k_I(\Gamma(T) + a) \\ &= \dot{\tilde{T}}^\top(ku + k_I(\Gamma(T) + a)) \end{aligned} \tag{4.34}$$

Using u from (4.33) the resulting equation ((4.34)) becomes

$$\frac{d}{dt}P_d \leq -\alpha\dot{\tilde{T}}^\top\dot{\tilde{T}} \leq 0.$$

■

The controller obtained is a PI controller with respect to power balancing outputs. The controller needs model information to compute u^*, but the system attains stability for error in u^*.

4.2.1.6 Parameter Identification

The parameters of the model (4.29) such as resistances (R) and capacitances (C) are calculated using the approach given in Goyal and Barooah (2010); Gouda et al. (2003). The individual resistances/capacitances of each wall or surface is calculated based on the total resistance/total capacitance (R_{total}/C_{total}) of each wall. The data from Travesi et al. (2001), such as the thickness and thermal properties of construction layers used in the ERS building is used for calculation of the total resistances/capacitances of each wall. The total resistance and capacitance of each surface in the ERS building is calculated as follows:

$$R_{total} = \left(\sum_{j=1}^{n} \frac{x_j}{k_j}/A\right) \tag{4.35}$$

$$C_{total} = A\sum_{j=1}^{n} x_j \rho_j c_{p,j} \tag{4.36}$$

where j represents individual layer of the wall, x is thickness of the layer, k is the layer R-value, A represents area, ρ is the layer density, and $c_{p,i}$ is the specific heat of each layer. Using the scaling coefficients Goyal and Barooah (2010) in Table 4.1, the indiviudal resistances/capacitances of the wall can be found as

Table 4.1 Coefficients used to calculate resistance and capacitance values

Surface	e_1	e_2	e_3	h_1	h_2
External Wall	0.4	0.5	0.1	0.85	0.15
Internal Wall	0.2	0.6	0.2	0.5	0.5

$$R_m = e_m R_{total} \tag{4.37}$$

$$C_n = h_n C_{total} \tag{4.38}$$

where m = 1, 2, 3; 1 is the outermost and n= 1, 2; 1 is the outermost. The parameters calculated are an indicative of typical buildings based on the material properties. However, by using some system identification techniques we can estimate the parameters accurately.

4.2.1.7 Simulation results

In order to show the effectiveness of the proposed approach, simulations were conducted on the RC network model (4.29) of the testbed described in Section 4.2.1.4. The RC network model representation of the 8 zone building shown in Fig. 4.6, consists of a total 41 nodes including the ambient node: 8 nodes $\{1, \cdots, 8\}$ are the zone nodes, 8 internal wall nodes $\{9, \cdots, 16\}$, 16 external wall nodes $\{17, \cdots, 32\}$, the space between the zones in different directions correspond to remaining 8 nodes $\{33, \cdots, 40\}$ and ambient node $\{41\}$. The total number of edges $m = 48$. The resistance and the capacitance values calculated using the procedure given in Section 4.2 is given in Table 4.2. Different operating conditions are considered, where each of the zones temperatures may have different set points, with similar outside air conditions. The procedure of finding the parameters used for the simulation are described in section 4.2.1.6. The objective is to regulate the zone temperatures such that $\tilde{T} = \tilde{T}^*$. The gains k and k_I are chosen to satisfy performance specification such as settling time etc.

Same setpoint for AHU-A and B zones: Preliminary analysis is conducted by considering same setpoint for all the zones served by two AHU's. Fig. 4.7(a) shows the actual outside air temperature data (represented as T_∞ in the dynamic model (5.22) in the month of April 2016. The simulations are conducted using the actual settings at the ERS testbed, where the supply air temperature (SAT) is kept at $61^\circ F$, using the actual outside air temperature during the day shown in Fig. 4.7(a), the temperature setpoint for all the zones is $68^\circ F$ and all the zones are initialized with different temperatures. The results of the temperature profile and the mass flow rate are shown in Fig. 4.7(b) and Fig. 4.7(c) respectively. Due to the initial temperatures being high compared to the setpoint, the massflow rate should be high initially to cool the temperature and it gradually reduces as the temperature reaches close to the setpoint. The controller effectiveness in terms of transient and steady state performance of the temperature profile can be enhanced by appropriately tuning the gains.

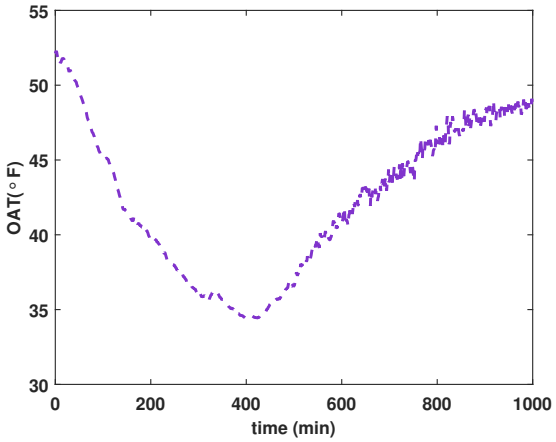

(a) Outside Air Temperature

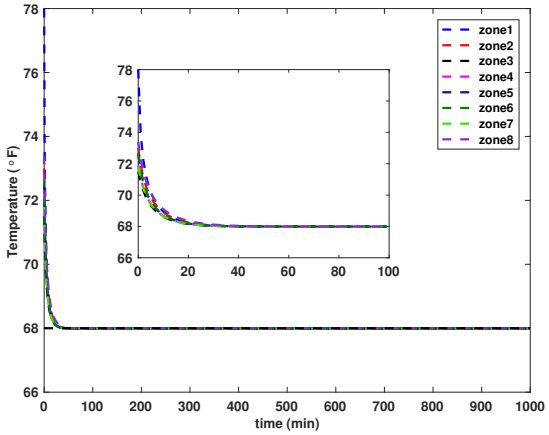

(b) Zone temperature

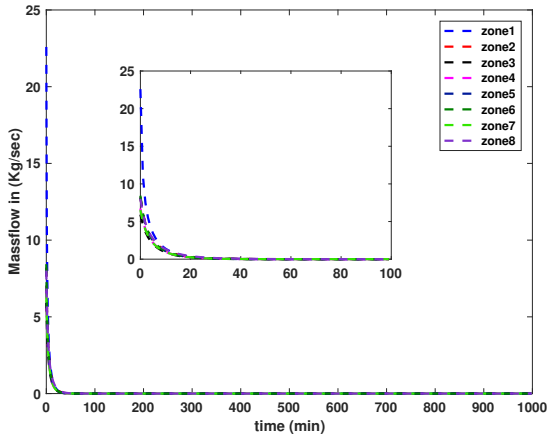

(c) Control input

Figure 4.7 Trajectories of outside air temperature and zone temperature, mass flow rate for constant setpoint

Different setpoint for AHU-A and B zones: Taking into account the actual setup at IEC, where there are two AHU's and each of the AHU's supplying the air to four zones located in different directions. For the simulation, different reference setpoints are used for zones served by different AHU's to show the performance of the proposed controller under these conditions. For the four zones (zone 2, zone 4, zone 5, zone 7) supplied by the AHU-A system we have considered the setpoint to be $68°F$ and for AHU-B systems it is $70°F$. We can see the control effort i.e the mass flow rate needed to stabilize the zone temperatures in AHU-B system is less compared to AHU-A system this is due to the change in setpoints; for AHU-A system we need more cold air to stabilize the system and hence more damper opening compared to AHU-B system. Fig 4.8 and 4.9 show the temperature profile of the zones and the control input needed to stabilize the zone temperature.

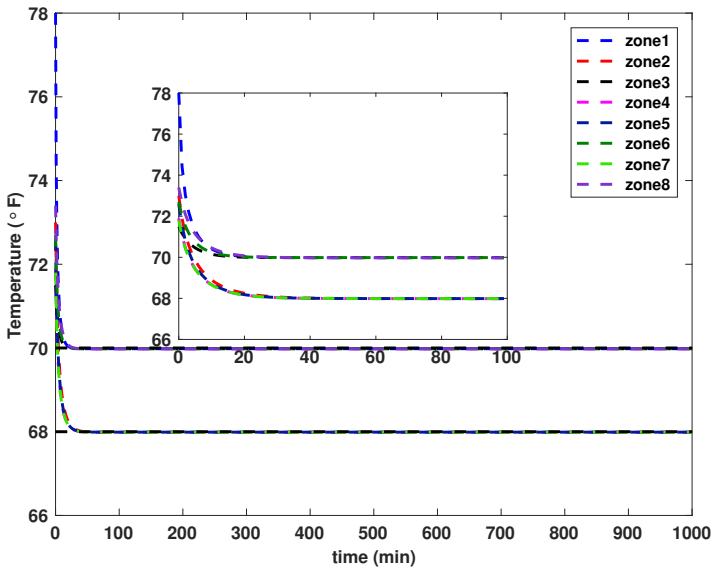

Figure 4.8 Zone temperature (AHU-A zones setpoint is $68°F$ and $70°F$ for AHU-B zones)

Remark 20 *It is to be noted however that there will be trade-offs between control power and performance and the extent of such trade-off will depend on the specific system under consideration. The primary intent of the simulation examples was to demonstrate the effectiveness of the method-*

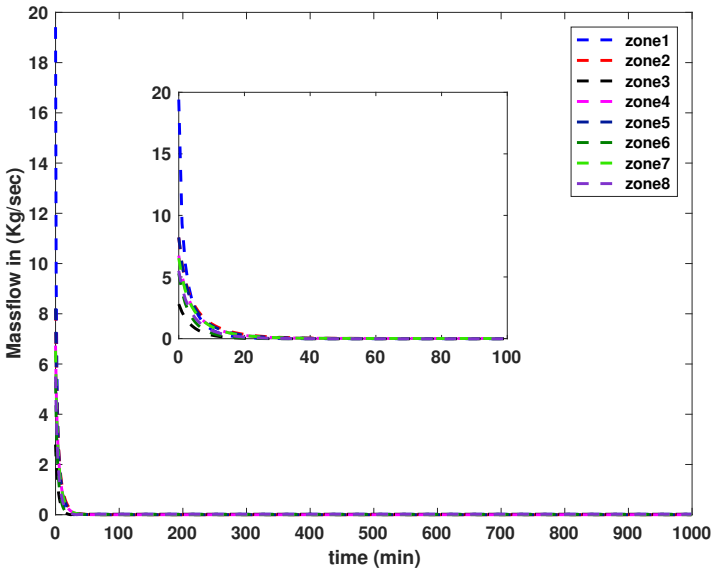

Figure 4.9 Control input

ology, however, in practice, the increase in control power will also be limited by actuator constraints. Nevertheless as discussed above controller can be tuned to improve the performance.

Occupancy and solar radiation analysis: In order to show robustness with respect to more general scenarios, we conducted simulations using a preloaded internal load profile which is shown in Fig. 4.13, which is the sum of heat gains due to occupancy and solar radiation, calculated using the profiles given in Fig. 4.10 and Fig. 4.11. The occupancy load is calculated based on the simulated test bed requirements based on Center (2010) using fraction of total occupancy from Fig. 4.11 and the solar load is calculated based on the hourly global horizontal irradiance data Fig. 4.10 collected from Wilcox and Marion (2008). For the simulation study, the solar data during the occupied hours is considered and a time series is generated by considering the hourly data point to be constant for that entire hour as shown in Fig. 4.13. We provided comparison of temperature and control profile with no disturbance, solar and total (solar + occupancy) as shown in Fig. 4.14 and Fig. 4.15 , it can be seen that the controller tries to keep the zone temperature around the set point.

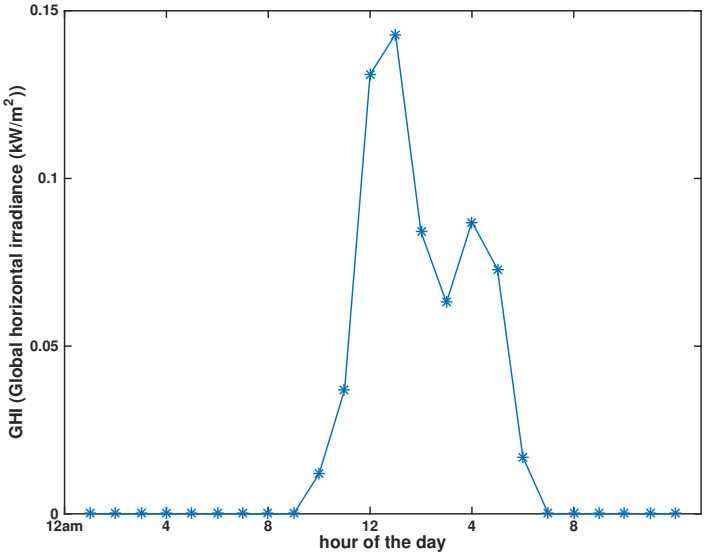

Figure 4.10 Solar GHI

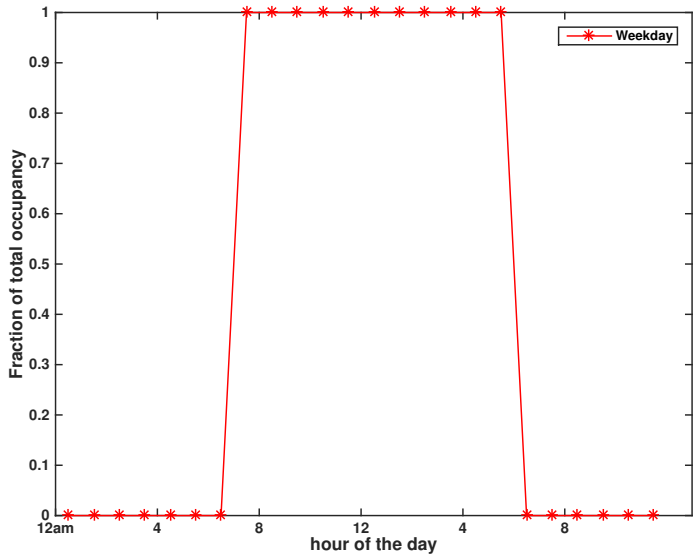

Figure 4.11 Fraction of total occupancy

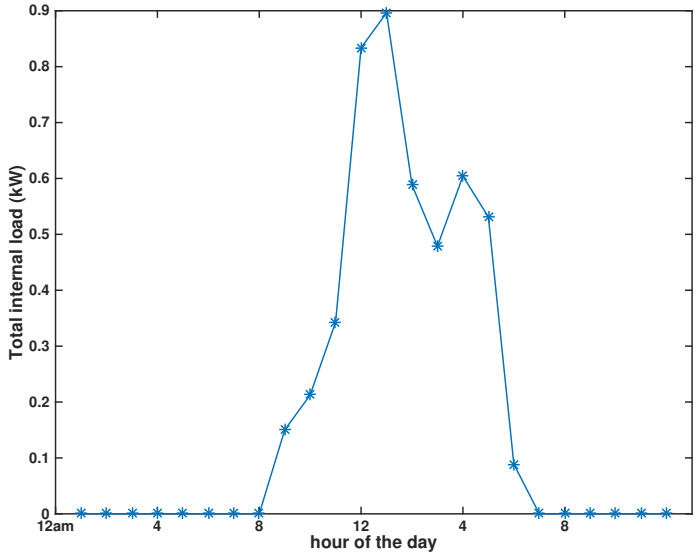

Figure 4.12 Total internal load

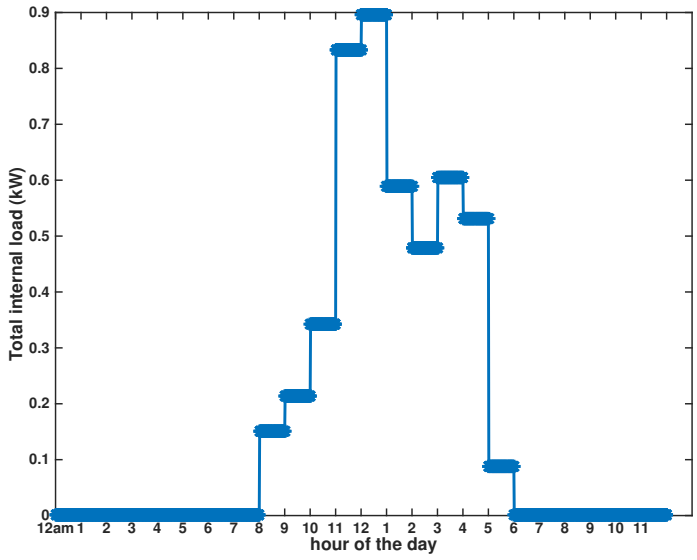

Figure 4.13 Total internal load (simulation)

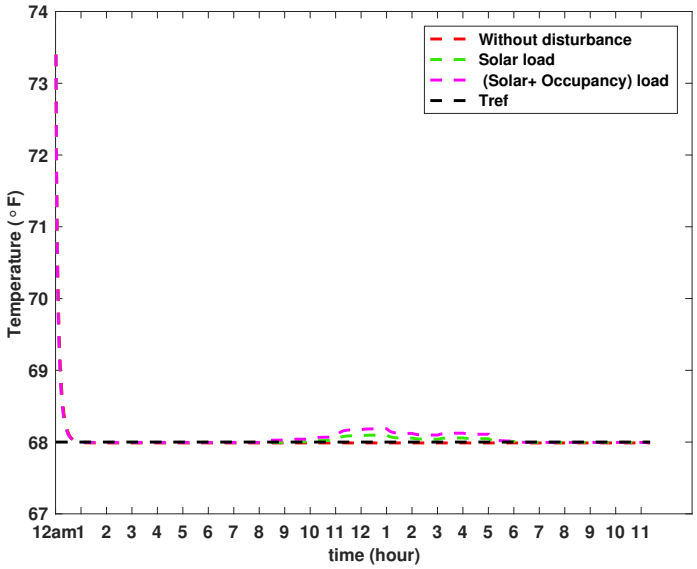

Figure 4.14 Zone temperature profile

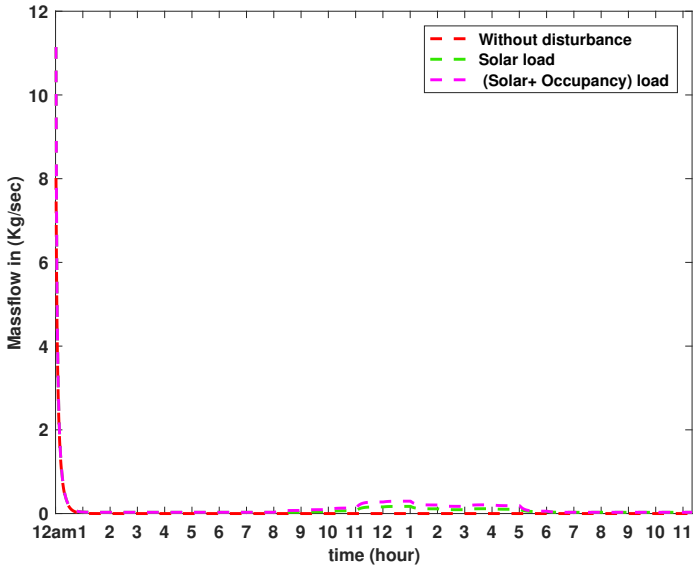

Figure 4.15 Control input profile

4.2.2 Heat exchanger

Buildings need efficient heating/cooling to maintain comfortable environment and heat exchangers form an integral part and widely used in air conditioning of buildings, as every subsystem in HVAC system has a role to play to enhance the overall building energy efficiency. Heat exchangers are one of the most important HVAC subsystems which efficiently transfer heat from one medium (water/air) to another (water/air). The effectiveness of heat exchangers strongly influences the thermal performance of building systems. To illustrate the proposed approach, a water-to-water heat exchanger is considered where, heating is accomplished either by geothermal or solar energy. A schematic of a simple tube-shell water-to-water heat exchanger model Jeltsema and Scherpen (2009) is shown in Fig. 4.16. The inlet and outlet temperatures of cold stream are given by T_{ci}, T_{co} whereas the corresponding temperatures on hot-stream side are denoted by T_{hi}, T_{ho}, respectively. The control variables are the volumetric flow rates denoted by f_c, f_h; the thermal capacities for the cold and hot stream are denoted by C_c, C_h; and the heat transfer in the system is modeled by a thermal conductance G_{hc}. The differential equations governing the heat exchanger system are given by

$$\begin{aligned} C_c\dot{T}_{co} &= -G_{hc}(T_{co}-T_{ho})+\gamma_c(T_{co}-T_{ci})f_c \\ C_h\dot{T}_{ho} &= G_{hc}(T_{co}-T_{ho})+\gamma_h(T_{ho}-T_{hi})f_h \end{aligned} \tag{4.39}$$

The system of equation (4.39) can be written in Brayton-Moser form (4.2) with $x=[T_{co},T_{ho}]^\top$ and

$$\begin{aligned} P(x) &= \frac{G_{hc}}{2}(T_{co}-T_{ho})^2 \\ Q(x) &= \operatorname{diag}(-C_c,-C_h) \text{ and} \\ G(x) &= \begin{bmatrix} -\gamma_c(T_{co}-T_{ci}) & 0 \\ 0 & -\gamma_h(T_{ho}-T_{hi}) \end{bmatrix}. \end{aligned} \tag{4.40}$$

It can easily be verified that $P(x)$, $Q(x)$ and $G(x)$ in (4.40) satisfy Assumptions 9 and 13. From Proposition 10, the system defined in (4.39) is passive with storage function $P(x)$ in (4.40), input $u=[f_c,f_h]^\top$ and output

$$y=[\gamma_c(T_{co}-T_{ci})\dot{T}_{co},\gamma_h(T_{ho}-T_{hi})\dot{T}_{ho}]^\top. \tag{4.41}$$

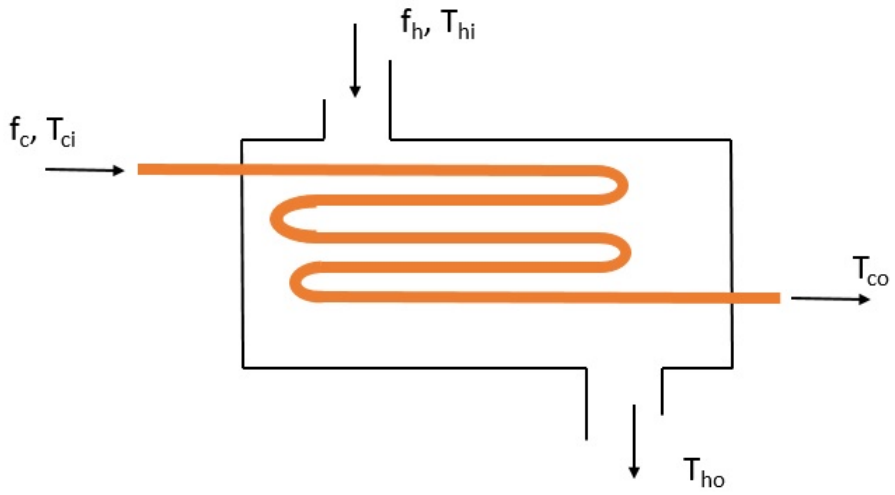

Figure 4.16 Heat exchanger model.

Further from Proposition 14, we have

$$\begin{aligned} \Gamma_1 &= \frac{\gamma_c}{2}(T_{co} - T_{ci})^2 \\ \Gamma_2 &= \frac{\gamma_h}{2}(T_{ho} - T_{hi})^2 \end{aligned} \tag{4.42}$$

Control objective: The control objective is to stabilize system (4.39) at operating point $[T^*_{co}, T^*_{ho}, u^*_1, u^*_2]$ satisfying (4.5) that is

$$u^*_1 = \frac{G_{hc}(T^*_{co} - T^*_{ho})}{\gamma_c(T^*_{co} - T_{ci})} \quad u^*_2 = -\frac{G_{hc}(T^*_{co} - T^*_{ho})}{\gamma_h(T^*_{ho} - T_{hi})} \tag{4.43}$$

Similar to Proposition 18, in this example, using Proposition 15 we can show that system (4.40) in the closed-loop with feedback controller

$$\begin{aligned} u_1 &= -\frac{\alpha}{k}\gamma_c(T_{co} - T_{ci})\dot{T_{co}} - \frac{k_1}{k}\left(\Gamma_1 - \Gamma^*_1 - \frac{k}{k_1}u^*_1\right) \\ u_2 &= -\frac{\alpha}{k}\gamma_c(T_{ho} - T_{hi})\dot{T_{ho}} - \frac{k_2}{k}\left(\Gamma_2 - \Gamma^*_2 - \frac{k}{k_2}u^*_2\right) \end{aligned}$$

is asymptotically stable at equilibrium $[T^*_{co}, T^*_{ho}]$ with Lyapunov function (4.10) defined with $k_I = \text{diag}(k_1, k_2)$ and $a = -kk_I^{-1}u^* - \Gamma(x)^*$. The objective is to achieve a desired outlet temperature of cold stream $T^*_{co} = 80°C$. This gives a desired equilibrium (T^*_{co}, T^*_{ho}), where T^*_{ho} is determined by χ

and T^*_{co}, the admissible equilibrium set χ is given by

$$\chi = \{(T_{co}, T_{ho}) \in \mathcal{S} | G_{hc}(T_{co} - T_{ho}) + \gamma_h(T_{ho} - T_{hi}) f_h = 0\}$$

and $\mathcal{S} = \{(T_{co}, T_{ho}) \in \mathbb{R}^2 | T_{co} > T_{ci}\}$. The parameters values used for the simulation are found in Cøengel (2007). From Fig. 4.17, it can been seen that the desired outlet temperature of cold stream is attained and lies on the equilibrium manifold, which shows the performance of the controller in regulating the temperature.

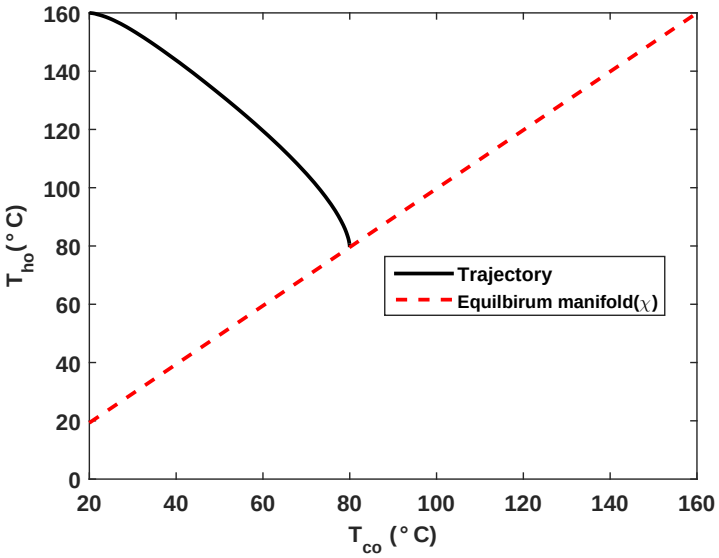

Figure 4.17 Closed loop trajectory.

4.3 Conclusions

A new paradigm, power shaping, is presented for synthesizing control of building HVAC systems using power shaping approach that exploits passivity property of the system. The controller design uses Brayton-Moser formulation for the system dynamics wherein the mixed potential function is the power function and a desired power function to the closed loop dynamics is obtained from new passive maps with differentiation at the output port-variable.

The proposed framework is employed on two representative building subsystem examples (building zone, heat exchanger) to demonstrate the applicability of the power-shaping approach. It is shown that HVAC subsystems has an inherent BM form and then power-shaping methodology can be used to design an effective controller. Mainly, the methodology is demonstrated on a simulated medium-sized commercial building with zones having different setpoint preferences and also disturbance analysis using occupancy and solar radiation profiles.

Table 4.2 Resistance and Capacitance values for the Simulated ERS testbed

Capacitance	Value	Resistance	Value
C_{29}, C_{31}, C_{23}, C_{21}, C_{19}, C_{17}	374kJ/K	$R_{2,10}$,$R_{5,13}$,$R_{8,16}$,$R_{4,12}$,$R_{1,9}$,$R_{3,11}$,$R_{7,15}$,$R_{14,6}$	0.0249K/W
C_{30}, C_{32}, C_{24}, C_{22}, C_{20}, C_{18}	2124kJ/K	$R_{13,14}$,$R_{15,16}$,$R_{11,12}$,$R_{9,10}$	0.0747K/W
C_{13}, C_{14}, C_{10}, C_{9}, C_{15}, C_{16}	179kJ/K	$R_{29,30}$,$R_{21,22}$,$R_{29,30}$,$R_{31,32}$	0.0817K/W
C_{1}, C_{2}, C_{3}, C_{4}, C_{5}, C_{6}, C_{7}, C_{8}	1.21kJ/K	$R_{7,29}$,$R_{8,31}$,$R_{4,23}$,$R_{3,21}$,$R_{11,7}$,$R_{2,19}$	0.0163K/W
C_{28}, C_{27}, C_{26}, C_{25}	156kJ/K	$R_{30,\infty}$,$R_{32,\infty}$,$R_{24,\infty}$,$R_{22,\infty}$,$R_{18,\infty}$,$R_{20,\infty}$	6.53K/W
C_{12}, C_{11}	325kJ/K	$R_{33,34}$,$R_{35,36}$,$R_{37,38}$,$R_{40,39}$	0.0609K/W, 0.0371K/W, 0.0660K/W, 0.126K/W
C_{33}, C_{34}	123kJ/K	$R_{2,33}$,$R_{3,34}$,$R_{28,\infty}$, $R_{26,\infty}$	0.0710K/W, 0.0710K/W, 100.02K/W, 100.02K/W
C_{35}, C_{36}	180kJ/K	$R_{4,35}$,$R_{5,36}$,$R_{27,28}$, $R_{25,26}$	0.0433K/W, 0.0433K/W, 0.0855K/W, 0.0855K/W
C_{37}, C_{38}	101kJ/K	$R_{6,37}$,$R_{38,7}$	0.0770K/W
C_{39}, C_{40}	59kJ/K	$R_{8,39}$,$R_{40,39}$,	0.1473K/W

CHAPTER 5. STABILITY ANALYSIS OF CONSTRAINED OPTIMIZATION DYNAMICS: APPLICATION TO SOCIAL WELFARE PROBLEM FOR BUILDING ENERGY SYSTEMS

Supply-demand balance is essential for stable operation of a power system. Increasing demand and rapid penetration of distributed energy resources into the existing grid induce more uncertainties towards the safe operation of the grid. Traditionally, conventional generators were employed to meet the additional demand. With increasing demand-side management programs, utilities provide incentives to consumers to lower the overall power demand. This results in reducing load during the time when prices are high. These programs lead to a process which involves both the supply and the demand-side resources to minimize the overall cost. In such a scenario, building systems are one of the strong contenders for providing ancillary services to the grid Hao et al. (2013). The advent of smart grid technologies provides sophistication to consumers and providers to schedule supply and demand at regular intervals of time. The idea of minimizing the energy costs of producer and user discomfort is formulated as a social welfare problem Chen et al. (2012).

One of the standard tools for designing algorithms to solve such optimization problems is through primal-dual gradient method. Recently, in Ma et al. (2016), primal-dual gradient method is used to solve the energy management problem in application to HVAC systems. The primary interest in using such method is multi-fold: 1) Gradient method is a well-established method for finding optimum for a class of constrained and unconstrained problems 2) The connection between optimization and control using gradient method and Lyapunov functions naturally relates the solution of the optimization problem to equilibrium points of a dynamical system 3) This procedure leverages to use the framework (BM) and tool (passivity) developed in Chapter 4 for stability analysis for a class of constrained optimization problems. In this process, we borrow tools such as the use of Krasovskii method of Lyapunov function which is an alternative for proving stability

Feijer and Paganini (2009) for saddle-point problems with applications to congestion control and general network utility maximization problems. In Feijer and Paganini (2010), the authors used this Krasovskii Lyapunov function and hybrid Lasalle's invariance principle Lygeros et al. (2003) to prove asymptotic stability of a network optimization problem. Also, tools from switched systems theory Zefran et al. (2001a) for analysis of inequality constraints. Using the duality between energy and co-energy Jeltsema and Scherpen (2009), the authors in Stegink et al. (2016) transformed these BM dynamics, partially into a port-Hamiltonian (pH) form. Stability analysis was presented using the invariance principle for discontinuous Caratheodory systems Cherukuri et al. (2016) and an incremental passivity property for the misfit dynamics.

5.1 Analysis of Constrained Optimization Problems Using Passivity

Consider the standard convex optimization formulation

$$\begin{aligned} \underset{x\in\mathbb{R}^n}{\text{minimize}} \quad & f(x) \\ \text{subject to} \quad & h_i(x) = 0 \quad i = 1,\dots,m \\ & g_i(x) \leq 0 \quad i = 1,\dots,p \end{aligned} \tag{5.1}$$

where, $x \in \mathbb{R}^n$ is the decision variable, $f(x) : \mathbb{R}^n \to \mathbb{R}$, $h_i(x) : \mathbb{R}^n \to \mathbb{R}$ (affine), $g_i(x) : \mathbb{R}^n \to \mathbb{R}$ are all continuous differentiable functions.

Suppose that Slater's condition is satisfied so that strong duality holds Boyd and Vandenberghe (2004). Then x^* is an optimal solution to (5.1) if and only if there exists $\lambda \in \mathbb{R}^m$, $\mu \in \mathbb{R}^p$ such that the **Karush-Kuhn-Tucker (KKT)** conditions

$$\begin{aligned} \nabla_x f(x^*) + \sum_{i=1}^{m} \lambda_i \nabla_x h_i(x^* + \sum_{i=1}^{p} \mu_i \nabla_x g_i(x^*)) = 0 \\ h_i(x^*) = 0 \quad \forall i \in \{1,\dots,m\} \\ g_i(x^*) \leq 0, \;\; \mu_i^* \geq 0, \;\; \text{and} \;\; \mu_i^* g_i(x^*) = 0 \quad \forall i \in \{1,\dots,p\} \end{aligned} \tag{5.2}$$

are satisfied.

A brief note on Lagrange Duality: We consider (5.1) to be a primal problem. Let f^* denote its optimal value.

Consider the following Lagrange dual problem of (5.1):

$$\underset{\lambda\in\mathbb{R}^m,\mu\in\mathbb{R}^p_+}{\text{maximize}} \quad q(\lambda,\mu) \tag{5.3}$$

where q is the dual function given by

$$q(\lambda,\mu) = \underset{x\in\mathbb{R}^n}{\text{minimize}} \quad \mathcal{L}(x,\lambda,\mu) \tag{5.4}$$

and $\mathcal{L}$ is the Lagrange function given by

$$\mathcal{L}(x,\lambda,\mu) = f(x) + \sum_{i=1}^{m} \lambda_i h_i(x) + \sum_{i=1}^{p} \mu_i g_i(x) \tag{5.5}$$

Let q^* denote the optimal value of (5.3). It is well known that weak duality $q^* \leq f^*$ always holds and under the Slater's conditions, i.e., there exist a vector x such that $h_i(x) = 0 \quad \forall i \in \{1,\ldots,m\}$ and $g_i(x) < 0 \quad \forall i \in \{1,\ldots,p\}$, the strong duality $q^* = f^*$ also holds Boyd and Vandenberghe (2004). One of the classical dual methods for solving (5.3) is the saddle point algorithm of Arrow-Hurwicz-Uzawa Arrow et al. (1958) also known as Primal-Dual method.

Inspired from the early work of economists Arrow et al. (1958) and control system view point to convex optimization problems Wang and Elia (2011), which shows that there is a natural continuous time dynamics (primal-dual) associated with the Lagrangian of the optimization problem. The convergence of the dynamical system relates to the optimal solution of optimization problem under mild conditions. This control perspective to optimization problems provides many directions such as using passivity tool with its properties and BM formulation for better understanding of optimization problem and analysis. The optimization problem (5.1) is naturally represented as an interconnection of two systems (equality constrained system and inequality constraint) which is shown in Fig. 5.1

Given the interconnection structure, the key idea for stability analysis of (5.1) is to prove the passivity and stability of individual systems and using the compositional property of passivity (the interconnection of two passive systems is passive) results in stability analysis of whole optimization problem.

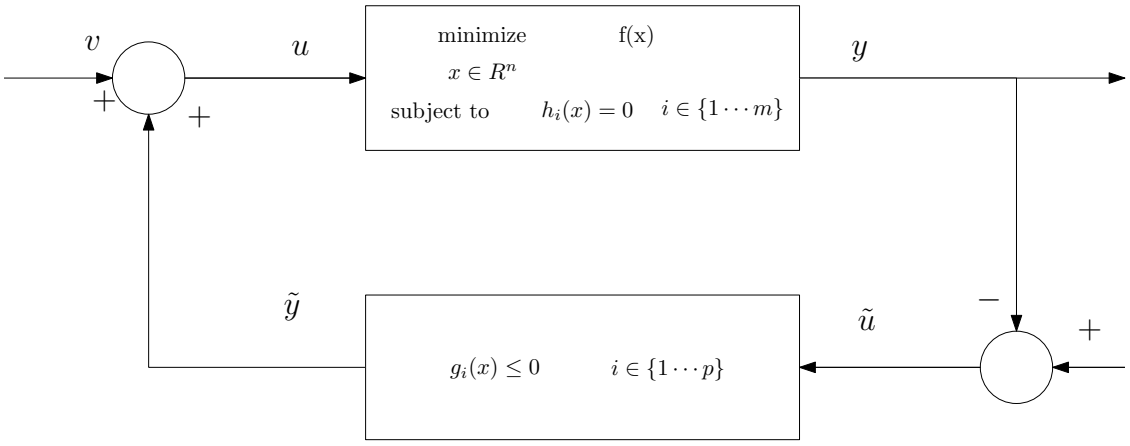

Figure 5.1 Interconnected optimization

Equality constrained optimization problem: Consider the following constrained optimization problem

$$\begin{aligned} \underset{x \in \mathbb{R}^n}{\text{minimize}} \quad & f(x) \\ \text{subject to} \quad & h_i(x) = 0 \quad i = 1, \ldots, m \end{aligned} \tag{5.6}$$

where $f : \mathbb{R}^n \to \mathbb{R}$ is continuously differentiable (C^1) and strictly convex and $h_i (\in C^1) : \mathbb{R}^n \to \mathbb{R}$ is affine. Assume (i) that the objective function has a positive definite Hessian $\nabla_x^2 f(x)$ and (ii) that the problem (5.6) has a finite optimum, and Slater's condition is satisfied i.e., the constraints are strictly feasible and strong duality holds Boyd and Vandenberghe (2004). The solution x^* is a optimal solution to (5.6) if there exists $\lambda^* \in \mathbb{R}^m$ such that the following Karush-Kuhn-Tucker (KKT) conditions are satisfied.

$$\begin{aligned} \nabla_x f(x^*) + \sum_{i=1}^{m} \lambda_i \nabla_x h_i(x^*) = 0 \\ h_i(x^*) = 0 \quad \forall i \in \{1, \ldots, m\} \end{aligned} \tag{5.7}$$

The Lagrangian of (5.6) is given by

$$\mathcal{L} = f(x) + \sum_{i=1}^{m} \lambda_i h_i(x) \tag{5.8}$$

Since strong duality holds for (5.6), (x^*, λ^*) is a saddle point of the Lagrangian $\mathcal{L}$ if and only if x^* is an optimal solution to (5.6) and λ^* is optimal solution to its dual problem. Consider the following

dynamics

$$\begin{aligned} -\tau_x \dot{x} &= \nabla_x f(x) + \sum_{i=1}^{m} \lambda_i \nabla_x h_i(x) + u \\ \tau_{\lambda_i} \dot{\lambda}_i &= h_i(x), \quad y = -x. \end{aligned} \tag{5.9}$$

where τ_x, τ_λ are positive definite matrices and input $u, y \in \mathbb{R}^n$. The unforced system ($u = 0$) of equations (5.9) represent primal-dual dynamics corresponding to (5.8) and the equilibrium corresponds to the KKT conditions (5.7).

The Brayton Moser formulation: Denote $z = [x; \lambda]$. The continuous time gradient laws (5.9), associated with (5.6), naturally admit a BM form (4.1), with $Q = \{-\tau_x, \tau_\lambda\}$ and $P(z) = f(x) + \lambda^\top h(x)$ as $Q\dot{z} = \nabla_z P + u$.

Proposition 21 *Let $\bar{z} = (\bar{x}, \bar{\lambda})$ satisfy (5.7). Assume $h(x)$ is affine and $f(x)$ strictly convex. Then the system of equations (5.9) are passive with port variables $(\dot{u}, \dot{y})$ Kosaraju et al. (2017). Further every solution of the unforced version ($u = 0$) of (5.9) asymptotically converges to $\bar{z}$.*

Proof. In BM formulation we represent the system dynamics in pseudo-gradient form, ($Q(z)$ and $P(z)$ are indefinite). Therefore $P(z)$ cannot be used as a Lyapunov function for stability analysis. A way of constructing a suitable Lyapunov function involves finding $\alpha \in \mathbb{R}$ and $M \in \mathbb{R}^{n \times n}$ Ortega et al. (2003); Kosaraju et al. (2017) such that

$$\tilde{P} = \alpha P + \frac{1}{2} \nabla_x P^\top M \nabla_x P. \tag{5.10}$$

Considering $\tilde{P}$ (5.10) with $\alpha = 0$ and $M = \frac{1}{2} diag\{\tau_x^{-1}, \tau_\lambda^{-1}\}$ we have

$$\tilde{P} \;\; = \;\; \frac{1}{2} \dot{z}^T Q^T M Q \dot{z} = \frac{1}{2} \dot{x}^T \tau_x \dot{x} + \frac{1}{2} \dot{\lambda}^T \tau_\lambda \dot{\lambda} \tag{5.11}$$

The time derivative of the storage function (5.11) along the system of equations (5.9) can be computed as

$$\dot{\tilde{P}} = -\dot{x}^\top \nabla_x^2 f(x) \dot{x} - \dot{x}^\top \dot{u} \leq -\dot{x}^\top \dot{u} = \dot{u}^\top \dot{y} \tag{5.12}$$

which implies that the system (5.9) is passive. Further for $u = 0$ we have $\dot{\tilde{P}} = 0 \implies \dot{x} = 0$ (x is some constant). Using this in the first equation of (5.9) we get that λ is a constant, proving

asymptotic stability of $\bar{z}$. ■

Inequality constraints: We now define the inequality constraint $g_i(\tilde{u}) \leq 0$ as the following hybrid dynamics

$$\tau_\mu \dot{\mu}_i = (g_i(\tilde{u}))^+_{\mu_i} \tag{5.13}$$

where $\tilde{u} \in \mathbb{R}^n$ and $i \in \{1 \cdots p\}$. The positive projection of $g_i(\tilde{u})$ can be written as

$$(g_i(\tilde{u}))^+_{\mu_i} = \begin{cases} g_i(\tilde{u}) & \mu_i > 0 \\ \max\{0, g_i(\tilde{u})\} & \mu_i = 0 \end{cases} \tag{5.14}$$

Note that the discontinuity in the above equations occurs when $g_i(\tilde{u}) < 0$ and $\mu_i = 0$, the value of $g_i(\tilde{u})^+$ switches from $g_i(\tilde{u})$ to 0. To make this more visible, we redefine these equations equivalently as follows; if (i) ($\mu_i > 0$ or $g_i(\tilde{u}) > 0$) then $(g_i(\tilde{u}))^+_{\mu_i} = g_i(\tilde{u})$ else (ii) $(g_i(\tilde{u}))^+_{\mu_i} = 0$. The projection is said to be active in the second case. Let $\mathcal{P}$ represent the power set of $\{1 \cdots p\}$, then we define the function $\sigma : [0,\ \infty) \to \mathcal{P}$ as follows

$$\sigma(t) = \{i \mid \text{ if } \mu_i(t) = 0 \text{ and } g_i(\tilde{u}) \leq 0 \, \forall i \in \{1, ..., p\}\} \tag{5.15}$$

where the projection is active. With $\sigma(t)$ representing the switching signal, (5.13) now takes the form of a switched system

$$\tau_\mu \dot{\mu}_i = g_i(\tilde{u}, \sigma) = \begin{cases} g_i(\tilde{u}); & i \notin \sigma(t) \\ 0; & i \in \sigma(t) \end{cases} \tag{5.16}$$

The overall dynamics of the p inequality constraints $g_i(\tilde{u}) \leq 0 \ \forall i \in \{1 \cdots p\}$ can be written in a compact form as:

$$\tau_\mu \dot{\mu} = g(\tilde{u}, \sigma) \tag{5.17}$$

where μ_i and $g_i(\tilde{u}, \sigma)$ are i^{th} components of μ and $g(\tilde{u}, \sigma)$ respectively. It is well known that, a sufficient condition for a switched system to be passive system is that the storage function should be common for all the individual subsystems. In general it is not easy to find such storage

functions. Here we use passivity property defined with 'multiple storage functions'Zefran et al. (2001b). Consider the following storage function(s)

$$S_{\sigma_q}(\mu) = \frac{1}{2}\sum_{i \notin \sigma_q} \dot{\mu}_i^2 \tau_{\mu_i} \quad \forall \sigma_q \in \mathcal{P} \tag{5.18}$$

Proposition 22 *The switched system (5.17) is passive with multiple storage functions S_{σ_q} (defined one for each switching state $\sigma_q \in \mathcal{P}$), input port $u_s = \dot{\tilde{u}}$ and output port $y_s = \dot{\tilde{y}}$ where $\tilde{y} = \sum_{\forall i} \mu_i \nabla_{\tilde{u}} g_i(\tilde{u})$. That is, for each $\sigma_p \in \mathcal{P}$ with the property that for every pair of switching times (t_i, t_j), $i < j$ such that $\sigma(t_i) = \sigma(t_j) = \sigma_p \in \mathcal{P}$ and $\sigma(t_k) \neq \sigma_p$ for $t_i < t_k < t_j$, we have*

$$S_{\sigma_p}(\mu(t_j)) - S_{\sigma_p}(\mu(t_i)) \leq \int_{t_i}^{t_j} u_s^\top y_s dt \tag{5.19}$$

Proof. For the proof, refer to Kosaraju et al. (2018) ■

Proposition 23 *The equilibrium set Ω_e defined by constant control input $\tilde{u} = \tilde{u}^*$ of (5.13)*

$$\Omega_e = \{(\bar{\mu}, \tilde{u}^*) \,|g_i(\tilde{u}^*) \leq 0, \;\; \bar{\mu}_i g_i(\tilde{u}^*) = 0 \;\; \forall i \in \{1, \ldots, p\}\} \tag{5.20}$$

is asymptotically stable.

Proof. For the proof, refer to Kosaraju et al. (2018) ■

The overall optimization problem: In this subsection we define a power conserving interconnection between passive systems associated with optimization problem with an equality constraint (5.9) and an inequality constraint (5.13).

Proposition 24 *Consider the interconnection of passive systems (5.9) and (5.13), via the following interconnection constraints $u = \tilde{y} + v$ and $\tilde{u} = x$, $v \in \mathbb{R}^p$. The interconnected system is then passive with port variables $\dot{v}$, $-\dot{x}$. Moreover for $v = 0$ the interconnected system represents the primal-dual gradient dynamics of the optimization problem*

$$\begin{aligned} &\underset{x \in \mathbb{R}^n}{\text{minimize}} \quad f(x) \\ &\text{subject to} \quad h(x) = 0, \quad g_i(x) \leq 0 \quad i = 1, \ldots, p \end{aligned} \tag{5.21}$$

and the trajectories converge asymptotically to the optimal solution of (5.21).

Proof. For the proof, refer to Kosaraju et al. (2018). The interconnected system is shown in Fig. 5.2 ■

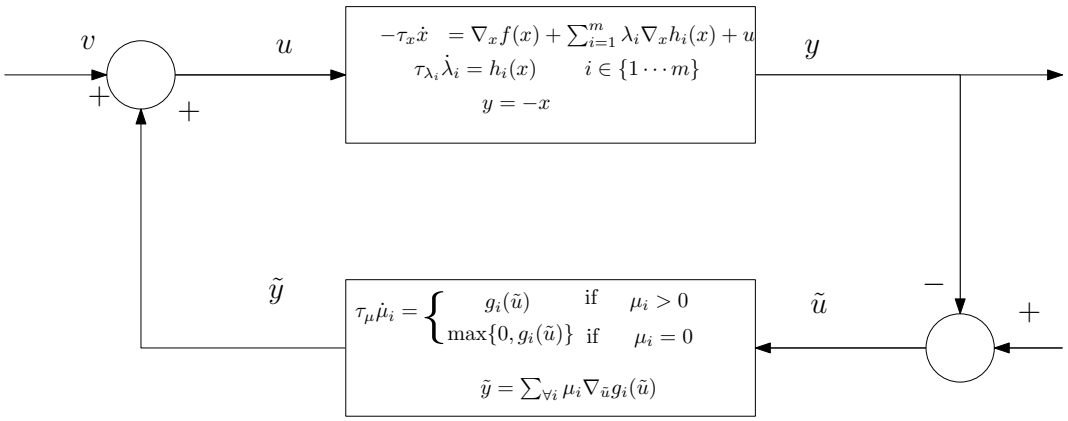

Figure 5.2 Individual Primal-dual dynamics interconnection

5.2 Building Energy Management Formulation

This subsection describes the mathematical formulation of the energy management problem of building HVAC systems. The problem is formulated by taking into account the interaction between the multiple consumers and a single producer in achieving social welfare. The rising opportunities for demand side flexibility enables the consumers to manage their load to reduce their costs, in this context, we model the coalition by group of consumers in order to have access to wholesale energy markets. The coalition coordinator or energy provider purchases the electricity from wholesale energy markets and resells to each member of the coalition using a simple price structure. A time-of-use (TOU) pricing is considered for the simulation study. Furthermore, each member of the coalition tries to maximize his own benefit by contributing to overall demand reduction. A schematic representation of the interaction between coalition coordinator and group of consumers is shown in Fig. 5.3. In order to illustrate the energy management problem, a simulated medium sized commercial building with different zones is considered. The zone thermal dynamics is one of the essential component of the modeling building energy systems.

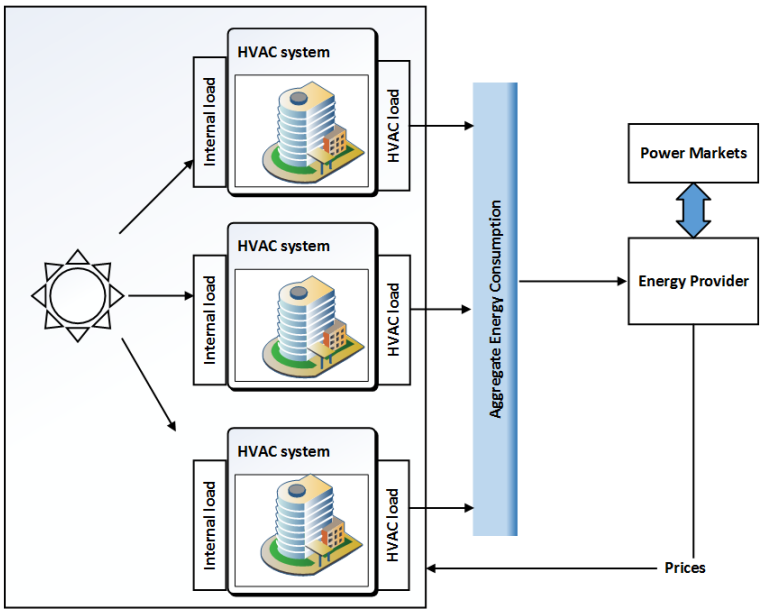

Figure 5.3 Coalition model of producer-consumer interaction

The thermal dynamics of a multi-zone building can be represented using a resistance-capacitance network and the governing dynamics are given by Chinde et al. (2016b):

$$C_i\dot{T}_i = \sum_{j\in\mathbb{N}_i} \frac{(T_j - T_i)}{R_{ij}} + \frac{(T_\infty - T_i)}{R_{i0}} + u_i + d_i \tag{5.22}$$

where $\mathbb{N}_i$ denotes all resistors connected to the i^{th} capacitor (includes zone and surface capacitances), T_i is the temperature of the i^{th} zone and, T_∞ denotes the ambient temperature. C_i is the thermal capacitance of the i^{th} zone, R_{ij} is the thermal resistance between zone i and zone j, R_{i0} is the thermal resistance between zone i and ambient conditions, u_i is the heating/cooling input to the zone i and d_i denotes the heat gain due to sources such as solar, occupancy etc.

The objective is to define the total welfare function of the coalition of consumers under the operational and market clearing constraints. The optimization problems for each consumer and producer at each time slot is given as below.

The optimization problem for each consumer i is given as follows

$$\begin{aligned} \underset{x_i}{\text{maximize}} \quad & u_i(x_i) - px_i \\ \text{subject to} \quad & x_i^{min} \leq x_i \leq x_i^{max}. \end{aligned}$$

Each of these consumers has a private utility function $u_i(x_i)$, which represents the utility the consumer derives by consumption of x_i units of power. p stands for the market price. We assume that for all time slots and across all consumers the utility function $u_i(x_i) : \mathbb{R} \to \mathbb{R}$ is concave and monotonically increasing function.

The objective of energy provider is to maximize his profits and is given by

$$\begin{aligned} \underset{\bar{x} \geq 0}{\text{maximize}} \quad & p\bar{x} - u(\bar{x}) \\ \text{subject to} \quad & \bar{x} = \sum_{i=1}^{N} x_i \end{aligned}$$

where, $\bar{x}$ denotes the total supply available to the consumers. We further assume the function $u(\bar{x}) : \mathbb{R} \to \mathbb{R}$ is convex and strictly monotonically increasing. Once we have the consumer and producer cost functions,

The social welfare problem is formulated as the net benefits of the consumers and producer Wei (2014), and is given by

$$\begin{aligned} \underset{x_i, \bar{x}}{\text{maximize}} & \sum_{i=1}^{N} u_i(x_i) - u(\bar{x}) \\ \text{subject to } \bar{x} = & \sum_{i=1}^{N} x_i \quad x_i^{min} \leq x_i \leq x_i^{max} \end{aligned}$$

Using the generic formulation discussed above, the energy management of HVAC system is formulated by considering the discomfort and generation costs as consumer and producer utility functions, respectively Ma et al. (2016). This can be formulated as

$$\begin{aligned} \underset{T_i, q}{\text{minimize}} \quad & -\left(\sum_{i=1}^{N} U_i(T_i) - U(q) \right) \\ \text{subject to} \quad & \sum_{i=1}^{N} \theta \left(\sum_{j \in \mathbb{N}_i} \frac{(T_j - T_i)}{R_{ij}} + \frac{(T_\infty - T_i)}{R_{i0}} + d_i \right) = q \\ & T_i^{min} \leq T_i \leq T_i^{max} \quad i \in \{1, \ldots, N\} \end{aligned} \tag{5.23}$$

where, $U_i(T_i) = b_i - \gamma_i(T_i - T_i^{ref})^2$, $U(q) = \rho_1 q^2 + \rho_2 q + \rho_3$ $(\rho_1 > 0)$ and θ denotes the conversion factor from energy consumption to energy demand Henze and Krarti (2005). The coefficients $\gamma_i > 0$ determine the tradeoff between cost and comfort Hämäläinen et al. (2000). The steady state dynamics of (5.22) is considered to relate energy supply and demand. In the compact notation, the Lagrangian is given as

$$\begin{aligned} \mathcal{L} &= U(q) - U(T) + \lambda^T(AT + b - q) \\ &\quad + \mu_l^T(T^{min} - T)^+ + \mu_h^T(T - T^{max})^+ \end{aligned} \tag{5.24}$$

where, $U(T) = \sum_{i=1}^{N} U_i(T_i)$. The primal dual dynamics of (5.24) is given as

$$\begin{aligned} \tau_T \dot{T} &= \nabla U(T) - A^T\lambda + \mu_l - \mu_h \\ \tau_q \dot{q} &= -\nabla U(q) + \lambda \\ \tau_\lambda \dot{\lambda} &= AT + b - q \\ \tau_{\mu_l} \dot{\mu_l} &= (T^{min} - T)^+_{\mu_l} \\ \tau_{\mu_h} \dot{\mu_h} &= (T - T^{max})^+_{\mu_h} \end{aligned} \tag{5.25}$$

Proposition 25 *The primal-dual dynamics* (5.25) *converges asymptotically to the optimal solution of* (5.23).

Proof. Since the optimization problem (5.23) has a strictly convex cost function and affine constraints, the result follows from Propositions 21 - 24. ∎

5.3 Simulation Results

In this section, a simulated study is conducted using a building model emulating the ERS testbed ERS (2015), which represents a small-sized commercial building as shown in Fig. 5.4. This simulated model consists of two side-by-side independent and similar zones marked as A and B and distributed in four directions, East, South, West, and North, respectively. These zones are served

using two air handling units (AHU) marked A and B, where each AHU will be serving four Variable Air Volume systems (AHU A serving 4 zones (A) in different directions). For simulation purposes, four zones marked as A, distributed in four different directions supplied by a single air handling unit (AHU (A)) are considered. The parameters used for the simulation are shown in Table 5.1.

To illustrate the effect of load reduction during a price surge, a simulated TOU pricing is considered. TOU pricing essentially provides consumers with different rates at different times in a 24 hour period. Fig. 5.5 shows the convergence of the algorithm to its optimal value and also the interplay between supply and demand.

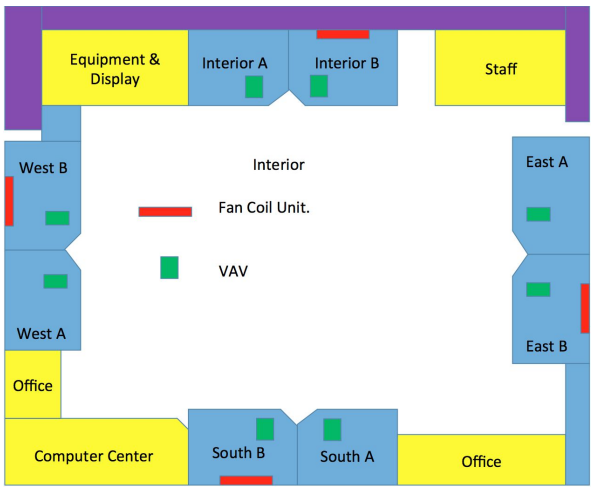

Figure 5.4 Schematic of the simulated building model

Table 5.1 Parameter settings

T_∞, T_{min}, T_{max}, T_i^{ref}	30, 18, 24, 20.5
Inertial time constants (τ_T, τ_q, τ_λ,τ_{μ_l},τ_{μ_h})	1
ρ_1, ρ_2, ρ_3	0.5, 2, 0
b_i, d_i, θ	40, 0.5, 3
R_{10}, R_{20}, R_{30}, R_{40}	11.5,11.5,11.5,15.5

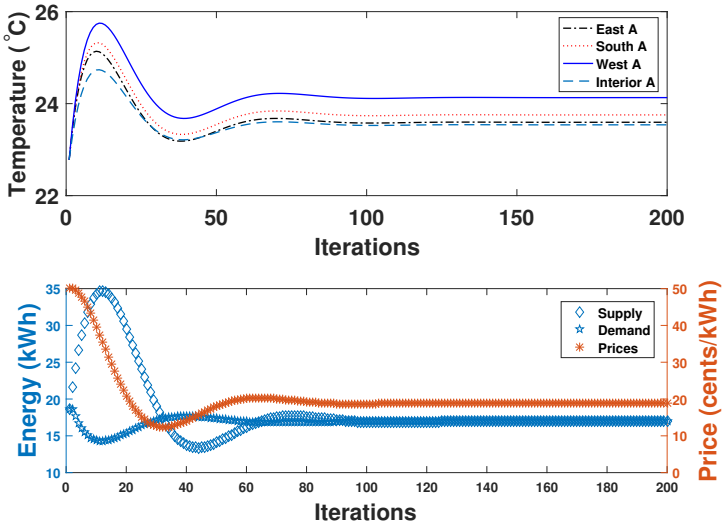

Figure 5.5 Zone temperature, Supply (q)-demand and pricing profiles

In order to evaluate the proposed algorithm for the 24 hour period, the internal load profile as shown in Fig. 5.6 is used which is the sum of heat gains due to occupancy and solar radiation. The occupancy load is computed based on the simulated test bed requirements based on ERS (2015) using the fraction of total occupancy profile (100% occupancy during occupied hours (9am to 5pm) and 30% during unoccupied hours). Similarly the solar load is calculated based on the global horizontal irradiance data collected from Typical Meteorological Year (TMY3) weather file Wilcox and Marion (2008). The outside air temperature profile Wilcox and Marion (2008) for summer is considered as shown in Fig. 5.7 to illustrate the interplay between increase in cooling load and the TOU pricing. The temperature profile for a particular zone (East A) is shown in Fig. 5.7 to illustrate the zone behavior to the TOU pricing for a hot summer day. It can be seen that during the time when prices are high the zone temperatures vary while contributing to the overall demand reduction.

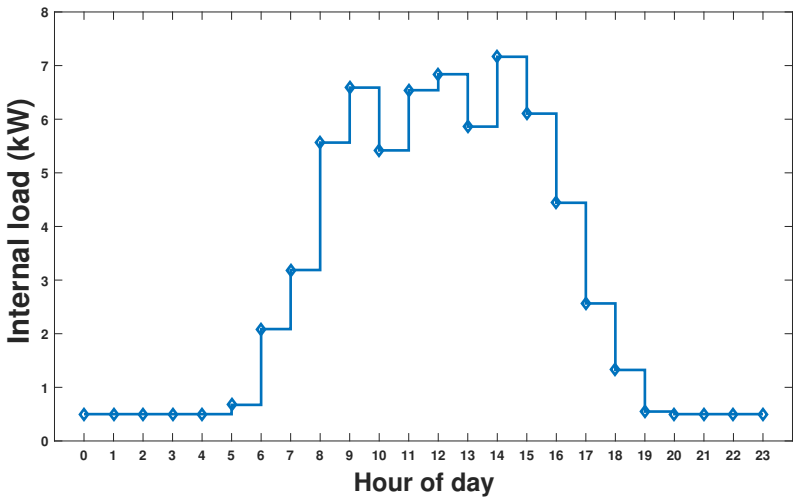

Figure 5.6 Internal load

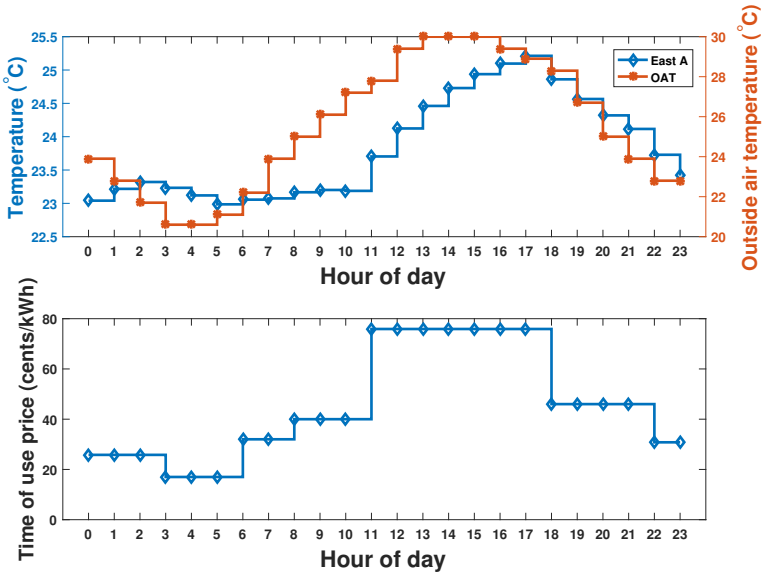

Figure 5.7 Time of use prices and zone temperatures

As a result there is a reduction in cooling load of the building as shown in Fig. 5.8 in comparison to the building when there is no energy management. Hence, the proposed algorithm effectively reduces the peak load, resulting in overall cost reduction.

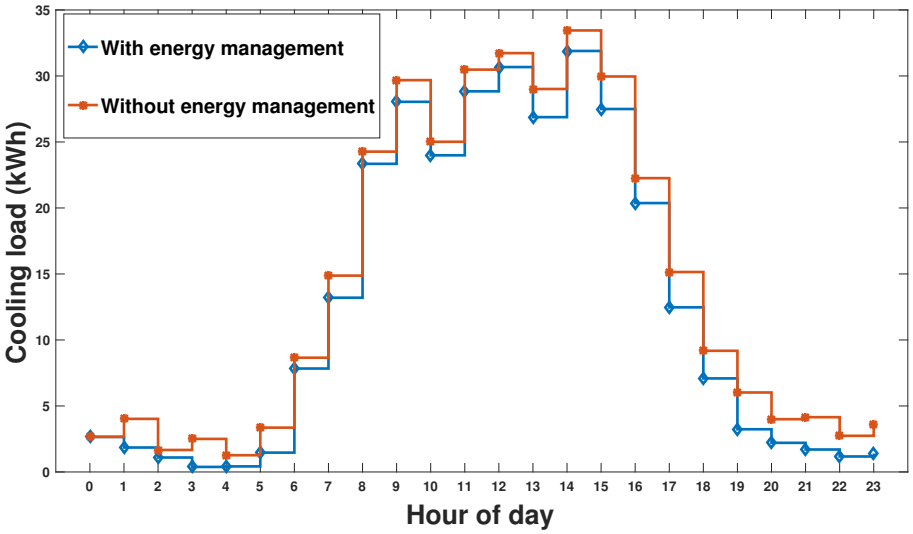

Figure 5.8 Cooling load

5.4 Conclusions

On the demand-side, buildings have the huge potential for providing ancillary services to the grid either by adjusting operational setpoints or adjusting individual components to track a regulation signal. Specifically, social welfare problem is formulated to maximize benefits of both the producers and consumers and is cast as a standard optimization problem. The standard optimization problem is naturally represented as an interconnection of two subsystems 1) equality constrained optimization problem 2) inequality constraints. The framework (BM) and the tool (passivity) used in Chapter 4 are leveraged to analyze these subsystems individually and using the compositional property of passivity the overall system stability is guaranteed. Firstly, the primal-dual equations of equality constrained optimization problem admit a BM representation. The Lyapunov functions derived from Krasovskii method are used to establish passivity and stability of the system. Secondly, the inequality constraints dynamics are represented as a switched system using the notion of passivity for hybrid systems both passivity and stability are established. The overall convergence is guaranteed by proving the asymptotic stability of individual subsystems using the compositional

property of passivity. This procedure is supported by energy management problem in buildings to reduce the overall demand by varying the zone temperature values during the high prices whereby producers incur low generation costs and consumers stay in their comfortable bands.

CHAPTER 6. A VOLTTRON™ BASED IMPLEMENTATION OF SUPERVISORY CONTROL USING GENERALIZED GOSSIP FOR BUILDING ENERGY SYSTEMS

Building energy systems comprising of many subsystems with local information and heterogeneous preferences demand the need for coordination in order to perform optimally. The performance required by a typical airside HVAC system involving a large number of zones are multifaceted involves attainment of various objectives (such as optimal supply air temperature) which requires coordination among zones. As previous Chapters are devoted to modeling (Chapter 3), control (Chapter 4) and optimization (Chapter 5), this chapter is mainly focused to outline a real-life implementation of the Generalized Gossip-based distributed optimization framework on the Iowa Energy Center's Energy Resource Station (ERS) testbed with the objective to reduce energy costs while maintaining zone comfort. These goals are accomplished by implementing the proposed framework within a distributed multi-agent control platform VOLTTRON™, recently developed by the Pacific Northwest National Laboratory (PNNL). The platform is aimed at improving energy efficiency and participate in demand response by controlling the loads in buildings.

6.1 Problem Setup

Buildings are complex energy systems composed of multiple subsystems which have different mathematical structures and evolve in different scales either in time or space. These components are interconnected due to which there are inherent dependencies between the local and the system-wide events. Building efficiency needs to be considered as a means to provide occupant comfort and safe indoor environment and also building systems, in particular, has distributed nature, which demands the need for distributed control architectures and optimization. There are several disadvantages associated with the centralized optimization such as handling large scale systems with

given time complexity and scalability issues often lead to the path for distributed optimization. The computational complexity in the distributed setup is addressed primarily based on the modularity in the modeling and control design phases. Distributed optimization problems arise in various fields of engineering where the set of agents coordinate to perform the task optimally.

Multi-agent coordination and control framework is adopted and tested in diverse applications and in the context of building systems application Cai et al. (2015) provides a multi-agent control methodology for optimal control of centralized air conditioning systems. We have proposed a modular optimization framework in Jiang et al. (2016), where the supervisory optimization scheme is completely decoupled from the data-driven micro-level modeling aspect leading to a significantly scalable and flexible architecture. The primary goals of the proposed framework are to achieve scalability, robustness, flexibility and low-cost commissioning. We present a formulation of the proposed methodology with regards to an illustrative example scenario for air-side heating, ventilation and air-conditioning (HVAC) system as shown in Fig. 6.1. In this energy supply-demand problem, individual zones become energy consumers that are served with conditioned air by an air handling unit (AHU).

6.1.1 Air-side HVAC (AHU-VAV) system

The general layout of a typical AHU-VAV HVAC system is shown in Fig. 6.1. While a central AHU provides conditioned air to each variable-air-volume (VAV) box, VAVs in turn supplies conditioned air to each zone. From a supervisory decision-making perspective, a few setpoints (e.g., supply air temperature (SAT) setpoint, mixed air temperature setpoint and duct static pressure setpoint) need to be determined for energy usage minimization while maintaining zone comfort levels. For simplicity, SAT setpoint is considered as the optimization variable to demonstrate the effectiveness of the proposed algorithm. Consider a situation where every zone in a building has the same comfort requirement and the same external/internal loads. In that case, a common SAT setpoint can be determined that satisfies the requirement of each zone. However, in reality due to the diversity of zones, AHU SAT is typically kept at a very low value (e.g., $55^{\circ}F$) such that VAVs

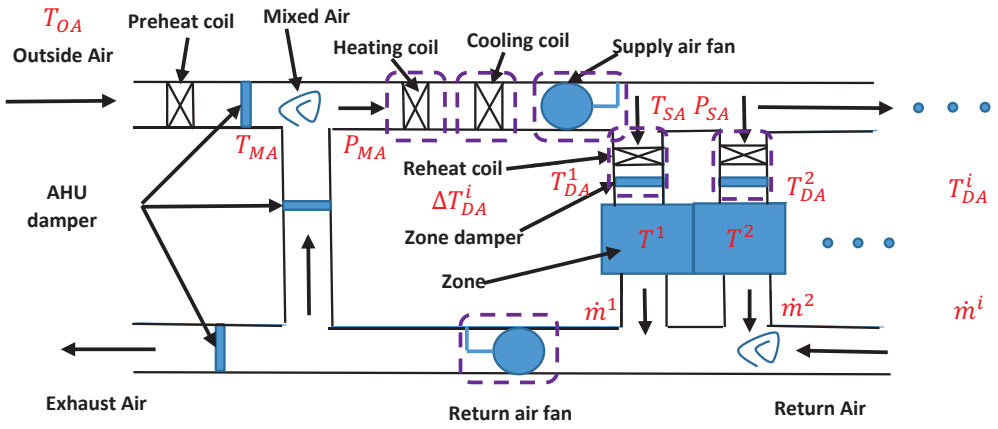

Figure 6.1 Typical layout of an AHU-VAV HVAC system

can reheat the supply air as needed before it enters the zones. Therefore, optimization can help decide a variable setpoint that reduces the excess energy use in this 'first cooling and then reheating' process. SAT setpoint can be further optimized based on the knowledge of outside air condition and zone thermal dynamics. On the specific energy consumption, the energy consuming components considered are the cooling/heating energy consumed by AHU, the reheat energy consumed by VAV boxes and the power cost by return air and supply air fans. Additionally, energy consumption by some other electrical equipments, e.g., chillers, chiller pumps, and water loop pumps are used for energy calculation and not for the optimization process as the SAT setpoint is the unique decision variable. For more details on the problem description and the assumptions refer to Jiang et al. (2016).

Cooling/heating Energy: In AHU, there are two modes, i.e., cooling and heating modes corresponding to cool down and heat up the mixed air temperatures respectively. In this paper, we only consider the cooling mode for the problem formulation. The following expression describes the cooling energy consumed by the cooling coil in the AHU

$$E_C = \alpha_c \dot{m} c_p (T_{SA} - T_{MA}) = \alpha_c \sum_{i \in \mathcal{V}} \dot{m}^i c_p (T_{SA} - T_{MA})$$

where i represents i^{th} zone in a building, $\mathcal{V} = \{1, 2, ..., N\}$. The heating mode follows the similar formula with reheat energy coefficient.

Reheat Energy: Energy consumed by a reheat coil in a VAV box can be expressed by the following formula

$$E_{RH} = \alpha_h \sum_{i \in \mathcal{V}} \dot{m}^i c_p (T^i_{DA} - T_{SA})$$

Fan Power: In this work, we simplify the fan power as a second order polynomial which is function of the air flow rate

$$E_F = a_0 + a_1 \dot{m} + a_2 \dot{m}^2$$

where a_0, a_1 and a_2 are the polynomial coefficients.

Actual Energy: The total amount of actual energy including the cooling energy consumed in AHU, the reheat energy consumed in VAVs and the fan power can be written as

$$E_{Act} = E_C + E_{RH} + E_F$$

As mentioned above, the mixed air consists of return air and outside air such the relation among these three variables, i.e., T_{MA}, T_{RA} and T_{OA} can be expressed as $T_{MA} = \lambda T_{RA} + (1-\lambda) T_{OA} = \lambda \frac{\sum_{i \in \mathcal{V}} \dot{m}^i T^i}{\sum_{i \in \mathcal{V}} \dot{m}^i} + (1-\lambda) T_{OA}$, where λ herein indicates the fraction of return air in mixed air.

Furthermore, at a reheat coil, the relation between discharge air temperature T^i_{DA} and supply air temperature T_{SA} in a VAV box is expressed by $T^i_{DA} = T_{SA} + \Delta T^i_{DA}$. ΔT^i_{DA} is the difference between supply air temperature and discharge air temperature which in this context is with respect to VAV reheat coil parameters, namely, inlet hot water temperature (T_{wi}), inlet hot water mass flow rate ($\dot{m}^i_w$), inlet air temperature (i.e., supply air temperature, T_{SA}) and air mass flow rate ($\dot{m}^i$). Also, the zone temperature model can be described in this case as a function with regards to several parameters: $T^i = f(T_{SA}, \dot{m}^i, \Delta T^i_{DA}, T_{OA})$. Regarding more details about specific expression of the zone thermal dynamics refer to Chinde et al. (2015). The major constraints in this energy optimization problem due to the capabilities of actuators and comfort requirements which are considered as follows:

$\dot{m}^i \in [\dot{m}^i_{min}, \dot{m}^i_{max}]$: Due to the VAV damper capacity the air flow rate is bounded above and below;

$T_{SA} \in [(T_{SA})_{min}, (T_{SA})_{max}]$: the supply air cannot be heated up or cooled down infinitely due to the capacity of a heating or cooling coil;

$T^i \in [T_{HSP}, T_{CSP}]$: the zone temperature is controlled between the cooling and heating temperature setpoints based on the real test bed requirements;

$\Delta T^i_{DA} \in [(\Delta T_{DA})_{min}, (\Delta T_{DA})_{max}]$: the discharge air temperature is as well controlled in between a range due to the capacity of a reheat coil.

The proposed supervisory control framework based on distributed optimization aims at minimizing the building energy consumption while satisfying different zone comfort requirements. Based on the above discussion the cost function proposed for determining the optimal AHU SAT can be expressed as follows

$$\begin{aligned} & T^*_{SA} = \underset{T_{SA}}{\operatorname{argmin}}\, J \\ & \text{s.t. } T_{SA} \in [(T_{SA})_{min}, (T_{SA})_{max}] \\ & \text{where } J = \omega E_{Act} + (1-\omega)\rho \sum_{i \in \mathcal{V}} \dot{m}^i \|T^i - T^i_{ref}\|_2^2 \end{aligned} \tag{6.1}$$

where, ω is defined as the weight index that indicates the trade-off between the energy consumption and zone comfort requirements. For avoiding the issue of scaling between energy and comfort cost values, we also introduce a scaling parameter ρ. With the above setup, the overall distributed optimization problem is stated as follows.

$$\begin{aligned} & T^*_{SA} = \underset{T_{SA}}{\operatorname{argmin}} \sum_{i=1}^{N} J^i \\ & \text{s.t. } T_{SA} \in [(T_{SA})_{min}, (T_{SA})_{max}] \\ & \text{where } J^i = \omega\{\alpha_c \dot{m}^i c_p (T_{SA} - \lambda \frac{\sum_{i \in \mathcal{V}} \dot{m}^i T^i}{\sum_{i \in \mathcal{V}} \dot{m}^i} \\ & - (1-\lambda) T_{OA}) + \alpha_h \dot{m}^i c_p \Delta T^i_{DA} + (a_0 + a_1 \dot{m}^i + a_2 (\dot{m}^i)^2)\} \\ & + (1-\omega)\rho \|T^i - T^i_{ref}\|_2^2 \end{aligned} \tag{6.2}$$

The third term on the right hand side of cost function should be $a_0 + a_1 \sum_{i \in \mathcal{V}} \dot{m}^i + a_2 (\sum_{i \in \mathcal{V}} \dot{m}^i)^2$ in the global objective function. The term of $a_2 (\sum_{i \in \mathcal{V}} \dot{m}^i)^2$ affect the distributed characteristics of our solution approach. In this context, it is bounded above by $a_2 \sum_{i \in \mathcal{V}} (\dot{m}^i)^2$ using Cauchy-Schwartz inequality Zhang et al. (2016). Therefore, rather than minimizing the consumption directly, we minimize its upper bound.

6.2 Distributed Optimization Using Generalized Gossip

This section describes a solution approach for the distributed building energy optimization problem formulated above. The approach uses a recently proposed Generalized Gossip-based algorithm. Theoretical contributions to the proposed framework can be found in Jiang et al. (2015).

6.2.1 Background of Generalized Gossip protocol

Consider an undirected graph $\mathcal{G} = (\mathcal{V}, \mathcal{A})$ consisting of N agents, where $\mathcal{V} = \{1, 2, ..., N\}$ and $\mathcal{A} \subseteq \mathcal{V} \times \mathcal{V}$. If $(i, j) \in \mathcal{A}$, then agent i can communicate with agent j. Let the distributed building energy optimization problem be defined on the network as follows:

$$\begin{aligned} &\text{minimize } f(x) = \sum_{i=1}^{N} f^i(x) \\ &\text{subject to } x \in \mathbb{X} \end{aligned} \tag{6.3}$$

where $f^i : \mathbb{R}^M \longrightarrow \mathbb{R}$ are agent level objective functions (possibly convex or non-convex), $\mathbb{X}$ is a nonempty, closed, and compact subset of $\mathbb{R}^M$. x is a vector whose i^{th} component is represented by x^i.

The basic definitions Boyd et al. (2003); Johansson et al. (2008) and assumptions used are:

Definition 26 *A vector $g \in \mathbb{R}^M$ is a subgradient of a convex function $f : \mathbb{R}^M \longrightarrow \mathbb{R}$ at a point $z \in \mathbb{R}^M$ if*

$$f(y) \geq f(z) + g^T(y - z), \forall y \in \mathbb{R}^M$$

Definition 27 *The set of all subgradients of a convex function of f at $z \in \mathbb{R}^M$ is called the subdifferential of f at z, and is denoted by $\partial f(z)$:*

$$\partial f(z) = \{g \in \mathbb{R}^M | f(y) \geq f(z) + g^T(y - z), \forall y \in \mathbb{R}^M\}$$

Assumption 28 (Subgradient boundedness) *There exists a scalar G for all $i = 1, ..., N$ such that*

$$\|g^i(x)\|_2 \leq G, \forall g^i(x) \in \partial f^i(x), \forall x \in \mathbb{X}$$

Note, this assumption can be derived from the *Lipschitz continuity* relationship.

A vector notation of the update law for the proposed algorithm (Nedic and Ozdaglar (2009) and Sarkar et al. (2013)) for the optimization variable is as follows:

$$x(k+1) = (1-\theta)\Pi(k)x(k) + \theta(x(k) - \nabla(k)) \tag{6.4}$$

where $\nabla(k)$ is the subgradient of f^i at $x^i(k)$ computed by agent i. $\Pi \in \mathbb{R}^N \times \mathbb{R}^N$ is the agent interaction matrix. θ is the user-defined control parameter.

6.2.2 Optimization algorithm overview

The proposed supervisory optimizer aims to determine optimal AHU supply air temperature based on information exchange among local zones. The crucial advantage of this framework is that local zones can use any local controllers and suitable modeling scheme. However, as long as they can compute subgradient for local cost function for energy optimization and achieving comfort, the supervisory control layer can run the generalized gossip protocol for global energy optimization.

In this context, each local zone needs modeling of thermal dynamics in order to compute subgradients for their local cost functions (refer Jiang et al. (2016)). For the analysis, although we use a data-driven ARX modeling scheme for zones, any other technique with same input-output conditions can be seamlessly accommodated. However, the local cost functions may be nonsmooth and nonconvex and therefore, subgradients can be found using numerical differentiation for handling nonsmooth functions, but for the case of nonconvexity which arises due to bilinear terms (for example., mass flow rate times temperature) are handled by fixing one variable. The modeling and optimization scheme also consider the local controllers for heating/cooling coil in AHU and dampers, reheat coils in VAV boxes. Currently, simple PI controllers are used for these local controllers (which is common for most of the HVAC equipment in commercial buildings Bengea et al. (2015).

The basic workflow of the supervisory control framework is illustrated in Fig. 6.2. In this framework, an optimization interval is considered within which it is assumed that predictions from zone thermal modeling would be reliable, as well as the optimized AHU supply air temperature setpoint,

would be appropriate. The supervisory decision-making process begins with subgradient-based optimization depending on the initial conditions. The building operation starts with optimized AHU supply air temperature setpoint. After expiry of the optimization interval, the supply air temperature setpoint is re-optimized based on current conditions.

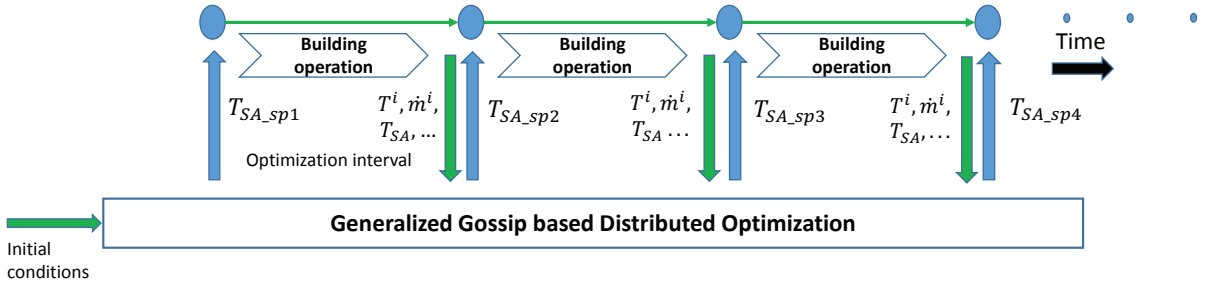

Figure 6.2 Workflow of the supervisory control framework

A schematic representation of the analysis (simulation and experimental) conducted on the ERS testbed which is further described in this section is shown in Fig. 6.3.

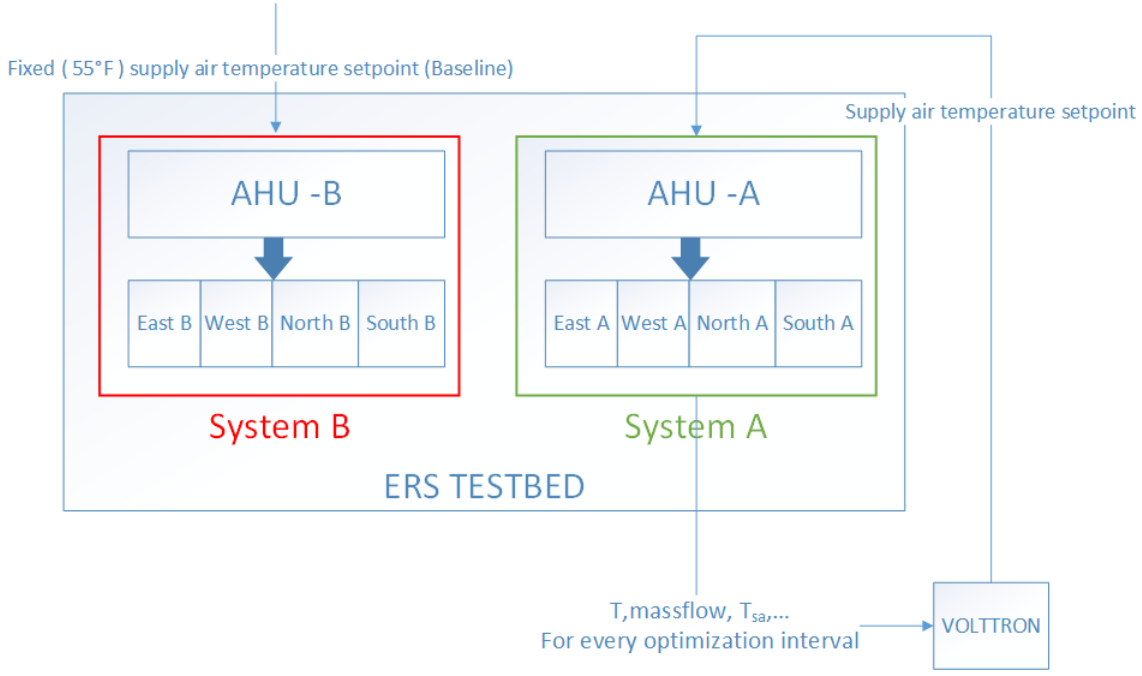

Figure 6.3 Workflow of the simulation/experimental analysis conducted on ERS testbed

The following algorithmic format gives a detailed overview of the entire process.

Algorithm 1 Supervisory Control Algorithm

initialize $\zeta, \theta, T_{SA}(0), T_{SA}(1), \Pi, \alpha_0$
set $u = 1$
loop over u (until building operation schedule expires)
set $k = 2$
loop over k
for $i = 1$ to N **do**
    calculate $J^i(k-1), J^i(k+1)$
    $g^i(k) \approxeq \frac{J^i(k+1) - J^i(k-1)}{2\zeta}$
end for
$T_{SA}(k+1) = P_{\mathbb{X}}[(1-\theta)\Pi T_{SA}(k) + \theta(T_{SA}(k) - \alpha_k g(k))]$
if (termination criterion met) **then**
    Break
else
    $k = k + 1$
end if
end loop over k
Run the building operation with $T_{SA_{sp}} = T_{SA}(k+1)$ over the span of one optimization interval
$T_{SA}(1) = T_{SA_{act}}$ at the last time instant of building operation
$u = u + 1$
end loop over u

For signifying a complete collaboration among zones and simplicity, Π in this context is defined as a uniformly doubly stochastic matrix which indicates that the network is fully connected. u is the number of cycles; each cycle includes one distributed optimization process among local zones and

the simulated building operation over one optimization interval. k indicates iteration number in optimization. $T_{SA_{act}}$ is the actual supply air temperature while $T_{SA_{sp}}$ is the supply air temperature setpoint. ζ denotes the step size.

For validating the proposed algorithm, a simulation study is performed on one AHU supplying four zones based on the physical Energy Resource Station testbed in the Iowa Energy Center Center (2010). The zone thermal modeling was performed using actual historical data collected from the testbed during winter season. For validating the algorithm under different ambient conditions, the testing period in this case study is one month (three different days are shown for the illustration of results). As shown in Fig. 6.4 and Fig. 6.5, optimized supply air temperature setpoint varies under different ambient conditions and is different from the constant baseline condition.

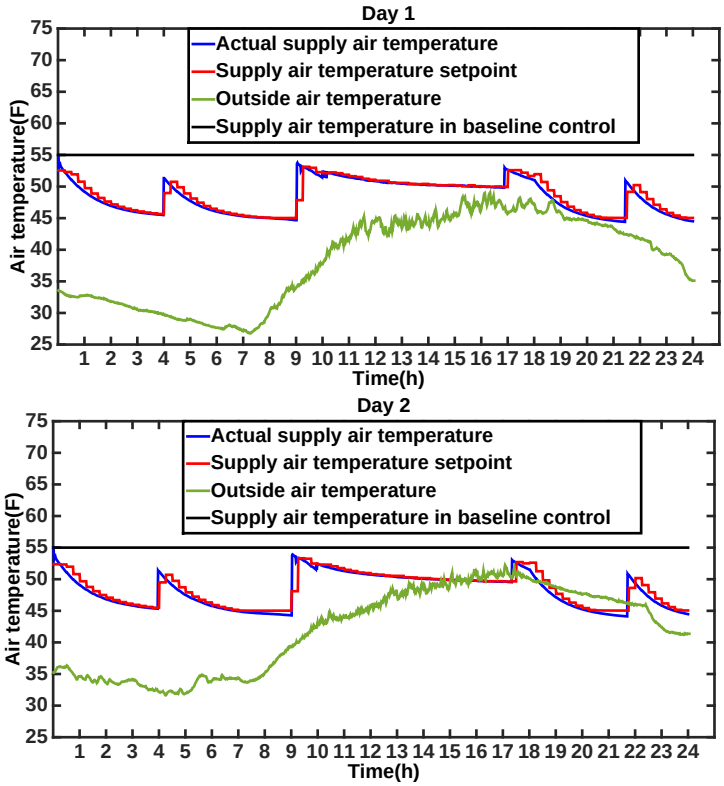

Figure 6.4 AHU supply air temperature under supervisory control and baseline control with different outside air temperatures (Day 1 and Day 2).

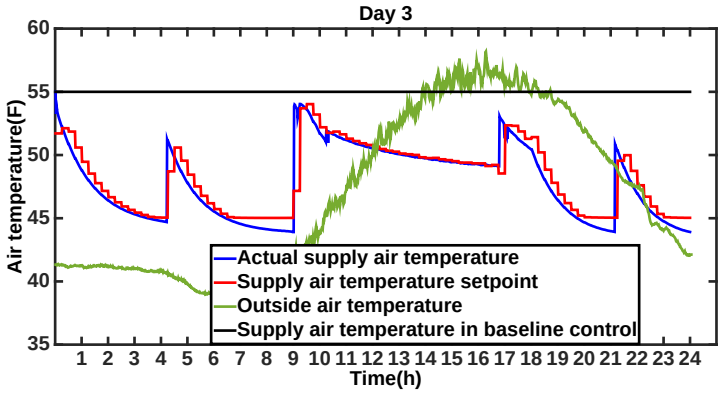

Figure 6.5 AHU supply air temperature under supervisory control and baseline control with different outside air temperatures (Day 3).

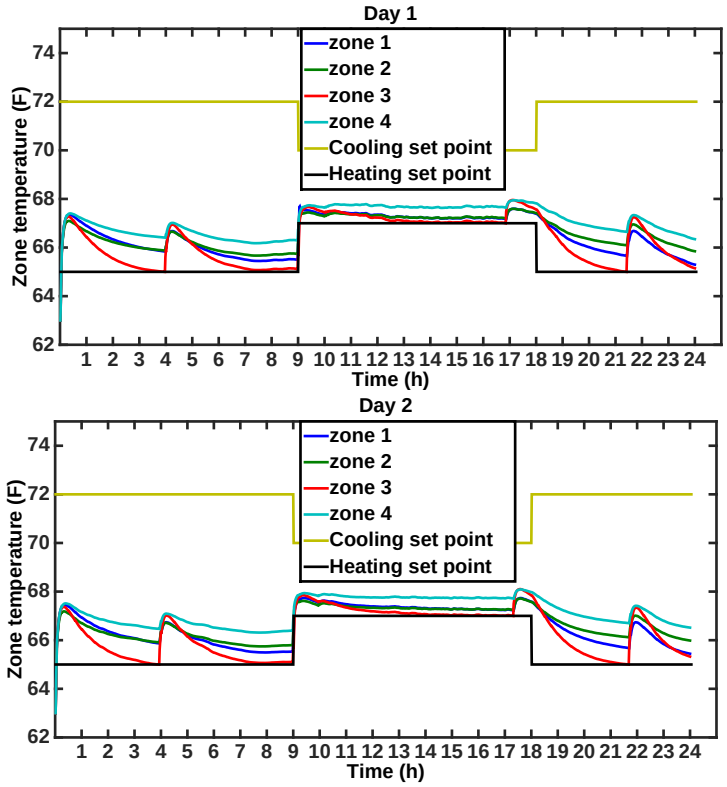

Figure 6.6 Zone temperature regulation during days with different outside air temperatures under supervisory control (Day 1 and Day 2).

Zone temperature regulation performance for all 4 zones with different heating/cooling setpoints during unoccupied and occupied hours is shown in Fig. 6.6 and Fig. 6.7.

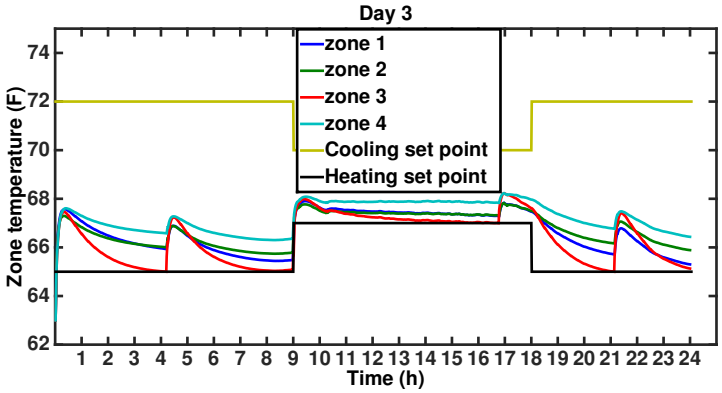

Figure 6.7 Zone temperature regulation during days with different outside air temperatures under supervisory control (Day 3).

The reason why local zone temperature control aims at approaching heating setpoint is because the testing was performed in the winter season in order to save energy. Figure 6.8 shows that in all 28 days, zone temperature by the proposed supervisory control scheme consumes less energy compared to baseline control. The energy consumption during 6 representative days by AHU heating/cooling coils, VAV reheat coils and AHU fans under baseline and supervisory control is shown in Fig. 6.9.

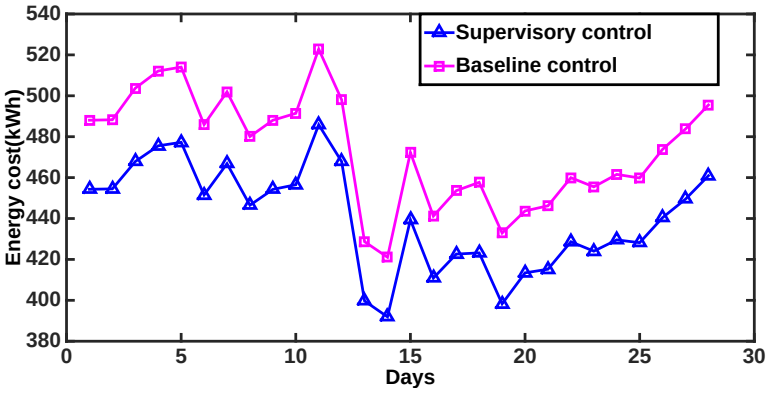

Figure 6.8 Energy cost in 28 test days in winter

The results demonstrate that in the supervisory framework cooling/heating energy consumed in AHU and the fan energy is reduced compared to baseline control, which validates the effectiveness of the proposed algorithm and control framework for HVAC systems.

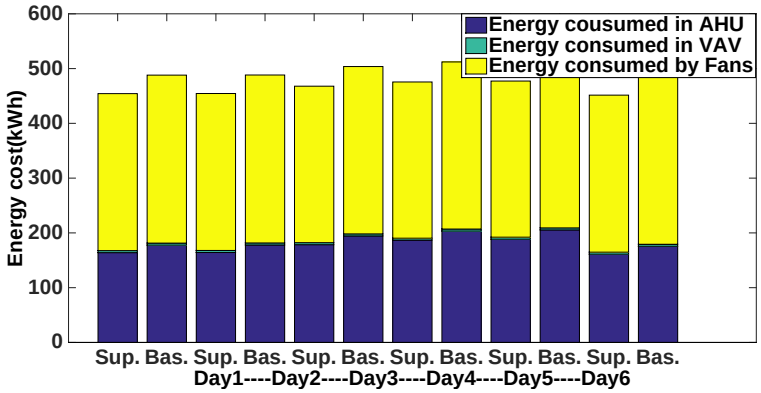

Figure 6.9 Energy consumed in AHU, VAV and by fans by supervisory control and baseline control.

6.3 VOLTTRON^{TM} Platform: Overview & Implementation

VOLTTRON^{TM} Lutes et al. (2014); Haack et al. (2013a) is an open source language-agnostic distributed control and sensing platform developed by Pacific Northwest National Laboratory (PNNL) and targeted towards managing wide spectrum of applications which includes heating, ventilation, and air-conditioning (HVAC) systems, Building to grid applications etc. This open source platform provides benefits in terms of adding additional features and functionality to software such as developing agents and enables integration of various systems to communicate and provides robust environment. The platform has default BACnet, Modbus drivers and provides frameworks for building custom drivers. VOLTTRON^{TM} supports numerous database options of which SQLite is considered as the VOLTTRON^{TM} Historian due to its automatic database creation during the launch and easy to use. The configuration of VOLTTRON^{TM} for the proposed testbed application is shown in Fig. 6.10.

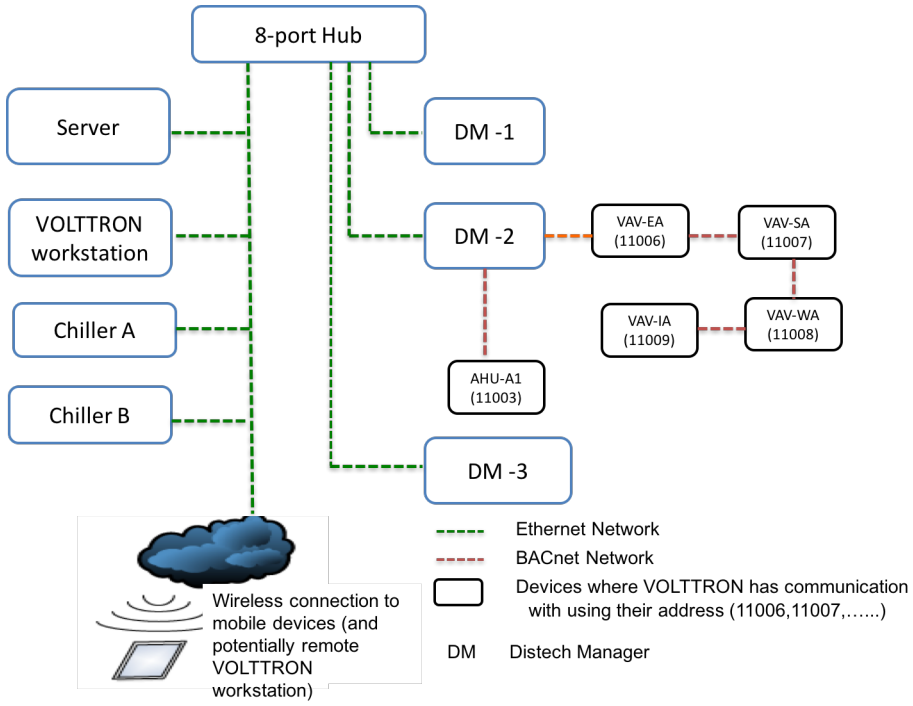

Figure 6.10 Configuration of VOLTTRON^{TM}: there are two networks, i.e., Ethernet network and BACnet network; in the Ethernet network, server, VOLTTRON^{TM} workstation, chiller A, chiller B, and Distech managers are connected; in the BACnet network, AHU and VAVs are connected

VOLTTRON^{TM} workstation is connected to the physical system network over BACnet/IP network and the devices of interest as shown in Fig. 6.10 such as (VAV-EA, VAV-SA etc.,) support BACnet protocol, hence it provides advantage to use default drivers and configure them appropriately.

The software architecture of VOLTTRON^{TM} based implementation is shown in Fig. 6.11. There are several default agents developed in VOLTTRON^{TM} such as the actuator agent, weather agent, listener agent etc., the only agent which implements the proposed algorithm in the VOLTTRON^{TM} framework is the optimization agent. A detailed description of these agents developed in VOLTTRON^{TM} can be found inChinde et al. (2016a); Haack et al. (2013b). Briefly speaking, the work flow is the use of master driver and BACnet proxy agent to collect data (zone temperatures, mass flow rates

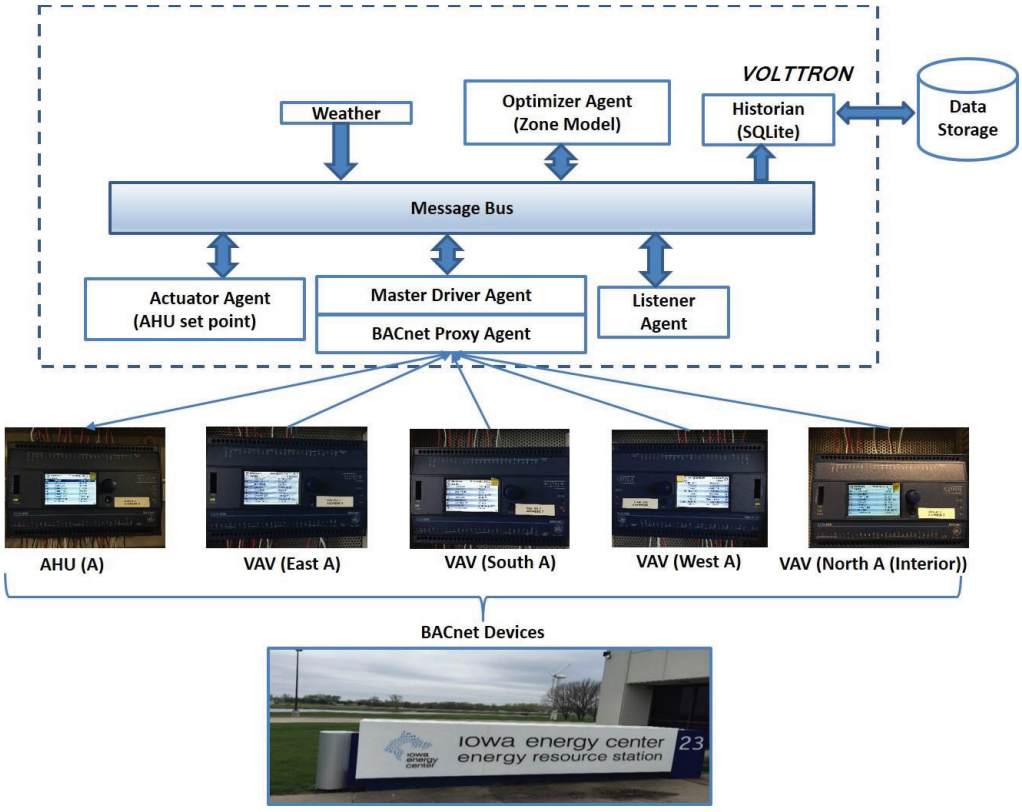

Figure 6.11 Software architecture of VOLTTRON^{TM} based implementation: in the VOLTTRON^{TM}, the BACnet proxy agent connects the BACnet devices (AHU and VAVs); through the master driver agent, they can publish information to the message bus; other agents can subscribed those published information; data from the message bus is stored via historian agent

etc.,) from the individual devices and to publish them onto the message bus. The optimization agent subscribes to the data from message bus and process the information based on the algorithm to publish the optimized supply air temperature setpoint onto message bus which then through actuator agent is sent directly to the device. A more detailed description on the implementation aspects is reported in Chinde et al. (2016a).

For the implementation purpose, we have considered A-test rooms served by air handling unit AHU-A.

6.3.1 VOLTTRON^{TM} agents: Description

The VOLTTRON^{TM} user guide provides a systematic procedure, templates, and examples for developing agents and to install the VOLTTRON^{TM} platform, by which one can develop simple agents for their own purpose. In the proposed setup we have built optimization agent on the top of VOLTTRON^{TM} which avails the existing benefits. The agents in VOLTTRON^{TM} are given as follows: (1) BACnet Proxy agent (2) Master Driver Agent (3) Weather Agent (3) Optimization agent (4) Weather agent (5) Listener Agent (6) Actuator Agent. The functionalities of individual agents are described below:

1. BACnet Proxy Agent: Device communication on a network happens through the virtual BACnet device and this agent is specifically used for communicating with the BACnet devices and managing the virtual BACnet device.

2. Master Driver Agent: Coordination among the drivers of devices is accomplished using this agent.

3. Weather agent: This agent interacts with remote applications such as online weather services like Weather Underground (www.wunderground.com). The weather information is used by the Zone Model to calculate the temperatures needed for computing the subgradients.

4. Optimization Agent: This agent serves the purpose of predicting the temperatures given the weather information and the parameters of the zone model identified using the data from the

ERS test bed. The algorithm described in Jiang et al. (2016) is implemented in Python to calculate the subgradients based on which the optimal AHU supply air temperature (SAT) is calculated.

5. Listener Agent: It logs all the activity on the message bus and is useful in testing the agent functionality in terms of publishing the required data. It can be used as a starting point for developing other agents.

6. Actuator Agent: This agent has the capability to assert control over the devices by accepting commands from the agents and scheduling times to issue commands to devices.

Message Bus in VOLTTRON^{TM} is a common place where data from all the agents and the devices are collected. All agents use publish/subscribe mechanism to communicate with the other agents. All the data published onto the message bus either by the devices or the agents will be collected by the historian and stores for retrieval or analysis purpose such as plotting etc.

6.3.2 Implementation

A detailed description of the steps from installing to configuring devices and writing agents can be found in Lutes et al. (2014). We briefly provide the implementation steps in our setting below:

- Install the VOLTTRON^{TM} by following the steps given in user guide Lutes et al. (2014) and move to the developer branch. ECLIPSE an integrated development environment (IDE) is used as a tool for agent development.

- The machine running the VOLTTRON^{TM} is physically connected through Ethernet network to the DISTECH network manager (router) to which all the individual devices of interest are connected. For the sake of convenience, we have shown only the five devices (1AHU and 4 VAVs) in Fig. 6.11.

- Since the Host machine is Windows, we installed Virtual Machine (VM) to run Linux and VOLTTRON^{TM} and configured VM to use a bridged adapter to avoid problems with different IP address.

- The immediate step after installing VOLTTRON^{TM} is to find and configure the BACnet devices. The scripts such as bacnet_scan and grab_bacnet_config files which are there in the VOLTTRON^{TM} repository can be used to detect the devices and generates a registry configuration file in CSV format for the BACnet driver which consists of a list of point names. This points list can be changed based on user interest.

- Configure the BACnet Proxy Agent by filling the address field in the configuration file with the IP address of Linux machine and specify the subnet mask. Since the BACnet network is on a default port (47808) there is no need to mention the port number.

- Setup the Master Driver Agent which consists of list device configuration files. For each device, we need to create driver configuration file, CSV file and the entry in the Master Driver Agent configuration file.

- Import the VOLTTRON^{TM} into ECLIPSE and launch VOLTTRON^{TM}, BACnet Proxy Agent, Master Driver Agent and Listener Agent using the steps given in Lutes et al. (2014). The output console of Listener Agent displays the device topics and messages.

- Develop the Optimization Agent by subscribing to the data from the message bus and implementing the algorithm scheme provided in section (6.2).

- Launching the Optimization Agent similar to other agents and it publishes the Supply Air Temperature (SAT) setpoint to message bus. Launching Historian agent stores the data to the SQLite database.

- Launch the Actuator Agent and schedule the timing to override the SAT setpoint of the AHU device.

6.3.3 Experimental results and discussion

This section presents the results obtained from the implementation of proposed algorithm using VOLTTRON^{TM} software. Note, that the real testbed works within two modes, i.e., occupied mode

(6:00 AM - 6:00 PM) and unoccupied mode (6:00 PM - 6:00 AM). As the testbed consists of two AHU's (AHU-A and AHU-B), the proposed algorithm is implemented on system A (consists of AHU-A supplying four zones marked as A Fig. 5.4) while system B (AHU-B supplying other four zones marked as B) is operated using a baseline strategy for the comparison of these two systems. The baseline strategy is where, the system B supply air temperature setpoint is fixed at $55°F$.

For the real-time implementation, systems A and B are operated in the following time intervals due to the real test bed conditions:

1. 4:30 PM - 6:00 PM on 07/20/2016
2. 12:30 PM - 6:00 PM on 07/21/2016
3. 12:00 PM - 6:00 PM on 07/22-07/25/2016
4. 12:00 PM - 11:59 PM on 07/29/2016
5. 07/30/2016
6. 07/31/2016

The preliminary observation on energy analysis is conducted by looking into the profiles of key variables such as mixed air temperature, supply air temperature, supply air volumetric flow rate, and zone temperature. Figure 6.12 shows the mixed air temperature, supply air temperature, and supply air temperature set points for systems A and B. It can be observed that supply air temperature set point of system B is $55°F$ while the set point of system A is time-varying and higher than that of system B. Correspondingly the supply air temperatures of these two systems follow the same trend. The mixed air temperature of system B is lower than that of system A while the cooling energy consumed by system A is less than that of system B as the gap between mixed air temperature and supply air temperature is smaller for system A.

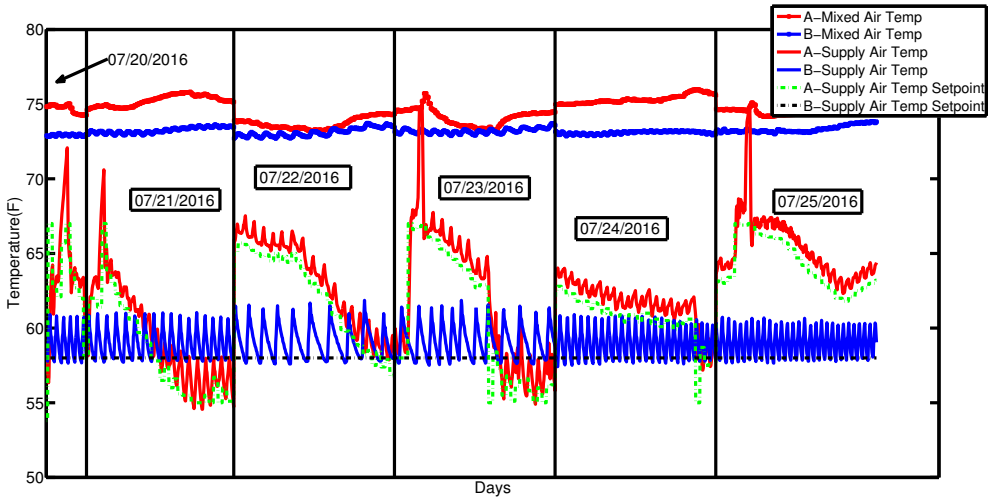

Figure 6.12 Mixed air temperature, supply air temperature and supply air temperature set point comparison between systems A and B from 07/20-07/25/2016

The same phenomenon can also be observed from Fig. 6.13.

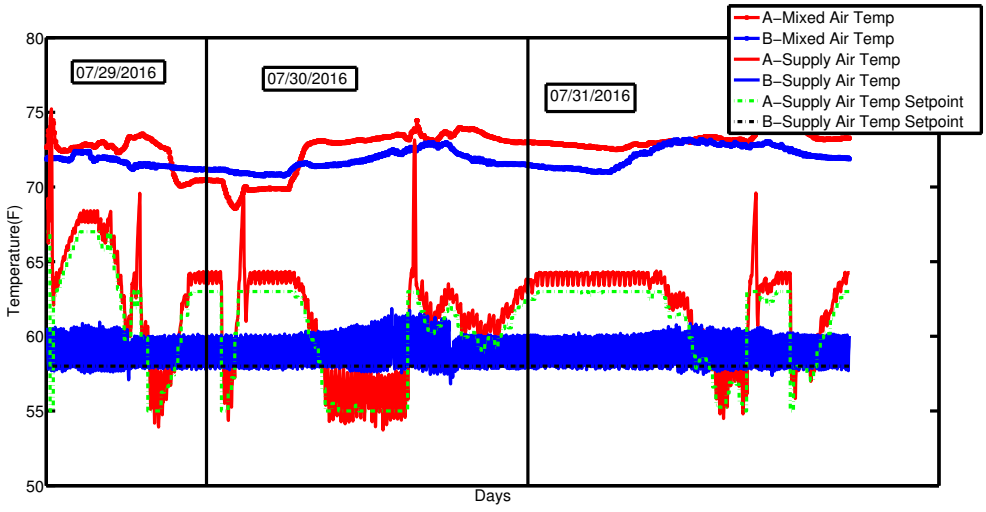

Figure 6.13 Mixed air temperature, supply air temperature and supply air temperature set point comparison between systems A and B from 07/29-07/31/2016

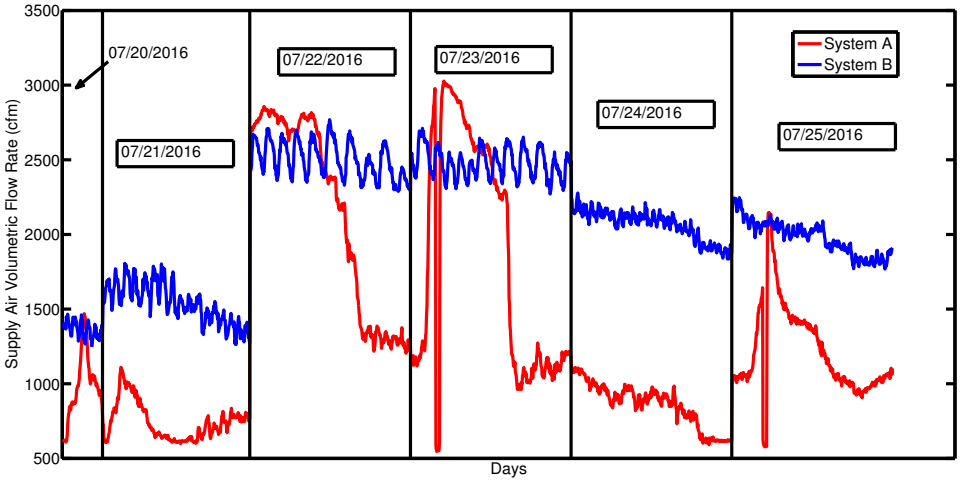

Figure 6.14 Supply air volumetric flow rate comparison between systems A and B from 07/20-07/25/2016

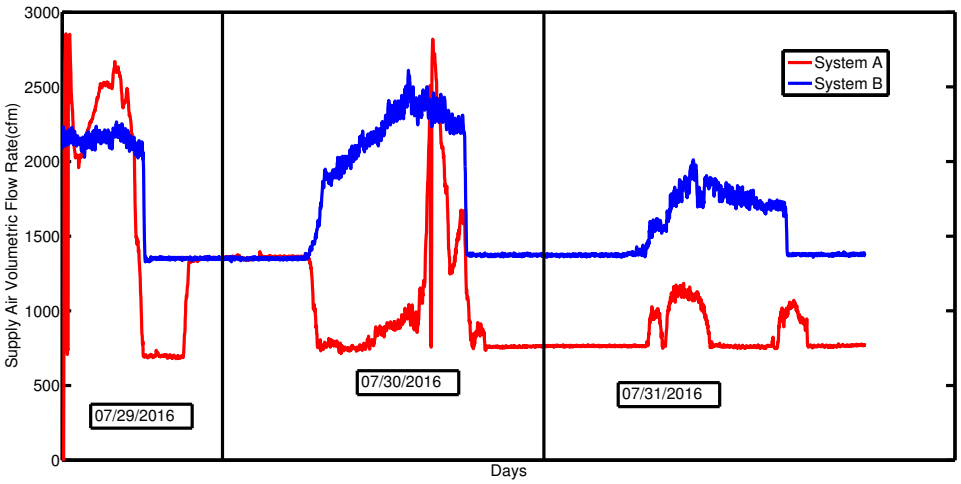

Figure 6.15 Supply air volumetric flow rate comparison between systems A and B from 07/29-07/31/2016

Figures 6.14 and 6.15 show the supply air volumetric flow rates of systems A and B which demonstrate that system A most of the time has lower air volumetric flow rate than system B. It accordingly indicates that system A consumes less fan power to pump conditioned air to local zones. Zone comfort requirement is also a key factor for addressing the difference between systems. Figure 6.16 show the east zone temperatures during 07/29 - 07/31/2016.

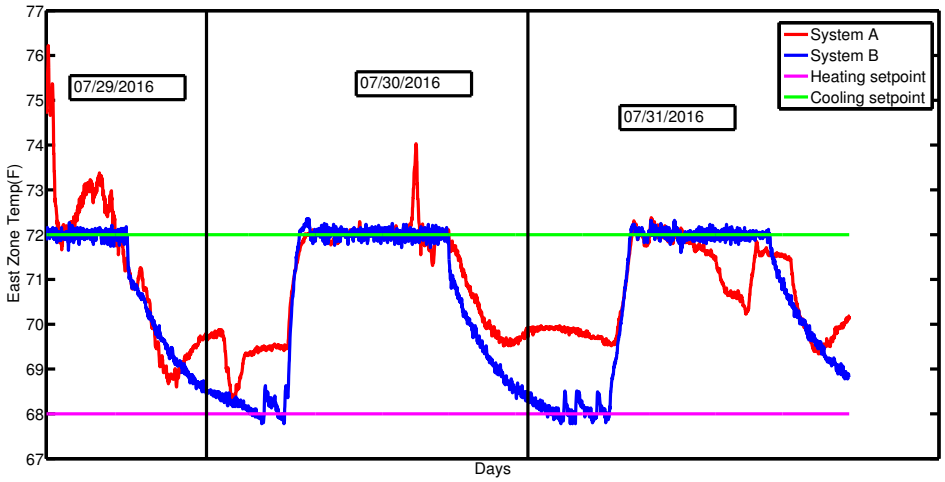

Figure 6.16 East zone temperature comparison between systems A and B

The temperatures of local zone controlled by AHU A are roughly maintained between the heating and cooling set points ($68°F - 72°F$). Also within the unoccupied mode system A outperforms system B as zone temperatures is controlled in the middle such that less reheat energy is consumed after the occupied mode begins.

The following Table 6.1 shows the total energy consumption of these two systems and it can be observed that from Table 6.1 the energy savings are 10.8% and 13.7% respectively in two different times. The major saving in system A is attributed to less energy consumed by the chiller and cooling energy consumed by the cooling coil in AHU. Therefore, the experimental results show that compared to the conventional control method the proposed supervisory control framework using

Table 6.1 Comparisons of energy consumption between systems A and B

Method	6 days with 31 hrs	3 days with 60 hrs
System B	2.3×10^6 BTU	3.4×10^6 BTU
System A	2.05×10^6 BTU	2.93×10^6 BTU

distributed optimization method can effectively achieve energy saving while maintaining thermal comfort requirements.

6.4 Conclusion

A supervisory control framework for agent-based building energy system using a novel distributed optimization framework is presented. A generalized gossip-based subgradient method is proposed to compute subgradients of the individual zones based on their individual cost functions. This method has the flexibility of using different modeling approaches for individual zones. The optimal setpoint (SAT) values are computed using the individual subgradients using a consensus protocol. The proposed framework is implemented on a real testbed at the Energy Resource Station in Iowa Energy Center using a recently developed agent-based distributed control platform, VOLTTRON^{TM}. Optimization agent has been developed in VOLTTRON^{TM} to realize the proposed framework which generates the optimal supply air temperature setpoint. Experimental results show that the proposed supervisory control framework based upon distributed optimization method can save energy by approximately 11% compared to the baseline strategy.

CHAPTER 7. CONCLUSIONS & FUTURE WORK

This dissertation has contributed to different areas of building energy systems such as modeling, control, and optimization. Mainly, it provides a framework (Brayton-Moser) and tool (Passivity) essential for analyzing complex building energy systems. In the following sections, we summarize the contributions of this dissertation and provide suggestions for future work.

7.1 Concluding Remarks

The concluding remarks of this dissertation are as follows.

In Chapter 1, a background was provided on the importance of reducing energy consumption in buildings along with the motivation for analyzing building systems through the methodology of tearing, zooming, and linking using BM framework and Passivity tool. We gave literature review on modeling, control, and optimization for building energy systems, and we outlined the contents of this dissertation.

In Chapter 2, a review of mathematical preliminaries needed to develop the results presented in this dissertation are provided.

In Chapter 3, comparative evaluation in terms of qualitative and quantitative metrics of representative modeling techniques belonging to different classes of models in the context of building zone temperature prediction are presented. Note: A bias in the temperature prediction can significantly affect the control of zone comfort and energy consumption. To the best of authors knowledge, there is no direct performance evaluation of different control oriented building thermal models reported using real building data. The results provide detailed analysis in terms of different metrics of individual modeling approaches and can be used as a guidelines for selecting appropriate modeling technique for diverse applications.

In Chapter 4, we proposed the power shaping paradigm to design controllers for two different HVAC subsystems, namely thermal zone model and heat exchanger system. These representative examples were chosen as they demonstrate most of the typical complexities found in building HVAC systems. Primarily, the building zone model which has a significant impact on the overall building energy efficiency. Firstly, the system dynamics are transformed into the BM framework and then the input-output map is identified that satisfies the passivity property. The advantage of using BM framework is that it naturally describes the dynamics of systems in terms of measurable quantities and for the case of building systems the individual zone temperatures are easily measurable. Secondly, stabilization is achieved by shaping the mixed potential function using the passive outputs such that the closed loop system with the total power function has a minimum at the desired equilibrium point. In our approach, we find the shaping function without the need to solve any partial differential equation (PDE). We explore the application of power shaping control in building systems context and show the building models have an inherent BM framework.

In Chapter 5, the BM framework and the passivity tool are further utilized for stability analysis of constrained optimization dynamics using the compositional property of passivity. Primarily, the convex optimization problem with only affine equality constraints admits a Brayton-Moser representation and is shown to be passive and stable. Secondly, the inequality constraints are modeled as a state-dependent switching system which is passive. Finally, the two systems are interconnected in a power conserving way whose dynamics represents the primal-dual gradient equations of the overall optimization problem and is passive using the compositional property of passivity. The aforementioned methodology is illustrated with energy management problem in buildings.

In Chapter 6, implementation and testing the effectiveness of the Generalized Gossip-based distributed optimization framework on the Iowa Energy Center's Energy Resource Station (ERS) testbed with the objective to reduce energy costs while maintaining zone comfort. These goals are accomplished by implementing the proposed framework within a multi-agent environment called

VOLTTRON^{TM}. The success of this experiment gives a way to deploy advanced control algorithms and optimization schemes which can benefit the building community.

7.2 Future Work

The potential future directions of research in continuation of this work is as follows:

- Extend the proposed framework to optimize whole building energy consumption which covers subsystems such as HVAC, on-site generation using renewables such as solar, wind etc., and energy storage. Also, implementing the whole building optimization using VOLTTRON^{TM} software.

- Developing a data-driven passivity framework for analysis (fault diagnosis) and control of engineering systems. Some useful references in this context are Lei et al. (2016); Romer et al. (2017); Maupong et al. (2017).

- The ability to use dissipativity/passivity for efficiently constructing Lyapunov functions and the intuitive notion of energy has ties with the convergence rate analysis of optimization methods. Recently Hu and Lessard (2017), dissipativity theory is used for understanding Nesterov's acceleration method.

7.3 Publications

Journal Publications

- Chinde, V., et al. "A Passivity-Based Power-Shaping Control of Building HVAC Systems." Journal of Dynamic Systems, Measurement, and Control 139.11 (2017): 111007.

- K. C. Kosaraju, V. Chinde, R. Pasumarthy, A. Kelkar and N. M. Singh, "Stability Analysis of Constrained Optimization Dynamics via Passivity Techniques," in IEEE Control Systems Letters, vol. 2, no. 1, pp. 91-96, Jan. 2018.

- Z. Jiang, V. Chinde, A. Kohl, S. Sarkar and A. Kelkar. "Supervisory Control and Distributed Optimization of Building Energy Systems" submitted to IEEE Transactions on Automation Science and Engineering.

Conference Publications

- V. Chinde, K. C. Kosaraju, Atul Kelkar, R. Pasumarthy, S. Sarkar, and N. M. Singh. "Building HVAC systems control using power shaping approach." In American Control Conference (ACC), 2016, pp. 599-604. IEEE.

- V. Chinde, A. Kohl, Z. Jiang, A. Kelkar, S. Sarkar. A VOLTTRON^{TM} based implementation of Supervisory Control using Generalized Gossip for Building Energy Systems, Proceedings in the 4th International High Performance Buildings Conference, (West Lafayette, IN), 2016.

- Jiang, Zhanhong, V Chinde, Adam Kohl, Soumik Sarkar, and Atul Kelkar. "Scalable supervisory control of building energy systems using generalized gossip." In American Control Conference (ACC), 2016, pp. 581-586. IEEE.

- V. Chinde, J. C. Heylmun, A. Kohl, Z. Jiang, S. Sarkar and A. Kelkar, Comparative Evaluation of Control-oriented zone temperature Prediction modeling strategies in Buildings, Proceedings of ASME Dynamics Systems and Control Conference, (Columbus, OH), 2015

BIBLIOGRAPHY

Afram, A. and Janabi-Sharifi, F. (2014). Review of modeling methods for hvac systems. *Applied Thermal Engineering*, 67(1):507–519.

Aranovskiy, S., Ortega, R., and Cisneros, R. (2015). Robust pi passivity-based control of nonlinear systems: Application to port-hamiltonian systems and temperature regulation. *arXiv preprint arXiv:1503.02935*.

Arcak, M. (2006). Passivity as a design tool for group coordination. In *2006 American Control Conference*, pages 6–pp. IEEE.

Arrow, K. J., Hurwicz, L., Uzawa, H., and Chenery, H. B. (1958). Studies in linear and non-linear programming.

Aswani, A., Master, N., Taneja, J., Culler, D., and Tomlin, C. (2012a). Reducing transient and steady state electricity consumption in hvac using learning-based model-predictive control. *Proceedings of the IEEE*, 100(1):240–253.

Aswani, A., Master, N., Taneja, J., Krioukov, A., Culler, D., and Tomlin, C. (2012b). Energy-efficient building hvac control using hybrid system lbmpc. *arXiv preprint arXiv:1204.4717*.

Aswani, A., Master, N., Taneja, J., Krioukov, A., Culler, D., and Tomlin, C. (2012c). Quantitative methods for comparing different hvac control schemes. In *Performance Evaluation Methodologies and Tools (VALUETOOLS), 2012 6th International Conference on*, pages 326–332. IEEE.

Aswani, A., Master, N., Taneja, J., Smith, V., Krioukov, A., Culler, D., and Tomlin, C. (June 2012d). Identifying models of hvac systems using semiparametric regression. *in the Proceedings of American Control Conference*.

Atam, E. (2017). Current software barriers to advanced model-based control design for energy-efficient buildings. *Renewable and Sustainable Energy Reviews*, 73:1031–1040.

Atam, E. and Helsen, L. (2016). Control-oriented thermal modeling of multizone buildings: Methods and issues: Intelligent control of a building system. *IEEE Control Systems*, 36(3):86–111.

Bacher, P. and Madsen, H. (2011). Identifying suitable models for the heat dynamics of buildings. *Energy and Buildings*, 43(7):1511–1522.

Behl, M., Nghiem, T., and Mangharam, R. (2013). Uncertainty propagation from sensing to modeling and control in buildings-technical report.

Bengea, S. C., Li, P., Sarkar, S., Vichik, S., Adetola, V., Kang, K., Lovett, T., Leonardi, F., and Kelman, A. D. (2015). Fault-tolerant optimal control of a building hvac system. *Science and Technology for the Built Environment*, 21(6):734–751.

Book, B. E. D. (2011). Energy efficiency and renewable energy. *US department of energy*.

Borja, P., Cisneros, R., and Ortega, R. (2016). A constructive procedure for energy shaping of porthamiltonian systems. *Automatica*, 72:230–234.

Boyd, S. and Vandenberghe, L. (2004). *Convex optimization*. Cambridge university press.

Boyd, S., Xiao, L., and Mutapcic, A. (2003). Subgradient methods.

Braun, J. E. (1990). Reducing energy costs and peak electrical demand through optimal control of building thermal storage. *ASHRAE transactions*, 96(2):876–888.

Brayton, R. and Moser, J. (1964). A theory of nonlinear networks i. *Quart. Appl. Math*, 22(1):1–33.

Burkhart, M. C., Heo, Y., and Zavala, V. M. (2014). Measurement and verification of building systems under uncertain data: A gaussian process modeling approach. *Energy and Buildings*, 75:189–198.

Cai, J., Braun, J. E., Kim, D., and Hu, J. (2016). A multi-agent control based demand response strategy for multi-zone buildings. In *American Control Conf.* Accepted.

Cai, J., Kim, D., Putta, V. K., Braun, J. E., and Hu, J. (2015). Multi-agent control for centralized air conditioning systems serving multi-zone buildings. In *American Control Conference (ACC), 2015*, pages 986–993. IEEE.

Center, I. E. (2010). Ers technical description. *Iowa Energy Center. Ankeny, I A.*

Chen, L., Li, N., Jiang, L., and Low, S. H. (2012). Optimal demand response: Problem formulation and deterministic case. In *Control and optimization methods for electric smart grids*, pages 63–85. Springer.

Chen, Q. (2009). Ventilation performance prediction for buildings: A method overview and recent applications. *Building and environment*, 44(4):848–858.

Chen, Q. and Zhai, Z. (2004). The use of cfd tools for indoor environmental design. *Advanced building simulation*, pages 119–140.

Cherukuri, A., Mallada, E., and Cortés, J. (2016). Asymptotic convergence of constrained primal–dual dynamics. *Systems & Control Letters*, 87:10–15.

Chinde, V., Heylmun, J. C., Kohl, A., Jiang, Z., Sarkar, S., and Kelkar, A. (2015). Comparative evaluation of control-oriented zone temperature prediction modeling strategies in buildings. In *ASME 2015 Dynamic Systems and Control Conference*, pages V002T34A009–V002T34A009. American Society of Mechanical Engineers.

Chinde, V., Kohl, A., Jiang, Z., Kelkar, A., and Sarkar, S. (2016a). A volttron based implementation of supervisory control using generalized gossip for building energy systems.

Chinde, V., Kosaraju, K., Kelkar, A., Pasumarthy, R., Sarkar, S., and Singh, N. (2016b). Building hvac systems control using power shaping approach. In *American Control Conference (ACC), 2016*, pages 599–604. IEEE.

Cøengel, Y. (2007). Heat and mass transfer: A practical approach.

Deng, K., Goyal, S., Barooah, P., and Mehta, P. G. (2014). Structure-preserving model reduction of nonlinear building thermal models. *Automatica*, 50(4):1188–1195.

Dincer, I. (2002). On thermal energy storage systems and applications in buildings. *Energy and Buildings*, 34(4):377–388.

Doe, U. (2012). Building energy software tools directory.

Donaire, A., Mehra, R., Ortega, R., Satpute, S., Romero, J. G., Kazi, F., and Singh, N. (2016a). Shaping the energy of mechanical systems without solving partial differential equations. *IEEE Transactions on Automatic Control*, 61(4):1051–1056.

Donaire, A., Mehra, R., Ortega, R., Satpute, S., Romero, J. G., Kazi, F., and Singh, N. M. (2016b). Shaping the energy of mechanical systems without solving partial differential equations. *IEEE Transactions on Automatic Control*, 61(4):1051–1056.

Dounis, A. I. and Caraiscos, C. (2009). Advanced control systems engineering for energy and comfort management in a building environmenta review. *Renewable and Sustainable Energy Reviews*, 13(6):1246–1261.

Eisenhower, B., Gasljevic, K., and Mezic, I. (2012). Control-oriented dynamic modeling and calibration of a campus theater using modelica. In *IBPSA-USA's SimBuild 2012 Conference The Future of Simulation for Buildings*.

ERS (2015). Energy Resource Station Technical Description. http://www.iowaenergycenter.org/energy-resource-station-ers/.

Favache, A. and Dochain, D. (2010). Power-shaping control of reaction systems: The cstr case. *Automatica*, 46(11):1877–1883.

Feijer, D. and Paganini, F. (2009). Krasovskii's method in the stability of network control. In *American Control Conference, 2009. ACC'09.*, pages 3292–3297. IEEE.

Feijer, D. and Paganini, F. (2010). Stability of primal–dual gradient dynamics and applications to network optimization. *Automatica*, 46(12):1974–1981.

Fux, S., Benz, M., and Guzzella, L. (2011). Comparing control-oriented thermal models for a passive solar house. In *submitted to CISBAT conference*.

Gao, N. and Niu, J. (2004). CFD study on micro-environment around human body and personalized ventilation. *Building and Environment*, 39(7):795–805.

García-Canseco, E., Jeltsema, D., Ortega, R., and Scherpen, J. M. (2010). Power-based control of physical systems. *Automatica*, 46(1):127–132.

Gogte, G., Venkatesh, C., Kazi, F., Singh, N., and Pasumarthy, R. (2012). Passivity based control of underactuated 2-d spidercrane manipulator. In *20th International Symposium on Mathematical Theory of Networks and Systems MTNS*.

Gouda, M., Danaher, S., and Underwood, C. (2002). Building thermal model reduction using nonlinear constrained optimization. *Building and Environment*, 37(12):1255–1265.

Gouda, M., Underwood, C., and Danaher, S. (2003). Modelling the robustness properties of HVAC plant under feedback control. *Building Services Engineering Research and Technology*, 24(4):271–280.

Goyal, S. and Barooah, P. (2010). Modeling thermal dynamics in multi-zone buildings. *University of Florida, Gainesville, FL, Tech. Rep.*

Goyal, S. and Barooah, P. (2012). A method for model-reduction of non-linear thermal dynamics of multi-zone buildings. *Energy and Buildings*, 47:332–340.

Goyal, S., Ingley, H. A., and Barooah, P. (2012). Zone-level control algorithms based on occupancy information for energy efficient buildings. In *American Control Conference (ACC), 2012*, pages 3063–3068. IEEE.

Goyal, S., Liao, C., and Barooah, P. (2011). Identification of multi-zone building thermal interaction model from data. In *Decision and Control and European Control Conference (CDC-ECC), 2011 50th IEEE Conference on*, pages 181–186. IEEE.

Haack, J., Akyol, B., Carpenter, B., Tews, C., and Foglesong, L. (2013a). Volttron: an agent platform for the smart grid. In *Proceedings of the 2013 international conference on Autonomous agents and multi-agent systems*, pages 1367–1368. International Foundation for Autonomous Agents and Multiagent Systems.

Haack, J., Akyol, B., Carpenter, B., Tews, C., and Foglesong, L. (2013b). Volttron: an agent platform for the smart grid. *in the Proceedings of the 2013 International Conference on Autonomous agents and multi-agent systems, Richland, SC*.

Haack, J., Akyol, B., Tenney, N., Carpenter, B., Pratt, R., and Carroll, T. (2013c). Volttron: An agent platform for integrating electric vehicles and smart grid. In *Connected Vehicles and Expo (ICCVE), 2013 International Conference on*, pages 81–86. IEEE.

Hämäläinen, R. P., Mäntysaari, J., Ruusunen, J., and Pineau, P.-O. (2000). Cooperative consumers in a deregulated electricity marketdynamic consumption strategies and price coordination. *Energy*, 25(9):857–875.

Hao, H., Kowli, A., Lin, Y., Barooah, P., and Meyn, S. (2013). Ancillary service for the grid via control of commercial building hvac systems. In *American Control Conference (ACC), 2013*, pages 467–472. IEEE.

Hao, H., Lin, Y., Kowli, A. S., Barooah, P., and Meyn, S. (2014). Ancillary service to the grid through control of fans in commercial building hvac systems. *IEEE Transactions on Smart Grid*, 5(4):2066–2074.

Henze, G. P. (2005). Energy and cost minimal control of active and passive building thermal storage inventory. *Journal of Solar Energy Engineering*, 127(3):343–351.

Henze, G. P., Felsmann, C., and Knabe, G. (2004). Evaluation of optimal control for active and passive building thermal storage. *International Journal of Thermal Sciences*, 43(2):173–183.

Henze, G. P. and Krarti, M. (2005). Predictive optimal control of active and passive building thermal storage inventory. Technical report, University Of Nebraska.

Heo, Y. and Zavala, V. M. (2012). Gaussian process modeling for measurement and verification of building energy savings. *Energy and Buildings*, (53):7–18.

Horan, J. and Finn, D. (2005). Cfd reliability issues in analysis of naturally ventilated buildings. *Passive and Low Energy Cooling for the Built Environment*, pages 53–58.

Hu, B. and Lessard, L. (2017). Dissipativity theory for nesterov's accelerated method. *arXiv preprint arXiv:1706.04381*.

Huang, H., Chen, L., Mohammadzaheri, M., and Hu, E. (2012). A new zone temperature predictive modeling for energy saving in buildings. *Procedia Engineering*, 49:142–151.

Huang, H., Chen, L., Mohammadzheri, M., Hu, E., and Chen, M. (June 2013). Multi-zone temperature prediction in a commercial building using artificial neural network model. *in the Proceedings of Control and Automation (ICCA), IEEE International Conference on*.

IEC (2010). Energy resource station (ers) technical description. *Iowa Energy Center Technical Report*.

Jeltsema, D. and Scherpen, J. (2009). Multidomain modeling of nonlinear networks and systems. *Control Systems, IEEE*, 29(4):28–59.

Jeltsema, D. and Scherpen, J. M. (2007). A power-based description of standard mechanical systems. *Systems & Control Letters*, 56(5):349–356.

Jiang, Z., Chinde, V., Kohl, A., Sarkar, S., and Kelkar, A. (2016). Scalable supervisory control of building energy systems using generalized gossip. In *American Control Conference (ACC), 2016 to appear*. IEEE.

Jiang, Z., Sarkar, S., and Kushal, M. (2015). On distributed optimization using generalized gossip. *in Proceedings of 54th Conference on Decision and Control, IEEE, Osaka.*

Jimenez, M. J. and Madsen, H. (2008). Models for describing the thermal characteristics of building components. *Building and Environment*, 43(2):152–162.

Johansson, B., Keviczky, T., Johansson, M., and H., J. K. (December, 2008). Subgradient methods and consensus algorithms for solving convex optimization problems. *in Proceedings of the 47th IEEE Conference on Decision and Control, Caucun, Mexico*, pages 4185–4190.

Khalil, H. K. and Grizzle, J. (1996). *Nonlinear systems*, volume 3. Prentice hall New Jersey.

Khamphanchai, W., Pipattanasomporn, M., Kuzlu, M., and Rahman, S. (2015). An agent-based open source platform for building energy management. In *Smart Grid Technologies-Asia (ISGT ASIA), 2015 IEEE Innovative*, pages 1–6. IEEE.

Khamphanchai, W., Saha, A., Rathinavel, K., Kuzlu, M., Pipattanasomporn, M., Rahman, S., Akyol, B., and Haack, J. (2014). Conceptual architecture of building energy management open source software (bemoss). In *Innovative Smart Grid Technologies Conference Europe (ISGT-Europe), 2014 IEEE PES*, pages 1–6. IEEE.

Kosaraju, K., Pasumarthy, R., Singh, N., and Fradkov, A. (2017). Control using new passivity property with differentiation at both ports. *Indian Control Conference (ICC)*, pages 7–11.

Kosaraju, K. C., Chinde, V., Pasumarthy, R., Kelkar, A., and Singh, N. M. (2018). Stability analysis of constrained optimization dynamics via passivity techniques. *IEEE Control Systems Letters*, 2(1):91–96.

Lei, Q., Munir, M. T., Bao, J., and Young, B. (2016). A data-driven fault detection method based on dissipative trajectories. *IFAC-PapersOnLine*, 49(7):717–722.

Li, P., ONeill, Z. D., and Braun, J. E. (2013). Development of control-oriented models for model predictive control in buildings. *Ashrae Trans*, 119(2).

Lin, Y., Barooah, P., and Meyn, S. P. (2013). Low-frequency power-grid ancillary services from commercial building hvac systems. In *Smart Grid Communications (SmartGridComm), 2013 IEEE International Conference on*, pages 169–174. IEEE.

Lin, Y., Middelkoop, T., and Barooah, P. (2012). Identification of control-oriented thermal models of rooms in multi-room buildings. In *IEEE CDC*.

Lutes, R. G., Haack, J., Katipamula, S., Monson, K., Akyol, B., Carpenter, B., and Tenney, N. (2014). Volttron: User guide.

Lygeros, J., Johansson, K. H., Simic, S. N., Zhang, J., and Sastry, S. S. (2003). Dynamical properties of hybrid automata. *IEEE Transactions on automatic control*, 48(1):2–17.

Ma, K., Hu, G., and Spanos, C. J. (2016). Energy management considering load operations and forecast errors with application to hvac systems. *IEEE Transactions on Smart Grid*.

Ma, Y. (2012). Model predictive control for energy efficient buildings.

Ma, Y., Anderson, G., and Borrelli, F. (2011). A distributed predictive control approach to building temperature regulation. In *American Control Conference (ACC), 2011*, pages 2089–2094. IEEE.

Mařík, K., Rojíček, J., Stluka, P., and Vass, J. (2011). Advanced hvac control: Theory vs. reality. *IFAC Proceedings Volumes*, 44(1):3108–3113.

Mathieu, J. L., Koch, S., and Callaway, D. S. (2013). State estimation and control of electric loads to manage real-time energy imbalance. *IEEE Transactions on Power Systems*, 28(1):430–440.

Maupong, T., Mayo-Maldonado, J. C., Rapisarda, P., et al. (2017). On lyapunov functions and data-driven dissipativity.

Minakais, M., Mishra, S., and Wen, J. T. (2014). Groundhog day: Iterative learning for building temperature control. In *Automation Science and Engineering (CASE), 2014 IEEE International Conference on*, pages 948–953. IEEE.

Minakais, M., Okaeme, C. C., Mishra, S., and Wen, J. T. (2017). Iterative learning control for coupled temperature and humidity in buildings. *IFAC-PapersOnLine*, 50(1):13420–13425.

Mukherjee, S., Mishra, S., and Wen, J. T. (2012). Building temperature control: A passivity-based approach. In *Decision and Control (CDC), 2012 IEEE 51st Annual Conference on*, pages 6902–6907. IEEE.

Nedic, A. and Ozdaglar, A. (Janury, 2009). Distributed subgradient methods for multi-agent optimization. *Automatic Control, IEEE Transactions on*, 54:48–61.

Nikolova, E. and Nikolova, S. E. (2003). The gradient method and lyapunov functions applied to decentralized optimization problems.

Oldewurtel, F., Parisio, A., Jones, C. N., Gyalistras, D., Gwerder, M., Stauch, V., Lehmann, B., and Morari, M. (2012). Use of model predictive control and weather forecasts for energy efficient building climate control. *Energy and Buildings*, 45:15–27.

Oldewurtel, F., Sturzenegger, D., and Morari, M. (2013). Importance of occupancy information for building climate control. *Applied energy*, 101:521–532.

Ortega, R., Jeltsema, D., and Scherpen, J. M. (2003). Power shaping: A new paradigm for stabilization of nonlinear rlc circuits. *Automatic Control, IEEE Transactions on*, 48(10):1762–1767.

Palensky, P. and Dietrich, D. (2011). Demand side management: Demand response, intelligent energy systems, and smart loads. *IEEE transactions on industrial informatics*, 7(3):381–388.

Privara, S., Cigler, J., Váňa, Z., Oldewurtel, F., Sagerschnig, C., and Žáčeková, E. (2013). Building modeling as a crucial part for building predictive control. *Energy and Buildings*, 56:8–22.

Rasmussen, C. E. (2006). Gaussian processes for machine learning.

Rasmussen, C. E. and Nickisch, H. (2010). Gaussian processes for machine learning (gpml) toolbox. *The Journal of Machine Learning Research*, 11:3011–3015.

Ríos-Moreno, G. J., Trejo-Perea, M., Castaneda-Miranda, R., Hernández-Guzmán, V. M., and Herrera-Ruiz, G. (2007). Modelling temperature in intelligent buildings by means of autoregressive models. *Automation in construction*, 16(5):713–722.

Romer, A., Montenbruck, J. M., and Allgöwer, F. (2017). Determining dissipation inequalities from input-output samples. *IFAC-PapersOnLine*, 50(1):7789–7794.

Ruano, A. E., Crispim, E. M., Conceiçao, E. Z., and Lúcio, M. M. J. (2006). Prediction of building's temperature using neural networks models. *Energy and Buildings*, 38(6):682–694.

Sarkar, S., Mukherjee, K., and Ray, A. (2013). Distributed decision propagation in proximity networks. *International Journal of Control*, 86(6):1118–1130.

Satpute, S., Mehra, R., Kazi, F., and Singh, N. (2014). Geometric–PBC approach for control of circular ball and beam system. *Proceedings of the Mathematical Theory of Networks and Systems MTNS*.

Sepulchre, R., Jankovic, M., and Kokotovic, P. V. (2012). *Constructive nonlinear control*. Springer Science & Business Media.

Spivak, M. (1979). A comprehensive introduction to differential geometry. volume four.

Srivastav, A., Tewari, A., Dong, B., Sarkar, S., and Gorbounov, M. (2014). Localized uncertainty quantification for baseline building energy modeling, automated diagnostics for facility equipment, systems, and whole buildings, fairmont press.

Stegink, T., De Persis, C., and van der Schaft, A. (2016). A unifying energy-based approach to stability of power grids with market dynamics. *IEEE Transactions on Automatic Control*, PP(99):1–11.

Travesi, J., Maxwell, G., Klaassen, C., Holtz, M., Knabe, G., Felsmann, C., Achermann, M., and Behne, M. (2001). Empirical validation of Iowa energy resource station building energy analysis simulation models. *IEA Task*, 22.

van der Schaft, A. J. (2011). On the relation between port-hamiltonian and gradient systems. *IFAC Proceedings Volumes*, 44(1):3321–3326.

Wang, J. and Elia, N. (2011). A control perspective for centralized and distributed convex optimization. In *50^{th} IEEE Conference on Decision and Control and European Control Conference (CDC-ECC)*, pages 3800–3805. IEEE.

Wei, E. (2014). *Distributed optimization and market analysis of networked systems*. PhD thesis, Massachusetts Institute of Technology.

Wen, J. T., Mishra, S., Mukherjee, S., Tantisujjatham, N., and Minakais, M. (2013). Building temperature control with adaptive feedforward. In *Decision and Control (CDC), 2013 IEEE 52nd Annual Conference on*, pages 4827–4832. IEEE.

Wilcox, S. and Marion, W. (2008). *Users manual for TMY3 data sets*. National Renewable Energy Laboratory Golden, CO.

Willems, J. C. (2007). The behavioral approach to open and interconnected systems. *IEEE Control Systems*, 27(6):46–99.

Willems, J. C. and Polderman, J. W. (2013). *Introduction to mathematical systems theory: a behavioral approach*, volume 26. Springer Science & Business Media.

Wu, S. and Sun, J.-Q. (2012a). Multi-stage regression linear parametric models of room temperature in office buildings. *Building and Environment*, 56:69–77.

Wu, S. and Sun, J.-Q. (2012b). A physics-based linear parametric model of room temperature in office buildings. *Building and Environment*, 50:1–9.

Yan, B. and Malkawi, A. (2012). Predicting system performance with uncertainty.

Zefran, M., Bullo, F., and Stein, M. (2001a). A notion of passivity for hybrid systems. In *Decision and Control, 2001. Proceedings of the 40th IEEE Conference on*, volume 1, pages 768–773. IEEE.

Zefran, M., Bullo, F., and Stein, M. (2001b). A notion of passivity for hybrid systems. *IEEE Conference on Decision and Control (CDC)*.

Zhang, M., Borja, P., Ortega, R., Liu, Z., and Su, H. (2017). Pid passivity-based control of port-hamiltonian systems. *IEEE Transactions on Automatic Control*.

Zhang, X., Shi, W., Li, X., Yan, B., Malkawi, A., and Li, N. (2016). Decentralized temperature control via hvac systems in energy efficient buildings: An approximate solution procedure. In *Signal and Information Processing (GlobalSIP), 2016 IEEE Global Conference on*, pages 936–940. IEEE.

Zhou, D. P., Hu, Q., and Tomlin, C. J. (2017). Quantitative comparison of data-driven and physics-based models for commercial building hvac systems. In *American Control Conference (ACC), 2017*, pages 2900–2906. IEEE.